NTNU
Norwegian University of
Science and Technology

Characterization of the airflow distribution in close proximity to the patient in an operating room

Anders Mostrøm Nilssen

NTNU

Norwegian University
of Science and Technology

Department of Energy
and Process Engineering

MASTER THESIS

for

Student Anders Mostrøm Nilssen

Spring 2018

Characterization of the airflow distribution in close proximity to the patient in an operating room

Karakterisering av luft fordelingen i nærheten av pasienten i en operasjonsstue

Background and objective

In modern hospitals, among surgical patients surgical-site infections (SSIs) are the most common hospital-acquired infections accounting for 36% of nosocomial infections. Tremendous efforts have been made to understand the general and procedure-specific patient risk factors for the development of postoperative surgical site infection. However, the nature of the turbulence airflow and the complex dynamic biochemical process prevent the identification and quantification of the effect of airflow on SSI. Ultra-clean ventilation systems and laminar airflow ceilings have been used in ORs to improve the cleanliness of indoor air. However, another individual study showed significantly higher severe SSI rates following knee prosthesis and significantly higher SSI rates following hip prosthesis under laminar airflow conditions. St. Olavs Hospital has 43 operating rooms and over 1000 patient bed.

The objective of this study is to characterise the airflow distribution in close proximity to a patient in operating rooms with different ventilation systems.

The following tasks are to be considered:

Tasks:
1) Literature review: state of the art analysis of the airflow distribution close to a patient and heat and mass transfer from a wound.
2) Model and calculate the heat and moisture exchange between the patient and the ambient air in an operating room.
3) Conduct experimental measurements of airflow distribution close to a patient in operating rooms.
4) Analyse the effect of the airflow distribution on heat and moisture exchange.
5) Provide suggestions and guidance to design the airflow distribution in operating rooms.
6) Prepare a conference article to disseminate the research results.

Within 14 days of receiving the written text on the master thesis, the candidate shall submit a research plan for his project to the department.

When the thesis is evaluated, emphasis is put on processing of the results, and that they are presented in tabular and/or graphic form in a clear manner, and that they are analyzed carefully.

The thesis should be formulated as a research report with summary both in English and Norwegian, conclusion, literature references, table of contents etc. During the preparation of the text, the candidate should make an effort to produce a well-structured and easily readable report. In order to ease the evaluation of the thesis, it is important that the cross-references are correct. In the making of the report, strong emphasis should be placed on both a thorough discussion of the results and an orderly presentation.

The candidate is requested to initiate and keep close contact with his/her academic supervisor(s) throughout the working period. The candidate must follow the rules and regulations of NTNU as well as passive directions given by the Department of Energy and Process Engineering.

Risk assessment of the candidate's work shall be carried out according to the department's procedures. The risk assessment must be documented and included as part of the final report. Events related to the candidate's work adversely affecting the health, safety or security, must be documented and included as part of the final report. If the documentation on risk assessment represents a large number of pages, the full version is to be submitted electronically to the supervisor and an excerpt is included in the report.

Pursuant to "Regulations concerning the supplementary provisions to the technology study program/Master of Science" at NTNU §20, the Department reserves the permission to utilize all the results and data for teaching and research purposes as well as in future publications.

The final report is to be submitted digitally in DAIM. An executive summary of the thesis including title, student's name, supervisor's name, year, department name, and NTNU's logo and name, shall be submitted to the department as a separate pdf file. Based on an agreement with the supervisor, the final report and other material and documents may be given to the supervisor in digital format.

☐ Work to be done in lab (Water power lab, Fluids engineering lab, Thermal engineering lab)
☒ Field work

Department of Energy and Process Engineering, 22. January 2018

Guangyu Cao
Academic Supervisor

Research Advisor: Liv-Inger Stenstad, Research Coordinator, Operating Room of the Future program, St. Olavs hospital
Jan Gunnar Skogås, Director of Operating Room of the Future program, St. Olavs hospital

Summary

The main objective of the master thesis is to characterize the airflow distribution in close proximity to a patient in a supine position, in two operating theatres with different ventilation systems. The two examined systems are a mixing and a laminar airflow system. Initially, the thesis was structured into three cases. Each case considered a subtask which was required to reach the main objective. Case 1 investigates the thermal plume of a human in a supine position in quiescent surroundings. Both Case 2 and 3 examine the airflow distribution above the patient and how it is affected by heat sources and obstacles. The ventilation system of Case 2 is a laminar system, while the operating theatre of Case 3 features a mixing system. A thermal manikin is used in Case 2 and 3 to simulate the heat loss of a patient.

Case 1 examines the thermal plumes of five human test subjects in a non-ventilated room. The objective of the case is to investigate the thermal plume of a human and use the findings to calibrate a thermal manikin. The results suggests that the human plume is most powerful above the upper body, with a maximum mean centerline velocity of 0.135 m/s.

Case 2 investigates if the airflow distribution above the patient is affected by heat sources and physical obstacles, at and around, the operating table. In addition to the thermal manikin are also three heated cylinders and two surgical lamps positioned around the table in various scenarios. The results indicates that the airflow distribution is affected by both heat sources and obstacles. Heat sources, especially the patient, led to lower velocities and increased values of temperature and turbulence intensity. Surgical lamps were found to change the airflow pattern downstream, indicating the importance of lamp positioning.

Case 3 studies the same scenarios and has the same objective as Case 2, but for an operating theatre with a mixing system. The results, compared to those of Case 2, suggests that the velocities and the levels of turbulence intensity are less affected by the heat sources. On the other hand, some of the temperatures are well above the values of Case 2. The levels of turbulence intensity are generally higher than in Case 2, ranging from 22 to 44 %. Also, the results indicates that the most significant changes from scenario to scenario occurred below a height of 15 cm above the surface of the patient.

A phenomenon observed in the results of both Case 2 and 3 is that the surgical lamps increase the velocities in two cross-sections. Neither of these cross-sections are close to, or beneath, the lamps. Based on the results of Case 2 and 3, it could prove wise to include as many heat sources and physical obstacles as possible during the design phase. The use of omnidirectional anemometers pose a limitation and complicates the analysis of the results. However, some of the findings in the thesis may be relevant to the design of ventilation systems in operating theatres.

Samandrag

Hovudmålet til master-oppgåva var å karakterisere luftstraumsfordelinga i umiddelbar nærleik til ein liggjande pasient i to operasjonsstove med ulike ventilasjonsanlegg. Dei to typane som vart undersøkte var fortynningsventilasjon og eit laminært luftstraumssystem. I starten vart hovudoppgåva delt opp i tre delar. Kvar del tok for seg ei deloppgåve som var naudsynt for å oppfylle hovudmålet. Del 1 utforskar den termiske pluma frå eit liggjande menneske i rolege omgjevnader. Båe del 2 og 3 undersøkjer luftstraumsfordelina over pasienten og korleis den vert påverka av varmekjelder og hindringar. Ventilasjonssystemet i del 2 er laminært, og i del 3 er det fortynningsventilasjon. Ein termisk dukke vart brukt i båe del 2 og 3 for å simulere ein pasient sitt varmetap.

Del 1 studerte dei termiske plumene til fem testpersonar i eit rom uten ventilasjon. Målet med delen var å undersøkje den termiske pluma over eit menneske og nytte funna til kalibrasjon av den termiske dukka. Resultata viser at den termiske pluma var sterkast ved overkroppen, med ein maksimal, gjennomsnittleg sentralsnøggleik på 0.135 m/s.

Del 2 undersøkte om luftstraumsfordelina over pasienten vert påverka av varmekjelder og fysiske hindringar som anten er rundt eller over operasjonsbordet. I tillegg til den termiske dukka vart tre oppvarma sylindrar og to operasjonslampar plasserte rundt operasjonsbordet i ulike scenario. Resultata viste at luftstraumsfordelinga vert påverka av varmekjelder og hindringar. Varmekjelder, særskild pasienten, resulterte i lågare snøggleikar og auka temperaturar og turbulensintensitetverdiar. Opersjonslampane endra luftstraumsmønsteret nedstrøms, noko som illustrerar at plassering av lampane er viktig.

Del 3 tok for seg dei same scenarioane og hadde det same målet som del 2, men i ei operasjonsstove med fortynningsventilasjon. Samanlikna med resultata frå del 2 viste resultata her at snøggleikane og nivåa av turbulensintensitet vart mindre påverka av varmekjeldene. På den andre sida, så var nokre av dei registrerte temperaturane godt over verdiar målt i del 2. Turbulensintensiteten var generelt høgare einn i del 2 og varierte mellom 22 og 44 %. Resultata avslørte òg at dei største endringane frå scenario til scenario fann stad opp til 15 cm over pasienten.

Det vart observert i båe del 2 og 3 at operasjonslampane auka snøggleikane i to tverrsnitt, når ein samanlikna med det føregåande scenarioet. Ingen av tverrsnitta var nære eller under operasjonslampane. Med bakgrunn i resultata frå del 2 og 3 kan det vere smart å inkludere så mange varmekjelder og hindringar som mogleg, når ein utformar anlegga. At omnidireksjonelle anemometer vart nytta båe avgrensar og kompliserar analysen av resultata. Likevel kan nokre av funna frå oppgåva vere relevante for utforming av ventilasjonssystem på operasjonsstove.

Preface

This master thesis was written at the Department of Energy and Process Engineering at the Norwegian University of Science and Technology in Trondheim, during the spring semester of 2018. The thesis was written in collaboration with the organization Fremtidens Operasjonsrom (FOR) at St. Olavs Hospital in Trondheim.

Anders Mostrøm Nilssen.
Trondheim, July 2018

Table of Contents

List of Tables

List of Figures

Abbreviations

BCP	=	Bacteria Carrying Particle
CBL	=	Convective Boundary Layer
CFD	=	Computational Fluid Dynamics
CFU	=	Colony Forming Units
HTM	=	Health Technical Memorandum
LAF	=	Laminar Airflow
NSD	=	Norsk senter for forskningsdata
OR	=	Operating Room
OT	=	Operating Theatre
SSI	=	Surgical Site Infection
UCV	=	Ultra clean Ventilation

Chapter 1

Introduction

1.1 Background and problem statement

Nosocomial, or hospital acquired, infections pose a problem for both patients and hospitals as they are associated with prolonged hospital stays for patients (Haley *et al.*, 1981), increased patient mortality (French and Cheng, 1991; Kaoutar *et al.*, 2004), as well as increased health care costs (French and Cheng, 1991). A study of hospitals in northern France identified nosocomial infections as the holder of fourth place at the list of causes for in-hospital deaths (Kaoutar *et al.*, 2004), and according to a study by Poggio do surgical-site infections (SSIs) rank as the second most common nosocomial infection in the US, accounting for 20 % (Poggio, 2013). In 2016, the Norwegian Institute of Public Health published statistics showing that 1 in 23 surgical patients had developed an infection in the surgical wound area, with 40 % of them being characterized as deep infections (Folkehelseinstituttet, 2016). As there is a growing attention towards the overconsumption of antibiotics and the antibiotic-resistant bacteria, the focus should be on preventing rather than curing SSIs.

Factors that may contribute to the risk of SSIs include among others; age and weight of the patient, latent underlying patient illness, the surgical staff's abilities, attention to hygiene, and contamination levels of bacteria and particles in the operating room (OR) (Weinstein and Bonten, 2017). Also, the role of the ventilation system has been investigated. Significant work has been put into creating ultra clean operating theatres with high-efficiency particulate air (HEPA) filters in order to reduce the prevalence of SSIs, but recent studies have indicated that the effort may have been uncalled for (Mchugh, Hill and Humphreys, 2015; Bischoff *et al.*, 2017). This means that there is a need for a thorough investigation of the airflow in the OR and the interaction between the ventilation system, thermal plumes, and airflow obstacles.

1.2   Objective of study

The main objective of this study is to characterize the airflow distribution in close proximity to a patient in a supine position in operating rooms with different ventilation systems. Two systems will be investigated; mixing and laminar airflow systems. In order to achieve the main objective three cases, each with its own sub-objective, were established. Two of them were field measurements performed at St. Olavs hospital, while the last one was lab measurements at Gløshaugen, NTNU. They were:

1. Study of the thermal plume above a thermal manikin and real human beings

2. Experiment with a thermal manikin in an operating theatre with a laminar airflow system

3. Experiment with a thermal manikin in an operating theatre with a mixing system

The assignment text of the thesis included modeling and measurements of both heat and moisture transfer from a patient during surgery. However, due to practical limitations, patient security, time constraints, and lack of adequate instruments, it was decided to focus only on heat transfer and thermal plumes. The decision was taken in agreement with the supervisor.

Conference articles

A subtask of the thesis was to prepare a conference article to disseminate the results. Two articles presenting the results from similar experiments conducted in autumn 2017 was submitted to two different conferences. They can be found in the appendices.

1.3   Structure and methodology

Initially on this master thesis a Gantt chart was made to plan and get an overview of the work. As time progressed, most of the tasks went as planned.

The thesis is divided into five main parts: literature review, a study of the thermal plume of a human in a supine position, experimental setup, results, and discussion. The literature review is meant to provide an analysis of the airflow distribution close to a patient and it includes; a brief presentation of the history of ventilation of operating theatres, a description of the two ventilation systems, a comparison of how various factors affect the performance of the ventilation system, Norwegian standards and guidelines, and a part about how a wound and its healing process is affected by the ambient air.

The second part is a study of the thermal plume of a human in a supine position. This part presents the theory for calculations of convective heat loss and other equations that are essential in order to test whether existing mathematical models can be applied to the human thermal plume. Part three presents the experimental setup, after which the results are presented. The fifth part comprises a discussion of the results and methods, as well as

suggestions for the design of airflow distributions in operating theatres and future studies. A conclusion follows the discussion.

Theory and literature in this thesis were found mainly by using the search engine of the university library and oria.no. A substantial part of the scientific articles come from the two databases ScienceDirect and Google Scholar.

Chapter 2

Literature Review

The chapter will present a literature review of ventilation of operating theatres. This includes presenting the two governing ventilation principles in operating theatres, a brief summary of the history of hospital ventilation, standards for OT ventilation, a comparison of two ventilation principles and how their performances are affected by different factors, and an assessment of the wound microenvironment.

2.1 Ventilation of operating theatres

The overall objective of the ventilation system in an operating theatre is to provide a healthy and secure indoor environment for the patient and the surgical staff. This includes keeping the temperature and relative humidity within specified ranges, safely removing and preventing bacteria from reaching critical areas, providing fresh clean air, removing anesthesia gases, and ensuring thermal comfort for the patient and the surgical staff. The design of the ventilation system has to take into account the way the air is removed from contaminated areas, and the amount of supply air needed in order to perform the task satisfactorily. The latter point is also a question of economy, as larger air volumes result in higher operational and building costs. Another important aspect is that even though two ventilation systems deliver the same amount of fresh air, the contamination removal efficiency of each system may differ.

Depending on the type of surgery there may be different requirements for the indoor environment in an operating theatre. For instance, the demands of a joint replacement procedure and a surgery involving significant burns could differ considerably (Nastas *et al.*, 2016). Therefore it may be reasonable to use operating theatres with different ventilation systems depending on the surgical procedure. According to Zoon, Loomans, and Hensen (2011), there are in general two main principles being used for ventilation of operating theatres: mixing and laminar airflow (LAF) systems.

2.1.1 Brief history

Surgery was for a long time usually performed at the hospital ward, but this changed in the 18th century when operating theatres were opened in order to improve the teaching of surgery (Stacey and Humphreys, 2002). A major revolution in operating theatre practice occurred after Lister's groundbreaking paper from 1867, where he proved the benefits of antisepsis (Lister, 1867). Following the paper, the design of operating theatres was focused on minimizing the risk of infection (Essex-Lopresti, 1999). In the 1930s the air quality of the operating theatre gained renewed interest (Lidwell, 1981), and in 1946 one of the first studies on wound infections and airborne bacteria was published (Stacey and Humphreys, 2002).

Blowers and Crew (1960) published a study in 1960 in which they investigated operating theatres across Britain and performed experiments in a dummy theatre. In the theatre, they investigated different airflow distribution systems, the effects of pressurizing, and airflow patterns among others. Based on their results they suggested some design specifications for operating theatres in order to remove contaminants effectively and avoid cross-contamination. The suggestions included filtering of the supply air in order to remove bacteria, pressurizing of the operating theatre to avoid contaminated air from adjacent rooms leaking in, and installation of doors between the operating theatre and adjacent rooms.

In the 1980s the focus of operating theatre design shifted towards ultra clean air ventilation (UCV) systems, as some major studies found that these systems could significantly reduce the number of airborne bacteria in an operating theatre (Whyte, Hodgson and Tinkler, 1982) and also reduce the risk of developing deep sepsis (Lidwell *et al.*, 1982), compared to conventionally ventilated theatres. However, recent studies have indicated that the basis for this focus may have been wrong. In 2017 Bischoff *et al.* (2017) concluded that ultra clean ventilation does not hold an advantage regarding SSIs compared to conventional ventilation, while another study found that the supposed correlation between LAF and lower rates of SSIs is uncertain and that recent studies actually suggests LAF be linked to higher rates (Mchugh, Hill, and Humphreys, 2005).

2.1.2 Mixing ventilation

Mixing ventilation is often referred to as conventional ventilation as far as ventilation of operating theatres is concerned. The principle is that air at high velocity is supplied to the room by air jets in order to stir the air in the entire room (Nilsson, 2003). A sketch of an operating theatre with a mixing system is shown in Figure 2.1. The movement of the air volume causes near uniform distribution of both temperature and contaminants in the room air, and increasing the ventilation rates leads to lower concentration of contaminants (Zoon, Loomans, and Hensen, 2011). As the supply velocity is quite high is it common to locate the supply device outside the occupancy zone, often in the ceiling (Nilsson, 2003). Due to the nearly uniform distribution of contaminants the exhaust devices may be placed arbitrarily (ibid.).
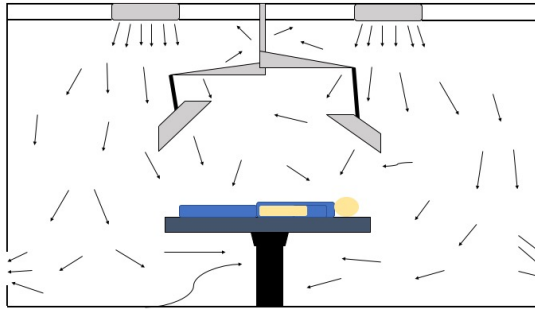
Figure 2.1: Principle of mixing system in an operating theatre

2.1.3   Laminar airflow

A system with laminar airflow is based on the principle of a piston flow, where the air is moving like a piston from the roof to the floor, floor to the roof or from a wall to the opposite side. In a laminar system the air is supplied from a large inlet area, with a uniform velocity distribution across the entire area (Nilsson, 2003). The supply velocity is unidirectional and must be high enough to overpower any convective airflow, and this causes a laminar system to require high airflow rates in order to keep the flow stable (ibid.). The air is diffused through a fine-meshed HEPA filter in order to remove 99.97 % of bacteria-carrying particles (BCP) in the size range of 5 to 60 μm, and bacteria itself with a size range of 1 to 2 μm (Friberg, 1998). A combination of laminar airflow and HEPA filters has been defined as an ultra clean air system (ibid.). The design of a laminar system often includes walls enclosing the supply area, as to prevent mixing of clean air and older, contaminated air (Friberg, Friberg and Burman, 1996). Figure 2.2 shows a sketch of a vertical laminar system.
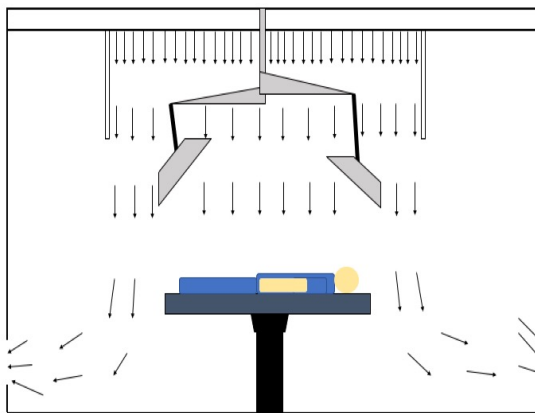
Figure 2.2: Principle of a vertical laminar system in an operating theatre

2.2 Comparison of laminar airflow and mixing systems in operating theatres

The performance and efficiency of LAF and mixing systems in operating theatres are often investigated in terms of the number of bacteria carrying particles in the room air or the number of particles that hits certain surfaces. The unit colony forming units (CFU) per cubic meter of air is frequently used when evaluating the cleanliness of the air. The Norwegian guidelines for operating theatres state threshold values for this measure, depending on the ventilation system of the operating room. Multiple studies have investigated they way in which different factors affect the efficiency of the two different ventilation systems, and Table 2.1 summarizes the findings. Unfortunately, studies on some of the factors and their influence were not found, with the majority of these concerning the mixing system. These fields have therefore been left blank in the table and should be investigated in the future.

Table 2.1: Comparison of mixing and laminar airflow ventilation

Factor	Mixing	LAF
Postion of the operating table and the surgical team		Significant (Department of Health, 2007).
Positioning of the surgical lamps		Significant (Aganovic *et al.*, 2017; Brohus, Balling and Jeppesen, 2006; Chow and Yang, 2005; Sadrizadeh, Holmberg and Tammelin, 2014). Crucial to the airflow distribution close to the patient, obstructs the airflow.
Number of personnel in the OT		Disputed. Rezapoor *et al.* (2018) and Sadrizadeh *et al.* (2014) found it to be significant, while Alsved *et al.* (2018) and Smith *et al.* (2013) did not.
Surgery staff clothing system	Significant (Tammelin, Ljungqvist and Reinmüller, 2012). Vital importance to staff source strength.	Significant (Sadrizadeh and Holmberg, 2014). Vital importance to staff source strength.
Door discipline	Disputed. Alsved *et al.* (2018) reported no correlation between the number of door openings and concentration of CFU, while Scaltriti *et al.* (2007) found the number of openings to be positively correlated to the number of bacteria in the OT.	Disputed. Alsved *et al.* (2018) and Erichsen Andersson *et al.* (2014) reported no significant effect, while Agodi *et al.* (2015) and Smith *et al.* (2013) stated that the contamination rate increases with the number of door openings.
Movement in the periphery area		Significant (Brohus, Balling and Jeppesen, 2006). Can cause transportation of bacteria to the sterile zone.
Posture of the surgical staff close to the patient		Significant (Chow and Yang, 2012; Sadrizadeh and Holmberg, 2014; Sadrizadeh, Holmberg and Tammelin, 2014). Causes formation of eddies and obstructs the airflow, which can elevate levels of BCP.

2.3 Norwegian standards and regulations for operating theatre ventilation

As different surgical procedures have different requirements in terms of the indoor environment, standards and guidelines regarding ventilation of operating theatres often provide ranges for the regulated parameters, rather than specific values. Standards and guidelines often provide recommendations for: supply air temperature, the number of air changes per hour (ACH) in the room, relative humidity, and supply air velocity. In a comparative review of European operating room ventilation standards, by Nastase *et al.* (Nastase *et al.*, 2016), the authors found that the national standards vary significantly. Requirements for general and ultra clean operating theatres in Norway (Aune, 2015) are listed in Table 2.2. The two categories of operating theatres also have different requirements in terms of air quality, which concerns the number of colony forming units per cubic meter of air. The Norwegian Board of Health Supervision (Andrew, Myhr and Skulberg, 1997) state that ultra clean and general operating theatres should keep the number of airborne microbes beneath 100 and 10 CFU/m^3, respectively. As can be seen in Table 2.2, the two types of OTs have similar requirements in every aspect, except airflow.

Table 2.2: Requirements for operating theatres in Norway

	Airflow	Pressure	Filtration	Supply location	Exhaust location
General (Mixing system)	20 ACH	Positive (5-10 Pa)	HEPA 14	Ceiling	2/3 at low level, 1/3 at ceiling
Ultra clean	Air velocity of 0.25-0.28 m/s	Positive (5-10 Pa)	HEPA 14	Ceiling	2/3 at low level, 1/3 at ceiling

The author has been unable to find Norwegian requirements for neither the relative humidity, nor the air temperature. Thus, the recommended range of 20-60 % relative humidity from the ASHRAE Standard 170 *Addendum d* (2011, cited in Rousseau, 2011) has been assumed. As for the air temperature, a recommended design air temperature range of 18-24°C is stated in both the Dutch recommendations C.b.z (2004, cited in Nastase *et al.*, 2016) and the German D.D.G.f (2002, cited in Nastase *et al.*, 2016), and is therefore considered a suitable range, with the caveat that the author considers it outside the scope of the scope of this thesis to explore the justification for this recommendation.

2.4 Turbulence intensity

Bailly and Comte-Bellot (2015) define a turbulent flow as flow characterized by arbitrary and unpredictable behavior. Eddies forming in a turbulent flow will cause variations in the velocity, meaning that the velocity at any time will be the sum of the mean and the turbulent component. Turbulence intensity is defined as the ratio between the root mean

square of the velocity fluctuations due to turbulence, and the local mean velocity (ibid.), and is often expressed in terms of %. Turbulence causes mixing of air and thus increases particle dispersion (Buchanan and Dunn-Rankin, 1998). As a result, the levels of turbulence intensity should be of interest in an operating theatre, but no standard or guideline describing what is considered a low, medium or high level was found. However, in a study by Karthikeyan and Samuel (2008), the authors refer to a turbulence intensity of 12.5 % as a high level.

2.5 Wound microenvironment and wound healing

One can distinguish between the internal and external wound microenvironment when considering a wound and its healing process. According to Kruse *et al.* (2015), the external microenvironment is the outer part of the wound, which borders to the wound surface. Parameters in the external microenvironment that affect the wound healing are temperature, pressure, the presence of certain gases, microbes, hydration and pH (ibid.). The wound temperature is dependent on both the blood flow and the ambient air temperature, and an increase in wound temperature is associated with vasodilatation (ibid.). Vasodilatation is the phenomenon of widened blood vessels (Arnesen, 2018), and it increases the transport of nutrients and oxygen to the wound (Kruse *et al.*, 2015), thus enhancing the healing process (Harper, Young and McNaught, 2014). Heat loss due to evaporation may lower the wound temperature. The velocity of the ambient air and the turbulence intensity both affect the convective heat loss of the wound (Murakami, Kato and Zeng, 1997).

The human skin acts as a vapor barrier, due to its low permeability, and therefore reduces the loss of fluid through evaporation (Scalise *et al.*, 2015). Following a traumatic injury or during a surgical procedure, the barrier effect is reduced locally and the evaporative loss of fluids increased (Kruse *et al.*, 2015), potentially causing the wound to dry. This is unfortunate, as studies by Scalise *et al.* (2015) and Vranckx *et al.* (2002) state that a wet or moist wound microenvironment enhances the wound healing process.

Chapter 3

Thermal plume of a human in a supine position

The chapter presents the requisite theory for the development of a mathematical model for the thermal plume of a human in a supine position.

3.1 Thermal plumes

A person in a supine position will experience heat transfer through several mechanisms: convection to the surrounding air, radiation to the surrounding surfaces, conduction to the solid materials in direct contact with the body, evaporation from the skin, and respiration. Heat loss caused by convection is the result of a temperature gradient between the skin and the surrounding air, as the surface temperature of a human exceeds the air temperature under normal conditions. The temperature difference induces a buoyancy-driven airflow, as heated air close to the skin will rise due to reduced density, and a thermal plume is formed (Goodfellow and Tähti, 2001). The formation of the plume and the amount of air entrained in the plume depend on several factors. Kondrashov, Sboev, and Dunaev (2016) point to the geometry and shape of the heat source, as well as the surface temperature, as essential factors for the formation and generation of a boundary layer. Zukowska, Popiolek, and Melikov (2010) claim that the surface temperature, geometry of shape and surface area of the heat source are important to the generation of the plume, while Goodfellow and Tähti (2001) state that the power and geometry of the heat source, as well as the temperature of the surrounding air, determine the amount of air entrained by the plume.

Zukowska, Popiolek, and Melikov (2010) divide a thermal plume into three main regions. The first one, known as the initial region, is the region closest to the heat source. It starts off as the convective boundary layer around the source before it transforms into a turbulent flow, and the plume develops (ibid.). The second region is known as the region of self-similarity of mean motion, and the plume in this region is characterized by turbu-

lent flow and axis-symmetry (ibid.). Also, both the velocity and temperature distribution have Gaussian profiles. As the plume develops more air is entrained and the maximum velocity gradually reduced. The third region depends on whether the plume develops in an environment with or without stratification. If there is no stratification will the plume spread linearly, while if there is will the plume reach its maximum height and spread out horizontally as a stratified layer (ibid.).

The thermal plume is elusive and sensitive to changes and may be subject to the phenomenon of plume axis wandering (Zukowska, Popiolek, and Melikov, 2010). The plume axis "wanders" off, and the vertical position changes from the one directly above the heat source. Zukowska, Popiolek, and Melikov (2010) claim it is caused by major fluctuations in the plume, which could originate from variations in the surrounding conditions, unstable flow in the convective boundary layer, or the heat source itself. The outcome of plume axis wandering could be increased scattering of obtained measurement results.

3.2   Convective heat output from a human

The convective heat output is an essential factor in order to predict how the thermal plume will develop and behave. The general equation for the convective heat output is presented in Equation 3.1

$$\dot{Q}_k = h_c * A_c * (T_s - T_0) \tag{3.1}$$

where $\dot{Q}_k$ is the convective heat output in W, h_c is the convective heat transfer coefficient in W/m^2*K, A_c is the convective surface area in m^2, T_s the surface temperature and T_0 the temperature of the surrounding fluid (Incropera *et al.*, 2013), the last two expressed in terms of K. The convective heat transfer coefficient, h_c, for a human was in a study by Kurazumi *et al.* (2008a) found to vary with body posture for natural convection. In the mentioned study the authors performed measurements in order to determine h_c for a person in a supine position. The authors suggest the following equation (Kurazumi *et al.*, 2008a)

$$h_c = 0.881 * \Delta T^{0.368} \tag{3.2}$$

where ΔT is the difference between the air temperature and the mean skin temperature, the latter corrected using convective heat transfer area (ibid.). The convective heat transfer area correction in Equation 3.2 is based on a convective heat transfer area ratio of 0.844, suggested by Kurazumi *et al.* in a study from 2004 (Kurazumi *et al.*, 2004). In the studies by Kurazumi *et al.* (2004) and by Kurazumi *et al.* (2008a) were the test subjects lying flat on the floor during the experiments for a person in the supine position.

The convective heat transfer area, A_c, in Equation 3.1 does also have to be determined as the convective heat transfer does not occur over the entire body surface when a person is in a supine position (Kurazumi *et al.*, 2004). Kurazumi has investigated the convective heat transfer area ratio in several studies and in a study from 2008 the authors found the

ratio to be 0.811 (Kurazumi *et al.*, 2008b). The formula for the convective heat transfer area is therefore as presented in Equation 3.3.

$$A_c = 0.811 * A \tag{3.3}$$

The body surface area, A, in Equation 3.3 must also be determined in order to calculate the convective heat output. In their study from 2010 proposed Yu, Lin and Yang (2010) a formula for the body surface area based on the weight and height. They developed the equation from a sample consisting of 270 human subjects, and in a test of accuracy demonstrated their equation a smaller estimation error than that of the widely used DuBois and DuBois formula (Yu, Lin and Yang, 2010). The equation by Yu, Lin and Yang is presented in Equation 3.4, where H is the height in cm, W the weight in kg, and A the body surface area in m^2.

$$A = 0.00713989 * H^{0.7437} * W^{0.4040} \tag{3.4}$$

The equations 3.1, 3.2, 3.3 and 3.4 were used during the analysis of the results of this thesis.

3.3 Mathematical models for thermal plumes

Eimund Skåret did in "Ventilasjonsteknisk Håndbok" from 2000 derive equations for thermal plume development. They are based on the assumption of quiescent surroundings with uniform air temperature (Skåret, 2000). The equations will be used during the analysis of the results from the experiments in the climate chamber at Gløshaugen.

Skåret (2000) suggested the formula given in Equation 3.5 for the centerline velocity above a point source. In the derivation of the point source equation, Skåret assumed axisymmetric flow (Skåret, 2000). The nomenclature is explained in Table 3.1.

$$U_m = \frac{1.63}{C_b^{2/3}} * \left(\frac{g\beta}{\rho c_p}\right)^{1/3} * \left(\frac{\dot{Q}_k}{z + z_0}\right)^{1/3} \tag{3.5}$$

Parameter	Description	Unit
U_m	Centerline velocity	m/s
C_b	Proportionality factor. Equal to the tangent of the spread angle α	-
g	Gravitational acceleration	m/s^2
β	Volumetric thermal expansion coefficient	1/K
ρ	Fluid density	kg/m^3
c_p	Specific heat capacity	kJ/kgK
$\dot{Q}_k$	Convective heat ouput	kW
z	Vertical distance from origin	m
z_0	Vertical distance from source to virtual origin	m

The value of 1.63 is based on the geometry of a point source. Skåret (2000) also suggested a formula for the centerline velocity above a line source. During the derivation of the equation, Skåret assumed plan symmetrical flow. The formula is presented in Equation 3.6.

$$U_m = \frac{1.37}{C_b^{1/3}} * \left(\frac{g\beta}{\rho c_p}\right)^{1/3} * \dot{Q}_k^{\,1/3} \tag{3.6}$$

Skåret (2000) states that the boundary lines of a convective flow are straight lines, as they are for normal jets, and therefore suggests a proportionality factor C_b equal to 0.235. When this value is applied in the Equation 3.5 and Equation 3.6 they turn into the following equations:

Point source

$$U_m = 4.27 * \left(\frac{g\beta}{\rho c_p}\right)^{1/3} * \left(\frac{\dot{Q}_k}{z + z_0}\right)^{1/3} \tag{3.7}$$

Line source

$$U_m = 2.22 * \left(\frac{g\beta}{\rho c_p}\right)^{1/3} * \dot{Q}_k^{\,1/3} \tag{3.8}$$

Some of the parameters in Table 3.1 are tabulated, and Skåret (2000) suggested values for them under regular temperatures. These values are presented in Table 3.2 and are in accordance with the values found in tables from Incropera *et al.* (2013).

Table 3.2: Parameter values under regular temperatures

Parameter	Value
ρ	1.2 kg/m^3
β	$1/300$ 1/K
c_p	1 kJ/kgK
g	9.81 m/s^2

3.3.1 Distance to the virtual origin z_0

A convective flow from a horizontal surface is significantly harder to evaluate than a flow from a point or line source, due to unstable behavior and because the air leaves different surface positions at different times (Goodfellow and Tähti, 2001). As a result are most of these surfaces treated as extended surfaces, where their centerline velocities and flow rates are calculated from a virtual source (ibid.). The virtual origin is located at the opposite side of the real surface along the plume axis, as illustrated in Figure 3.1, at a distance z_0 from the surface.
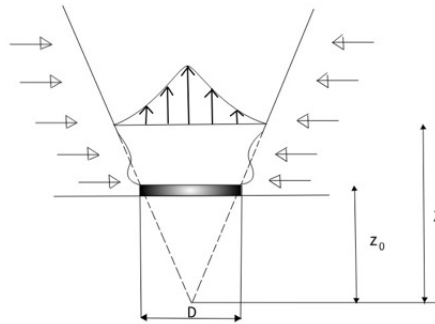
Figure 3.1: Extended surface and virtual origin

Formulas for the calculation of z_0 have been proposed by various researchers. Skåret (2000) stated that in practice will z_0 be in the range of 0-0.5 times the diameter of the source, while Goodfellow and Tähti (2001) suggested Equation 3.9 for a virtual source below a flat plate.

$$z_0 = 1.47 - 2.25 * D \qquad (3.9)$$

Morton, Taylor and Turner (1956, as cited in Goodfellow and Tähti 2001) suggested Equation 3.10 for the position of the virtual origin below a real source.

$$z_0 = 1.7 - 2.1 * D \qquad (3.10)$$

It was decided to use Equation 3.9 proposed by Goodfellow and Tähti during the comparison of theoretical and experimental values.

3.3.2 The proportionality factor C_b

The location of the virtual origin has a major impact on the spread angle, α, of a heat source. The distance from the plume axis to the plume boundary is often denoted as b, and it increases with increasing height above the heat source, z, as can be seen from Figure 3.1. The plume boundary b can be found experimentally through velocity measurements, and based on this may linear regression be utilized in order to find an expression for the plume boundary b. The linear expression will have the form presented in Equation 3.11.

$$b(z) = az + c \tag{3.11}$$

The a in Equation 3.11 may then be used to find the spread angle, α, of the heat source, and the proportionality constant can be calculated from the spread angle. The two relations are presented in Equation 3.12 and Equation 3.13.

$$\alpha = arctan\left(\frac{1}{a}\right) \tag{3.12}$$

$$C_b = tan(\alpha) \tag{3.13}$$

3.4 Models of the thermal plume from a human in supine position

Human thermal plumes are extremely individual as plumes depend heavily on biological factors like skin surface temperature and body geometry, for instance. Several studies have investigated the thermal plume of a human, with most studies focusing on a human in sitting or standing position. There is, however, a lack of studies investigating the thermal plume of human in a supine position, and the author was able to find only one study focusing on the plume centerline velocity. Storås (2017) performed measurements above a thermal manikin and proposed Equation 3.14 for the whole body as a line source, based on an experimentally determined proportionality factor of 0.286.

$$U_m = 2.08 * \left(\frac{g\beta}{\rho c_p}\right)^{1/3} * \dot{Q}_k^{1/3} \tag{3.14}$$

In the same thesis did Storås (2017) also propose two equations for the plume centerline velocity above the stomach of the manikin, while modeling the stomach as a point source. The first, Equation 3.15, was based on finding the proportionality constant, while the second one, Equation 3.16, was based on the assumption of a Gaussian distributed velocity profile.

$$U_m = 3.31 * \left(\frac{g\beta}{\rho c_p}\right)^{1/3} * \left(\frac{\dot{Q}_k}{z + z_0}\right)^{1/3} \tag{3.15}$$

$$U_m = 3.39 * \left(\frac{g\beta}{\rho c_p}\right)^{1/3} * \left(\frac{\dot{Q}_k}{z + z_0}\right)^{1/3} \tag{3.16}$$

Experimental setup

The chapter will describe the setup for the experiments performed both at St. Olavs hospital and the climate chamber at Gløshaugen, NTNU. It contains descriptions of the setup for each case, assessment of the instrumentation and information about the thermal manikin.

4.1 Case 1: Study of the thermal plume above a thermal manikin and real human beings

The first case was carried out in the climate chamber at Gløshaugen, NTNU. The room offers the possibility to turn off the ventilation system, making it possible to study the thermal plume of the thermal manikin and real human beings without disturbances caused by the ventilation system. It has a rectangular shape with a floor area of 9.2 m^2 and a height of 3.15 m, with a door of 1.77 m^2 as the single entry point. The door remained closed during the recordings. Figure 4.1 provides a sketch of the room.
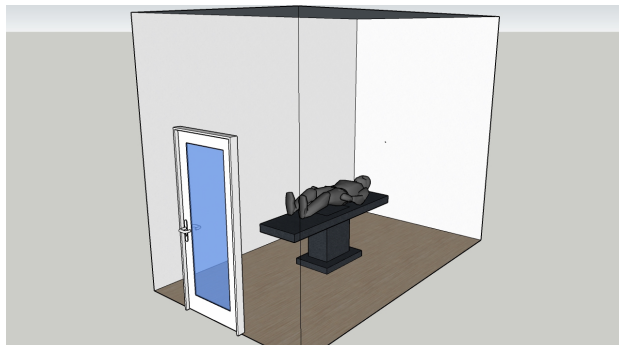
Figure 4.1: The climate chamber

The room features neither a cooling nor heating system, leaving ventilation through

the opening of the door as the only option for temperature control when the ventilation system in the room is turned off.

The objective of this case was to study the thermal plumes above real human beings in quiescent surroundings and to use the findings to adjust the thermal manikin so that its thermal plume resembled the one of a real human.

4.1.1 Thermal manikins

Thermal manikins have been used for over 70 years, with the first one being developed for the US army in the early 1940s (Holmèr, 2004). Their two main areas of application are the evaluation of the thermal insulation of clothing and the assessment of how a human body acts in various thermal environments (Foda and Sirèn, 2012). There are three main control modes for thermal manikins (ibid.): Constant Skin Surface Temperature, Constant Heat Flux, and Comfort Equation mode, commonly abbreviated CST, CHF, and CE, respectively. The most frequently used mode is the CST, which utilizes feedback control in order to maintain a specific skin surface temperature.

Advantages related to the use of thermal manikins are among others their ability to simulate local heat fluxes in three dimensions and to provide a fast and easy way for simulation in general. Another benefit from the use of manikins is that the method is both repeatable and possible to standardize (Holmèr, 2004).

4.1.2 The thermal manikin for the experiments

A male manikin was used during the experiments. The manikin is 190 cm tall and in standing position. The model is called Clark 4WI (white), produced by Morten Finckenhagen Butikkinnredninger AS and made out of fiberglass. As the manikin resembles a person with a standing posture is the left knee slightly bent, making it a protruding part.

Storås (2017) did in her master thesis use the same manikin as the one used in these experiments. She measured the surface area of each body part based on the assumption of a total body surface area of 1.98 m^2, where the total area was calculated by using the DuBois and DuBois formula. Table 4.1 provides an overview of the body parts and their surface area as measured by Storås (2017).

Table 4.1: The thermal manikin's body parts and their surface area

	Name of body part	Area [m^2]
1	Left foot	0.05
2	Right foot	0.05
3	Left leg	0.15
4	Right leg	0.15
5	Left thigh	0.23
6	Right thigh	0.23
7	Crotch	0.18
8	Head	0.11
9	Left hand	0.045
10	Right hand	0.045
11	Left arm	0.07
12	Right arm	0.07
13	Left shoulder	0.08
14	Right shoulder	0.08
15	Chest	0.22
16	Back	0.22
In total		1.98

The manikin is hollow and fitted with heating cable on the inside to achieve the wanted heat output. The cable has a heat output of 20 W/m, and the way it is wrapped is shown in Figure 4.2. The amount of heating cable in each body part is based on the ratio between the area of the body part and the total surface area. Unfortunately, the structure of the manikin makes it impossible to install heating cable in the hands and feet, and thus they can only reach the temperature of the surroundings.
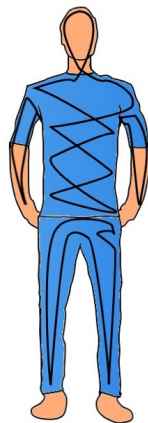
Figure 4.2: Heating cable placement inside the manikin

The manikin was representing a person in a supine position during the experiments and the metabolic rate was therefore assumed to equal 0.8 MET (Novakovic *et al.*, 2014). A metabolic rate of 1.0 MET is defined as a power production of 58.15 W/m^2 for a human (ibid.). Along with the total surface area were these numbers used to calculate the total heat output:

$$1.98m^2 * 58.15W/m^2 * 0.8 = 92.11W \qquad (4.1)$$

However, the manikin was designed for a heat output of 230 W, which means that it was oversized for this experiment. This made the surface temperature and heat output control challenging. The control strategy of the thermal manikin combined two of the strategies presented in chapter 2.5, as both the power supply and surface temperature was controlled. Temperature sensors are installed on the inside of the manikin in the arms, legs, and head and upper body, meaning that temperature control is divided into three regions. The three set point temperatures can be adjusted through a control panel, and the heating system is active until the setpoint temperature of each circuit is reached. Whenever one of the temperatures drop below the setpoint value is the heating system reactivated in the relevant circuit. Since the temperature is measured on the inside of the manikin, the thermo detector Bosch PTD 1 was regularly used in order to check the surface temperatures. The heating cable inside the manikin is not uniformly installed, causing significant variations in the skin surface temperature. This was noticeable in the forehead, where the temperature was relatively low, and in the left leg, where the temperature was higher than average.

The surface temperature of the manikin is essential to the development of the thermal plume and should be frequently controlled. According to Hanssen (1991, as cited in Novakovic *et al.* 2014) does the skin temperature for a real human vary between 32 and 34 °C under normal conditions, so in principle is that the desired range of temperature.

An energy meter was connected to the power cable of the manikin, making it possible to monitor the power supply. It was noted that the power supply experienced large variations, with a maximum value of 205 W and a minimum of 0 W. The maximum value appeared infrequently, and besides the initial heating, were high values observed only for short periods of time. It was also noted that the heating had a cyclical tendency, with short periods of high power being followed by longer periods of low power. The vast majority of the readings were below 92.11 W.

The thermal manikin was dressed in light clothing corresponding to an insulation level of 0.5 clo (Novakovic *et al.*, 2014).

4.1.3   Human subjects

In order to calibrate the thermal plume of the manikin were measurements above real humans performed. Since the manikin is a male, it was decided to only make use of male human subjects. Five healthy males participated and Table 4.2 provides an overview of some relevant participant data. The human subjects were dressed in the same clothing as the thermal manikin, with an insulation level of 0.5 clo.

Table 4.2: Participant data for case 1

	Range	Average
Age	23-39	27.8
Height [cm]	170-194	182.2
Weight [kg]	60-92	74.4

Contact with the Norwegian Centre for Research Data

As the measurements in this case involved real humans and collection of personal information, was the Norwegian Centre for Research Data, NSD, contacted. According to their guidelines was a Notification Form submitted, describing the project and how the privacy of the human participants would be protected. NSD carried out an assessment of the project and sent a reply describing which measures should be taken. The assessment from NSD is placed in the appendices.

4.1.4 Setup

The human subjects were laying down at the operating table while measurements were performed above them. The operating table consists of three rectangles. The first one, supposed to be at head height, is 28x23.5 cm. The middle one is 68x60 cm, and the one at the bottom 94x48 cm. Together they form an operating table which is 190 cm long. The table surface height is 70 cm above floor level. The temperature of the room increased during the measurements, as both real human beings and the thermal manikin emit heat. The door had to be opened between each measurement in order to move and adjust the sensors, and this provided a cooling effect. The door openings along with the heat emission from the experiment subjects caused a fluctuating temperature, and the room air temperature during the experiment was kept in the range of $23\pm0.5°C$. The ventilation system of the room was turned off during the experiment and the background velocity was measured to between 0.01 and 0.02 m/s by using the handheld anemometer TSI 962.

4.1.5 Measurement points

The measurements were performed at five cross-sections above the supine body. The cross-sections were located above the knees, the pelvis, the waist, the chest and the forehead, and were chosen to investigate the airflow above anatomical different locations. They are shown in Figure 4.3. At each cross-section were measurements performed at three heights; 5, 15 and 25 cm above the skin of the location. This approach was chosen as the geometry of a human body is complex and uneven, and thus locally fixed coordinate systems give airflow data at comparable heights.
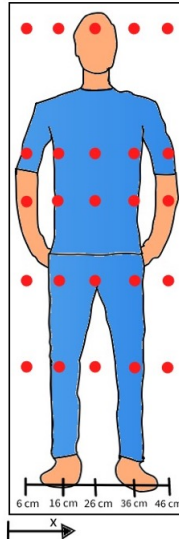
Figure 4.3: Measurement points case 1

4.2 Case 2: Experiment with a thermal manikin in an operating theatre with LAF

The second experiment took place in "Operasjonsstue 8" at "Bevegelsessenteret" at St. Olavs Hospital in Trondheim. The operating room has a vertical LAF ventilation system with a ceiling diffuser of 11.56 m^2, and the diffuser area is encircled by 110 cm long glass walls stretching towards the floor. There are two exhaust outlets mounted at the wall close to floor level, both with an area of 0.1917 m^2. The OR has an area of 56.58 m^2 and a ceiling height of three meters and is connected to an adjacent corridor through a door with an area of 3 m^2. The door remained closed during the recordings.

During surgery is the ventilation system set at full speed. The temperature control of the OT is based on temperature sensors in the exhaust ducts. Due to electrical equipment and metabolic heat production by the people in the OT is the supply air temperature somewhat lower than the setpoint temperature. During the experiments, the supply air temperature was measured to be 20±1°C. The relative humidity of the air in the OR is monitored at a display in the room and was observed to range from 8-29 % during the experiment.

The objective of this case was to control the state of the ventilation system in the OT and to study the airflow distribution above the patient. The latter includes the interaction of the laminar supply airflow and the convective airflows generated by the surgical staff, as well as the influence of surgical lights.

4.2.1 Scenarios and setup

Four different scenarios were considered for this case and Table 4.3 provides an overview of them.

Table 4.3: Scenarios in OT with LAF

Scenario	Description
1	Empty operating table
2	Only patient
3	Patient and surgical staff
4	Patient, surgical staff and surgical light

Prior to the experiment was the OT prepared as for a real surgical procedure. The operating table was set in the middle of the sterile zone, and other tables and equipment were removed from the zone. The height of the table was set to 90 cm. The patient was in each scenario represented by the thermal manikin previously described. The setpoint temperature of the theatre was set to $22.0°C$ in all of the scenarios, and the ventilation system set at full speed.

As the objective of this case was to control the OT ventilation system and to investigate the airflow distribution above the patient, the patient featured in scenario 2, 3 and 4, while a new element was introduced in each of the scenarios.

Observation of a real operation

In order to get a better understanding of the movement and positioning of the surgical staff, was the author invited to observe a real operation in "Operasjonsstue 8" at "Bevegelsessen-teret" at St. Olavs Hospital. The surgical procedure was a knee replacement. There were three persons in the sterile zone during the procedure: One surgical nurse at the foot end of the operating table, and two surgeons positioned at each side of the middle of the table. Also, there were two nurses in the operating theatre who remained outside the sterile zone. The surgical lamps were positioned above the foot and head end of the operating table, as can be seen in Figure 4.4, with the light focused on the middle of the table.
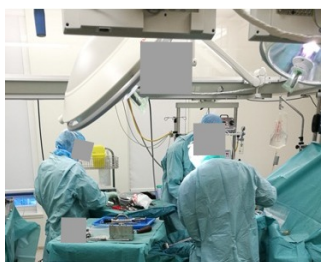
Figure 4.4: Picture from a real operation

Scenario 1: Empty operating table

In the first scenario was the objective to control the state of the OR ventilation system. Hence there were only an empty operating table in the sterile zone. Measurements above the empty operating table were conducted, and the results obtained in this scenario will serve as references for the other scenarios. A sketch of the setup can be seen in Figure 4.5.
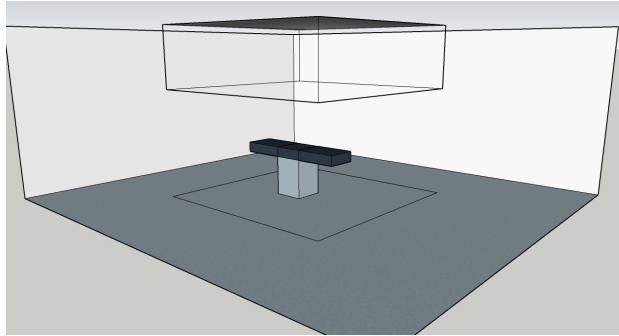
Figure 4.5: Sketch of scenario 1

Scenario 2: Only patient

Scenario 2 includes the patient in a supine position. The main objective of this master thesis is to characterize the airflow distribution close to the patient, hence is the patient now kept constant while additional elements are introduced. The manikin is positioned so that the heels are 14 cm from the short end of the operating table. The objective of this scenario is to study the interaction between the plume generated by the patient, and the laminar supply airflow. Figure 4.6 shows a sketch of the setup.
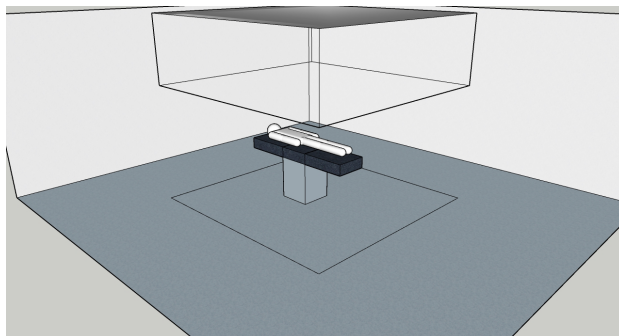
Figure 4.6: Sketch of scenario 2

Scenario 3: Patient and surgical staff

Scenario 3 includes the patient and the surgical staff, and the setup is illustrated in Figure 4.7. The staff is meant to represent two surgeons, standing at opposite sides of the operating table, and one nurse positioned at the foot end of the operating table. The staff and their presence are being simulated by cylinders containing light bulbs. Simulation of surgery staff by the use of geometrical shapes with a certain convective heat loss has been done in previous studies (Chow and Yang, 2005; Chow and Wang, 2012), and was therefore chosen for this thesis. Each cylinder is 140 cm tall, and have a diameter of 40 cm. In order to simulate the convective heat loss from the staff were light bulbs placed inside the cylinders, each bulb with a power of 100 W. As the convective heat loss from a person is dependent on several factors like skin surface temperature, level of activity and temperature of the surrounding air among others, is this a rough estimate. However, 100 W has been used in previous studies (Memarzadeh and Manning, 2002; Chow and Yang, 2005; Chow, Lin and Bai, 2006; Chow and Wang, 2012) and was hence chosen. The objective of this scenario is to study the influence of the surgical staff's thermal plumes on the airflow distribution above the patient.
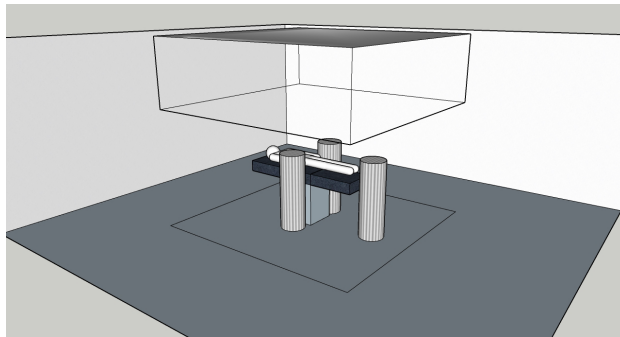
Figure 4.7: Sketch of scenario 3

Scenario 4: Patient, surgical staff and surgical lights

Scenario 4 includes the patient, the surgical staff, and surgical lights, and a sketch of the setup is shown in Figure 4.8. The two lamps both have a hemispherical shape and diameters of 60 and 85 cm respectively. Also, both feature halogen bulbs with filters preventing heat dissipation on the operating field and color temperatures of 4300 K. They are positioned directly above each short end of the operating table, focusing their light towards the lower abdomen of the patient. The largest lamp is positioned above the foot end, while the smaller one is above the head of the patient. Both lamp centers are 210 cm above floor level. The objective of this scenario is to study the influence of the surgical lamps on the airflow distribution above the patient. Figure 4.9 shows photos of each of the four scenarios.
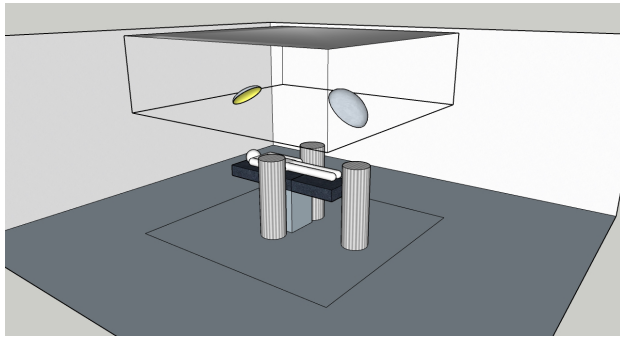
Figure 4.8: Sketch of scenario 4

(a) Scenario 1

(b) Scenario 2

(c) Scenario 3

(d) Scenario 4

Figure 4.9: Photos from the scenarios

4.2.2 Measurement points

The measurements were performed at the same five cross-sections as in Case 1, shown in Figure 4.3. At each cross-section were measurements performed at six heights; 5, 10, 15, 20, 25 and 30 cm above the surface of the location.

4.3 Case 3: Experiment with a thermal manikin in an operating theatre with a mixing system

The third experiment was conducted in "AHL 2" at "AHL-senteret" at St. Olavs Hospital in Trondheim. The operating theatre is equipped with a mixing ventilation system, with four ceiling-mounted diffusers. They are symmetrically positioned, one in each quadrant of the ceiling. As for the exhaust, there are two wall-mounted exhaust outlets and one close to the ceiling. The OT has an area of 59.7 m^2 and a ceiling height of 2.90 m. It is connected to an adjacent corridor through a door, and the door remained closed during the recordings. As opposed to the operating theatre in case 2, was the operating table of "AHL 2" mounted rigidly.

The ventilation system is set at full speed during surgery, and the temperature of the theatre is regulated by the temperature of the extract air.

4.3.1 Scenarios and setup

The same four scenarios were considered for Case 2 and 3 and the scenario objectives were the same, thus will the scenario descriptions in this section be brief. Table 4.4 provides an overview of scenarios.

Table 4.4: Scenarios in OT with mixing system

Scenario	Description
1	Empty operating table
2	Only patient
3	Patient and surgical staff
4	Patient, surgical staff and surgical light

Prior to the experiment was the OT prepared as for a real surgical procedure. The set-point temperature of the theatre was 22.0°C in all of the scenarios, the ventilation system to full speed, and the height of the operating table set to 90 cm above floor level. The patient was represented by the previously described manikin.

As the objective of this case was to control the OT ventilation system and to investigate the airflow distribution above the patient, the patient featured in scenario 2, 3 and 4, while a new element was introduced in each of the scenarios.

Scenario 1: Empty operating table

Measurements above an empty operating table were conducted in order to control the state of the ventilation system. As can be seen in Figure 4.10 were there some equipment and installations in the background. The equipment was either turned off or not possible to move.

Figure 4.10: Setup scenario 1

Scenario 2: Only patient

Scenario 2 includes a patient in supine position. The manikin is positioned so that the heels are 14 cm from the short end of the operating table. Figure 4.11 provides a picture of the setup.

Figure 4.11: Setup scenario 2

Scenario 3: Patient and surgical staff

Scenario 3 includes the patient and surgical staff, and a picture of the setup can be seen in Figure 4.12. The staff was represented by three cylinders of 140 cm height and 40 cm

diameter, and they each had their own light-bulb of 100 W. They were positioned the same way as in Scenario 3 in case 2, with one cylinder at the foot of the table and one cylinder at each of the long sides.

Figure 4.12: Setup scenario 3

Scenario 4: Patient, surgical staff and surgical lights

Scenario 4 includes the patient, the surgical staff, and surgical lights, and the setup is shown in Figure 4.13. The two lamp models are marLED V10 and marLED V16, both produced by KLS Martin Group. Both have a rectangular shape, and marLED V10 has concave long sides while marLED V16 has convex long sides. marLED V10 has a light head dimension of approximately 64x46 cm and marLED V16 a dimension of 87x64 cm (KLS Martin Group, 2008). They both use LED, and the color temperature was set to 4300 K for both lamps during the experiment. They are positioned directly above each end of the operating table, focusing their light towards the lower abdomen of the patient. The largest lamp is positioned above the head of the patient, while the smaller one is above the foot end. Both their centers are 210 cm above floor level.
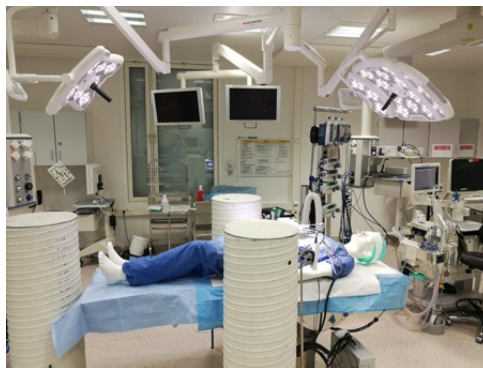
Figure 4.13: Setup scenario 4

4.3.2   Measurement points

The measurements were performed at three cross-sections above the supine body. The cross sections were located above the pelvis, the waist, and the chest, and are shown in Figure 4.14. At each cross-section were measurements performed at six heights; 5, 10, 15, 20, 25 and 30 cm above the skin of the location.
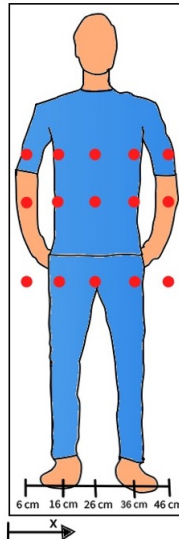
Figure 4.14: Measurement points case 3

4.4   Instrumentation

4.4.1   AirDistSyst 5000

The airflow distribution measurements were in all three cases performed by using the system AirDistSyst 5000 delivered by Sensor Electronic. The system was calibrated in advance, in order to ensure reliable and accurate data. The system consists of five omnidirectional thermoanemometers of the type SensoAnemo5100LSF, a power supply, a wireless transmitter SensoBee485, a computer connected receiver SensoBee USB, and a pressure sensor SensoBar 5301. The pressure sensor is connected to the anemometers in order to correct the recordings according to the barometric pressure. Further on are the anemometers connected in series, and one of them is connected to the transmitter. The transmitter sends the recordings to the receiver, which is connected to the computer through a USB connection. A software from Sensor Electronic has to be used in order to read and log the data. The pressure sensor, the anemometers and the transmitter are all connected by RJ 45 cables. Table 4.5 provides information about the range and accuracy of the anemometers, while Table 4.6 provides data about the pressure sensor.

Table 4.5: Range and accuracy of SensoAnemo5100LSF

	Range	Accuracy
Air speed [m/s]	0.05 to 5.00	$\pm 0.02 \pm 1.5\,\%$
Temperature [°C]	-10 to 50	± 0.2

Table 4.6: Range and accuracy of SensoBar5301

	Range	Accuracy
Pressure [hPa]	500 to 1500	± 3

In the software from Sensor Electronic was the recording time for each measurement row set to three minutes, with values being recorded every two seconds. The software records temperature, air velocity, turbulence intensity and standard deviation for each probe, and based on this were average values calculated for each measurement. It should be noted that the probes measure the magnitude of the velocity vector.

4.4.2 Bosch PTD 1

The thermo detector from Bosch PTD 1 was regularly used to check the surface and ambient temperatures in all of the experiments. Information about the range and accuracy of the detector within the relevant ranges can be found in Table 4.7.

Table 4.7: Range and accuracy of Bosch PTD 1

	Range [°C]	Accuracy [°C]
Surface temperatures	+10 to +30	± 1
Ambient temperatures	-10 to +40	± 1

4.4.3 TSI 962

The handheld thermoanemometer TSI 962 was used to measure the background velocity in Case 1, and information about the range and accuracy can be found in Table 4.8.

Table 4.8: Range and accuracy of TSI 962

	Range [m/s]	Accuracy
Air speed	0 to 50	$\pm 3\,\%$ or ± 0.015 m/s, whichever is greater

5

Chapter

Results

The chapter will present the results obtained from the experiments described in Chapter 4. It is divided into three main sections, one for each case described in Chapter 4. The sections for Case 2 and 3 are further divided into three main parts where velocity, temperature, and turbulence intensity plots are presented, respectively. The contours will be presented for one cross-section at a time, in order to show how the airflow distribution for each cross-section is affected from scenario to scenario. The results will be presented in the same order as the cases were presented in Chapter 4.

It should be noted that all of the recorded data was filtered for values below 0.05 m/s before they were processed further. All of the contours in this chapter were made using the contourf function in MATLAB. It is also important to underline that the anemometers measured the magnitude of the velocity, which means that they actually measured the speed. However, the values will be presented as velocities since that is common jargon within the field.

5.1 Case 1: Study of the thermal plume above a thermal manikin and real human beings

This section will present the results from experiment performed in the climate chamber at Gløshaugen. The results are based on the experimental setup explained in Chapter 4.1.

5.1.1 Measured centerline velocities

The results will be presented as velocity plots with one plot for each of the three heights and in ascending order in terms of height. Based on the measured velocities were the mean value for each human subject calculated, and these values were further used to calculate the mean value and standard deviation for the entire sample. The mean and standard deviation for the centerline velocity were then plotted for each cross section and height,

where the mean values are indicated with blue circles and the standard deviations as blue, vertical lines. As one of the objectives of this case was to calibrate the plume of the thermal manikin against a human thermal plume, were different setpoint temperatures for the thermal manikin tested. In the end were the temperatures in Table 5.1 used.

Table 5.1: Set point temperatures for the thermal manikin

Circuit	T_{set} [°C]
Head and upper body	40.0
Arms	34.0
Legs	34.0

The temperatures in Table 5.1 led to the skin surface temperatures in Table 5.2, which were measured using the thermo detector Bosch PTD 1.

Table 5.2: Measured skin surface temperatures of the thermal manikin

Area	$T_{skin,tm}$ [°C]
Forehead	31.8
Chest	37.0
Waist	36.7
Pelvis	32.0
Knees (average of both)	31.2

Only the centerline velocities will be presented, as the other sensors did not consistently record velocities within the range of the instruments. During the filtration it was observed that none of the recorded centerline velocities 5 cm above the knees of the thermal manikin exceeded or were equal to 0.05 m/s, and as a consequence will not the centerline velocities above the knees be included in this section. Plots including the centerline velocities above the knees for 15 and 25 cm has been put in the appendices.

The sensors used for this experiment were omnidirectional, but the direction of the airflow ca be assumed to be upwards as the dominant air movement in the room is caused by the thermal plume of the test subjects.

5 cm above the surfaces

The measured centerline velocities 5 cm above the surface of the forehead, chest, waist and pelvis are presented in Figure 5.1. The plot demonstrates a rather flat profile where the mean values are quite similar, ranging from about 0.079 to 0.090 m/s. The highest mean is recorded above the forehead and the lowest above the pelvis. The mean above the forehead also shows the largest standard deviation. It can also be observed that the mean value steadily decreases from the forehead to the pelvis.

As can be seen in Figure 5.1 are all of the values from the measurements above the thermal manikin within the range of the mean values plus minus standard deviations. The recorded values above the chest, waist and pelvis are all very close to the mean, while the velocity above the forehead is close to the upper limit.
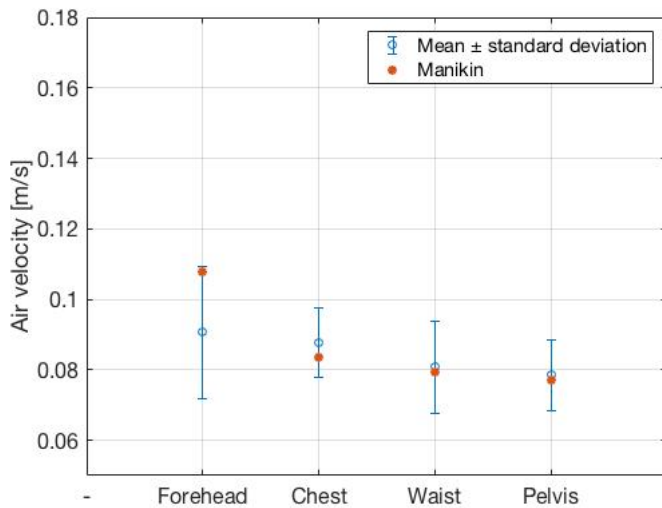
Figure 5.1: Measured centerline velocities 5 cm above surface

15 cm above the surfaces

The measured velocities 15 cm above the surface of the forehead, chest, waist and pelvis are presented in Figure 5.2. The mean velocity above the forehead is 0.11 m/s with a standard deviation of about 0.01 m/s, which is the lowest mean and lowest standard deviation, respectively. Above the chest is the mean centerline velocity 0.13 m/s, and thus the highest mean value in Figure 5.2. The standard deviation above the chest is the largest in the figure. As for the mean value and standard deviation above the waist and pelvis do the plot demonstrate similar values for the two, both with a mean value of 0.11 m/s.

The centerline velocity above the forehead of the manikin is almost equal to the mean value for the human subjects, and the velocity above the waist of the manikin is within the lower limit. The measured velocity above the chest and pelvis are both below the mean value minus the standard deviation, with the former being only slightly lower than the limit. However, the measured value above the pelvis of the manikin is almost 0.02 m/s lower than the lower limit.
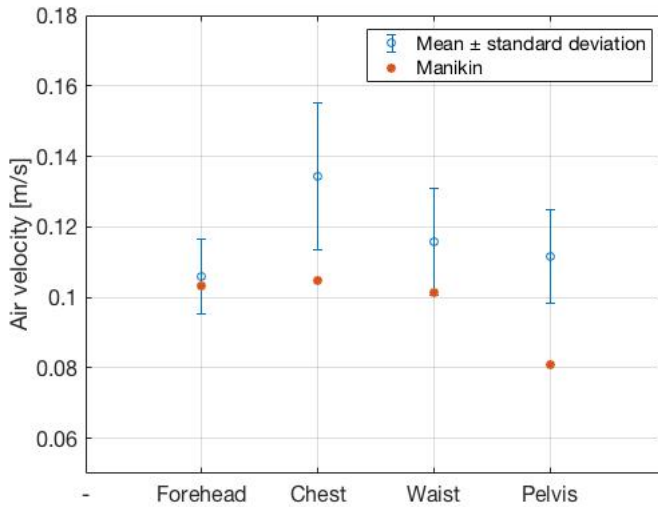
Figure 5.2: Measured centerline velocities 15 cm above surface

25 cm above the surfaces

The plot for the measured values 25 cm above the surfaces is presented in Figure 5.3. The plot shows that the highest mean values are those above the chest and the waist, both being 0.135 m/s. The mean value above the pelvis is slightly lower at 0.12 m/s. The mean value above the forehead, 0.085 m/s, is significantly lower than the three other mean values and also possesses the largest standard deviation of all.

The measured values above the forehead and pelvis of the manikin are both close to matching the corresponding mean values for the human subjects, while the value above the manikin's chest is just below the lower limit. At 0.105 m/s is the measured velocity above the manikin's waist 0.015 m/s lower than the lower limit from the human subjects.
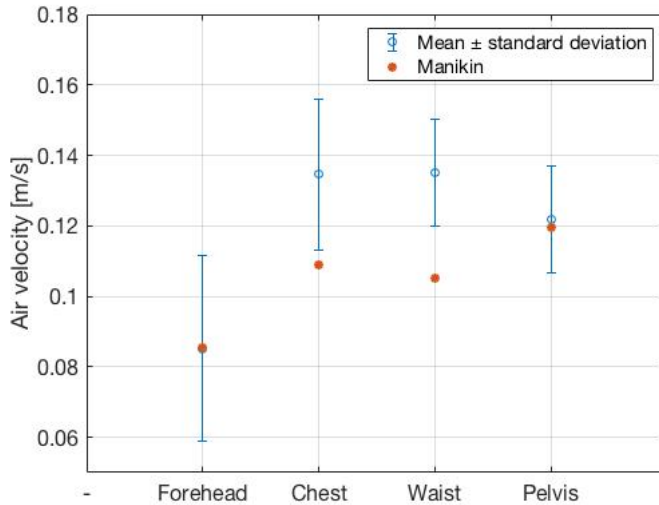
Figure 5.3: Measured centerline velocities 25 cm above surface

5.1.2 Set point temperatures for Case 2 and 3

Based on the results from Case 1 was it decided to use the setpoint temperatures in Table 5.1 for Case 2 and 3 as well, as they led to centerline velocities that were comparable to the measured velocities above the human subjects. Some of the values from the measurements above the manikin were outside the range based on the results from the human subjects, but none of these deviations exceeded 0.02 m/s which was the accuracy of the instruments.

5.2 Case 2: Experiment with a thermal manikin in an operating theatre with LAF

This section will present the results from the experiment performed in an operating theatre with a laminar system. The results are based on the experimental setup explained in Chapter 4.2.1. The order of the cross-sections: forehead, chest, waist, and pelvis. Each of the contours presented in this chapter is based on recordings from 30 different measurement points, where each point is the average value over a period of three minutes. The markings (a) - (d) below the plots correspond to scenario 1 - 4, meaning that (a) is Scenario 1, (b) is Scenario 2, and so on.

The results from the measurements above the knees have been put in the appendices, due to the lack of valid measurement data in Case 1.

5.2.1 Velocity contours

An important part of characterizing the airflow distribution close to the patient is to investigate the air velocity, and this sub-chapter will present the results concerning velocity.

Velocity distribution above forehead

Figure 5.4 presents the velocity contours above the forehead of the patient and it demonstrates that the profiles vary from scenario to scenario. Figure 5.4a is the reference, as it shows the velocity above an empty operating table. The figure indicates that the velocity is not uniformly distributed, as the recorded values range from 0.18 to 0.28 m/s. Also, the velocity field appears to be stratified with the highest values at the top of the contour and the lowest in the bottom. Figure 5.4b displays a large area of lower velocities close to the bottom. The velocity range from 0.18 to 0.30 m/s.

The contour for Scenario 3, Figure 5.4c, displays a velocity range of 0.16-0.28 m/s with the lowest values being located closest to the patient. Figure 5.4d displays the velocity contour with the inclusion of surgical lights. The plot indicates a top of higher values in the left part and a valley of lower values running along the line of a table width equal to 36 cm. The recorded velocities in Figure 5.4d range from 0.16 to 0.25 m/s.

Figure 5.4: Case 2: Velocity contours above forehead

Velocity distribution above chest

Figure 5.5 presents the velocity contours above the chest of the patient. Figure 5.5a acts as the reference case and it shows that the velocity field is not uniform, with values ranging from 0.15 to 0.26 m/s. In Scenario 2 Figure 5.5b demonstrates a large area of recorded velocities below 0.18 m/s. The values lie between 0.12 and 0.24 m/s.

Figure 5.5c shows that the airflow pattern with surgical staff included is characterized by lower values close to the patient, while the values range from 0.14 to 0.24 m/s. Figure 5.5d shows a profile with lower values close to the patient, and the value range is 0.16-0.26 m/s.
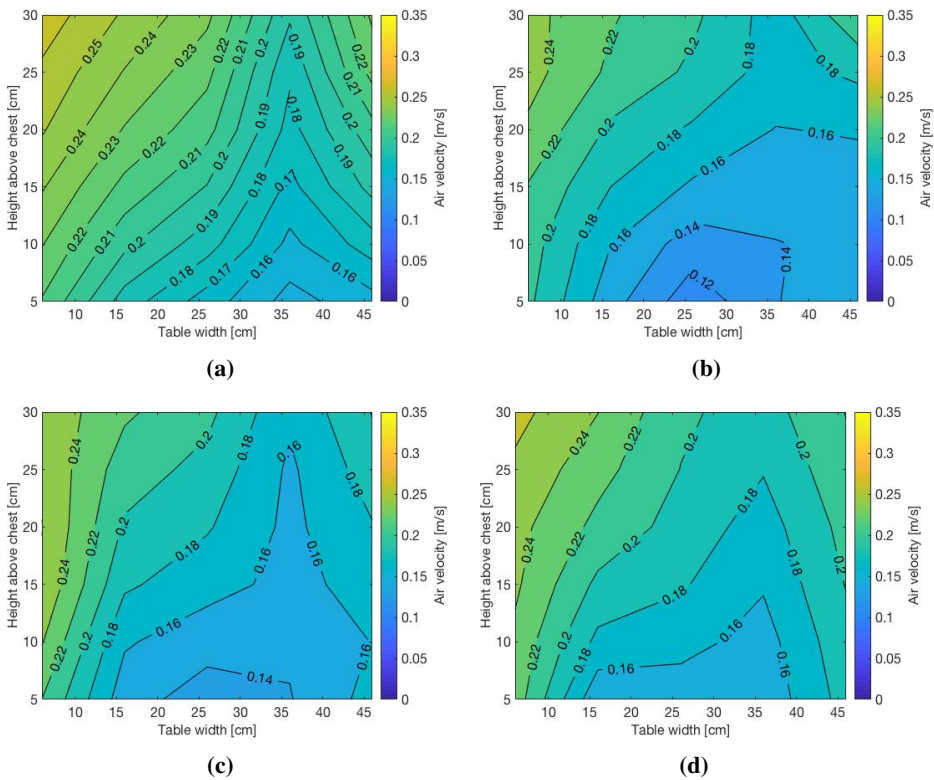
Figure 5.5: Case 2: Velocity contours above the chest

Velocity distribution above waist

Figure 5.6 presents the velocity contours above the waist for Case 2. The reference in Figure 5.6a shows a tendency of vertical layering of the velocity, with lower values occurring to the right and higher values to the left. The minimum is 0.18 m/s, while the maximum is 0.32 m/s. The contour for Scenario 2 is displayed in Figure 5.6b. The pattern in the figure has a concentric appearance where the center is located approximately at 5 cm height above the waist and 26 cm table width. The lowest velocity of 0.08 m/s is located in this center, while the highest value of 0.28 m/s is located in the top left corner.

Figure 5.6c displays higher values in the top left corner and lower values close to the patient, and the values range from 0.10 to 0.30 m/s. Figure 5.6d shows a profile characterized by lower values closest to the patient and higher values in the left part of the plot. The range is from 0.12 to 0.32 m/s.
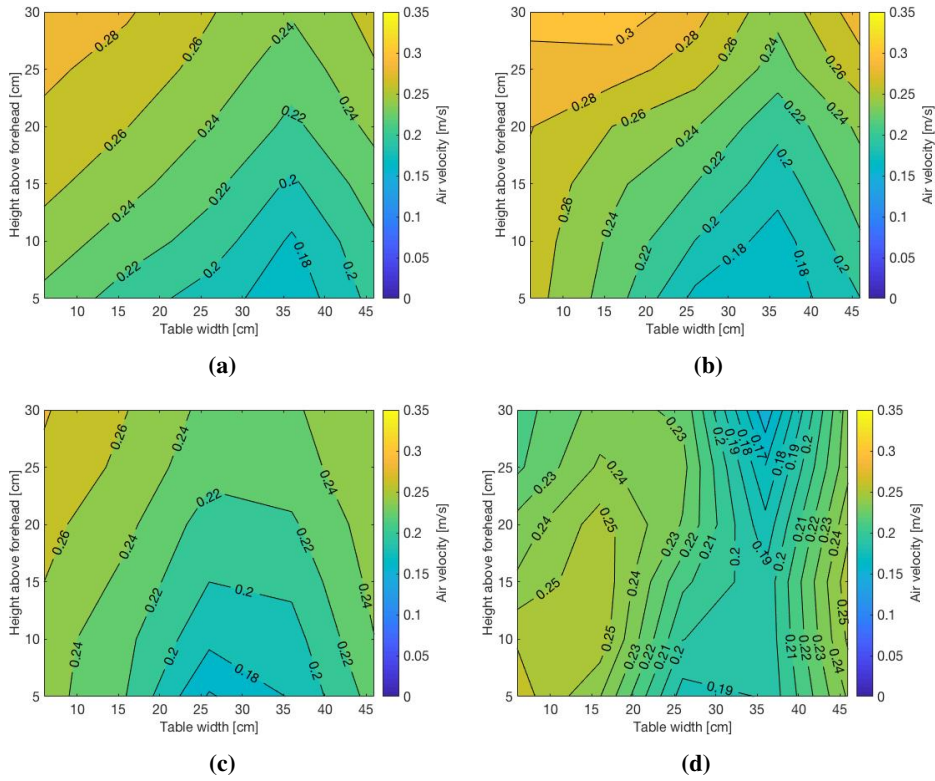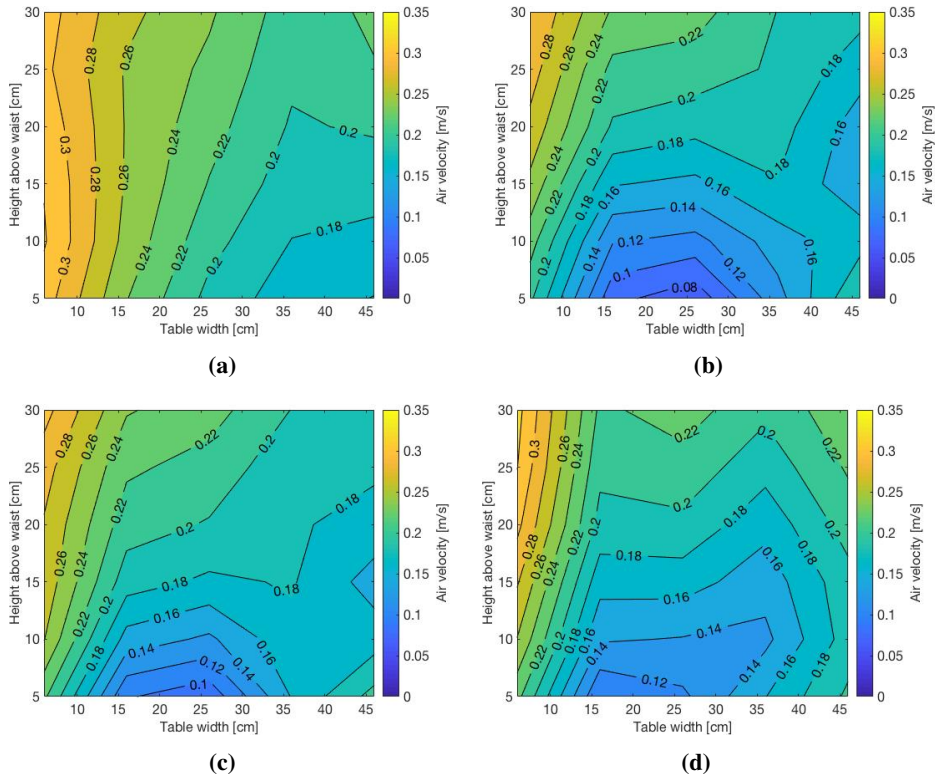

Figure 5.6: Case 2: Velocity contours above the waist

Velocity distribution above pelvis

Figure 5.7 presents the velocity contours above the pelvis for Case 2. Figure 5.7a shows a tendency of vertical layering of the velocity, with increasing values from right towards left. The highest value is 0.28 m/s, while the lowest is 0.18 m/s. The contour in Figure 5.7b shows a profile with a concentric look, semicircular layers and very low velocities at the bottom center of the plot. The velocities range from 0.06 to 0.20 m/s.

The airflow pattern in Figure 5.7c is dominated by higher values to the left and lower to the right, with the lowest located close to the patient. The values range from 0.08 to 0.24 m/s. Figure 5.7d displays a pattern where lower velocities are found to the right and higher to the left. The lowest and highest values are 0.10 and 0.30 m/s, respectively.

(a)

(b)

(c)

(d)
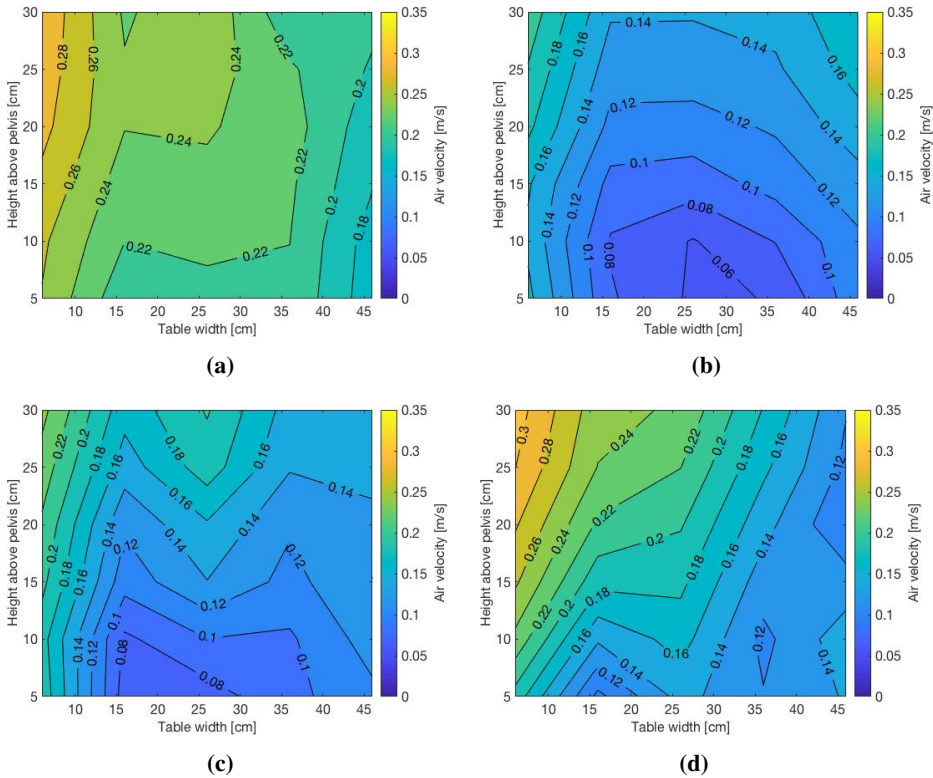
Figure 5.7: Case 2: Velocity contours above the pelvis

5.2.2 Temperature contours

This subchapter presents the temperature contours based on the measurements conducted in Case 2.

Temperature distribution above forehead

Figure 5.8 presents the temperature contours above the forehead. Figure 5.8a, Figure 5.8c and Figure 5.8d demonstrates very similar characteristics with the highest values located closest to the patient. Their temperature ranges are 21.75-22.00, 21.80-22.05 and 22.00-22.25°C, respectively. Figure 5.8b clearly shows stratification, and the values range from 19.60 to 21.00°C. The higher values are located near the patient. Note that the range of the colour bar in Figure 5.8b is from 19 to 23°C, while the three other colour bars in Figure 5.8 range from 21 to 23°C.

(a)

(b)

(c)

(d)
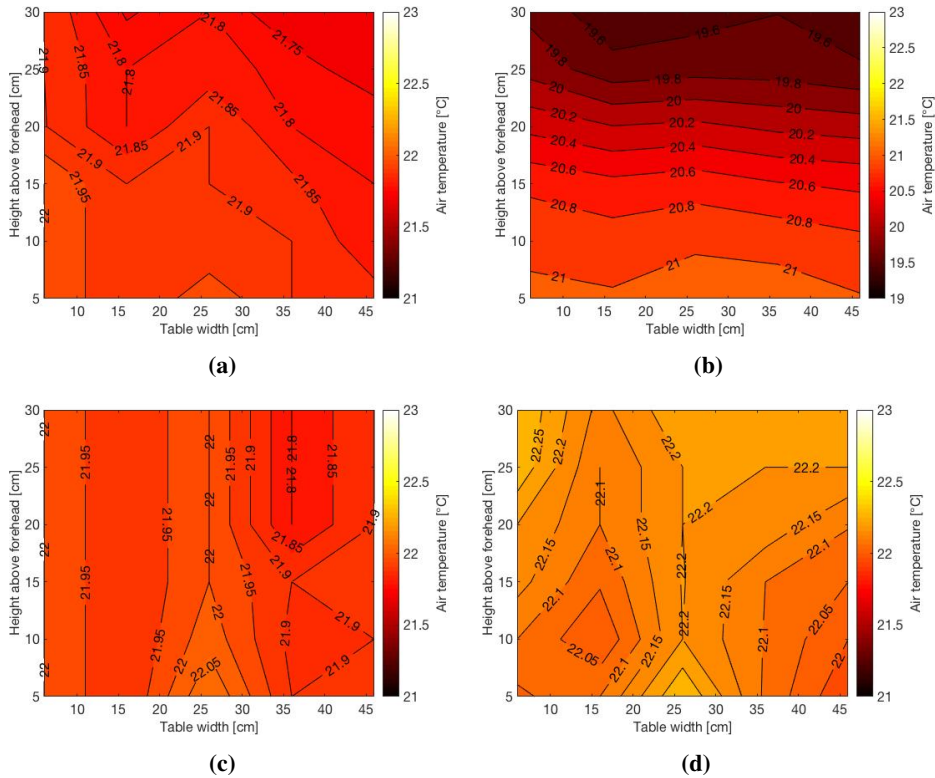
Figure 5.8: Case 2: Temperature contours above the forehead

Temperature distribution above chest

The temperature contours above the chest are presented in Figure 5.9. Figure 5.9a, Figure 5.9b, Figure 5.9c and Figure 5.9d paint a picture of almost homogeneous temperature fields with ranges of 21.60-21.85, 21.15-21.40, 21.95-22.20 and 21.85-22.25°C, respectively. The highest values in Figure 5.9a are found in the top left corner, while the highest values in Figure 5.9b, Figure 5.9c and Figure 5.9d are encountered close to the patient. A spot of higher temperatures occur in the top centre of Figure 5.9d.
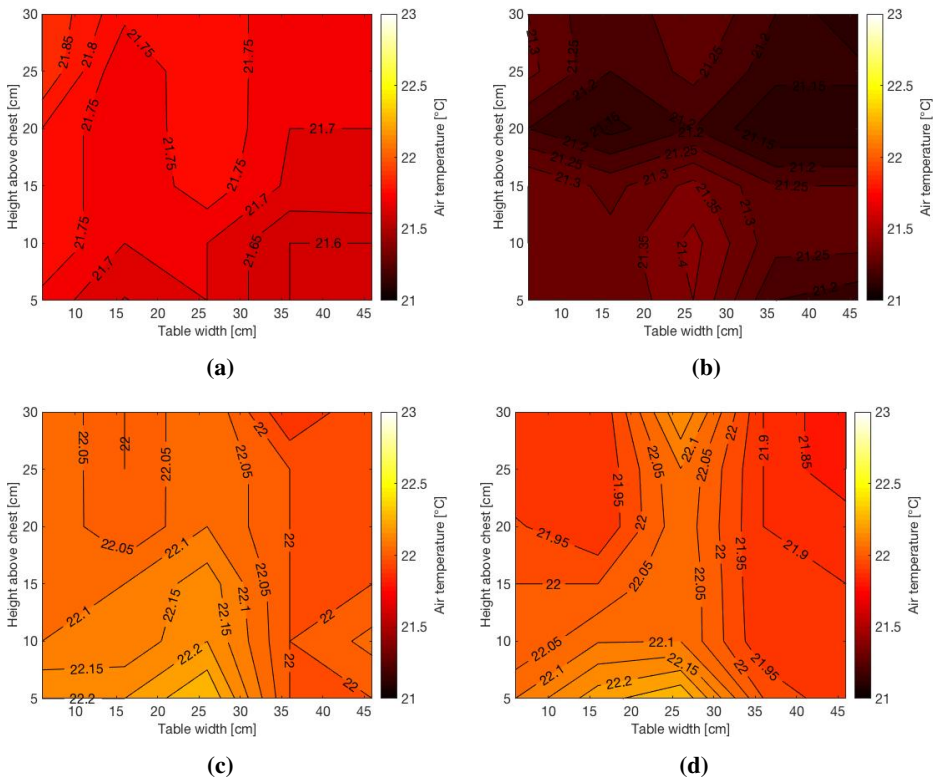
Figure 5.9: Case 2: Temperature contours above the chest

Temperature distribution above waist

The temperature contours in Figure 5.10 are those above the waist. Figure 5.10a shows a uniform temperature in the contour, with a range of only 21.52-21.62°C. Figure 5.10b and Figure 5.10c shows similar characteristics, with the higher temperatures being located in the bottom center of the contours. The range of values in Figure 5.10b and Figure 5.10c are 21.85-22.25 and 21.95-22.40°C, respectively.

Figure 5.10d demonstrates a profile where the maximum value of 22.5°C is found at a spot located 25 cm above the patient, and where the temperature drops in the horizontal direction from the spot. The values range from 21.90 to 22.50°C.
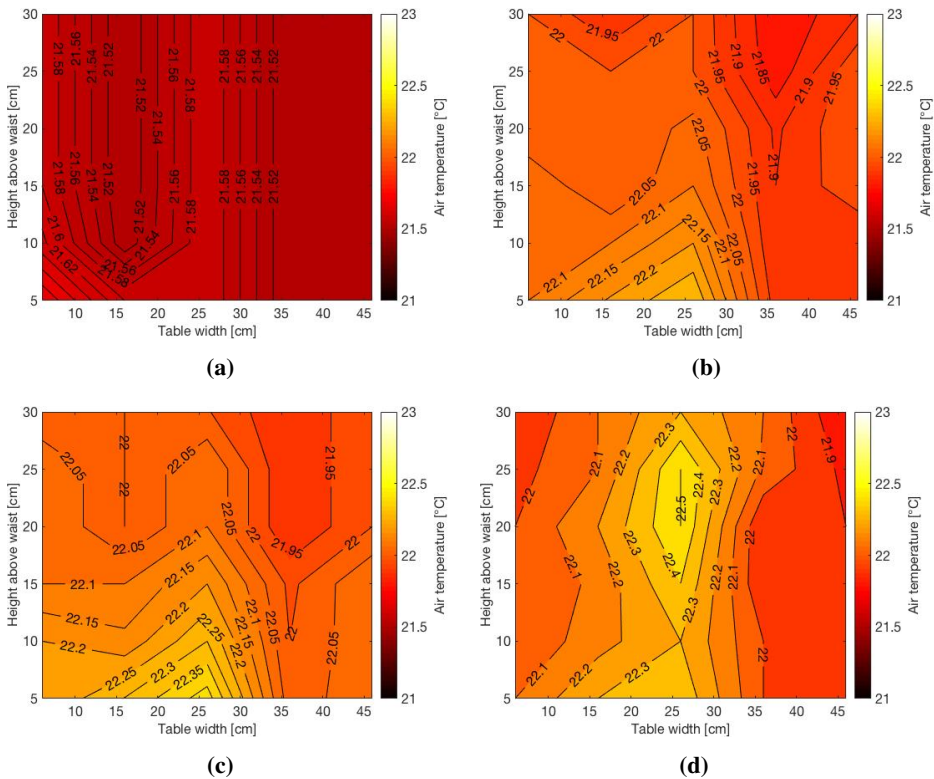
Figure 5.10: Case 2: Temperature contours above the waist

Temperature distribution above pelvis

The contours above the pelvis are shown in Figure 5.11. The contour in Figure 5.11a shows that the temperature field above the empty operating table is homogeneous, with the temperatures varying from 21.50 to 21.65°C.

In Figure 5.11b, Figure 5.11c and Figure 5.11d the highest temperatures are located at the bottom centre of the contours, and their temperatures lie between 21.95-22.40, 21.85-22.35 and 22.00-23.60°C, respectively. Note that the range of the color bar in Figure 5.11d differs from the others in Figure 5.11, as it spans from 21 to 24°C.

(a)

(b)

(c)

(d)
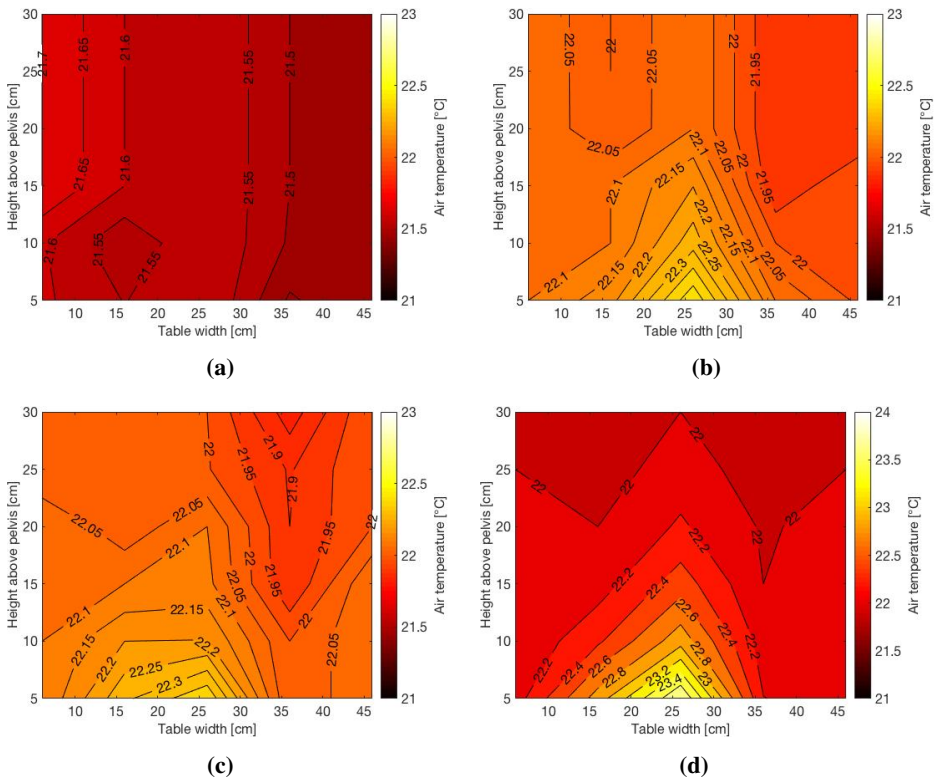
Figure 5.11: Case 2: Temperature contours above the pelvis

5.2.3 Turbulence intensity contours

This subchapter will present the turbulence intensity contours for each cross section and scenario in Case 2.

Turbulence intensity distribution above forehead

Figure 5.12 contains the turbulence intensity contours above the forehead. Figure 5.12a, Figure 5.12b and Figure 5.12c all contain large areas displaying values of around 3 %. The upper part of Figure 5.12d shows higher values than the bottom part, and the values range from 6 to 16 %.
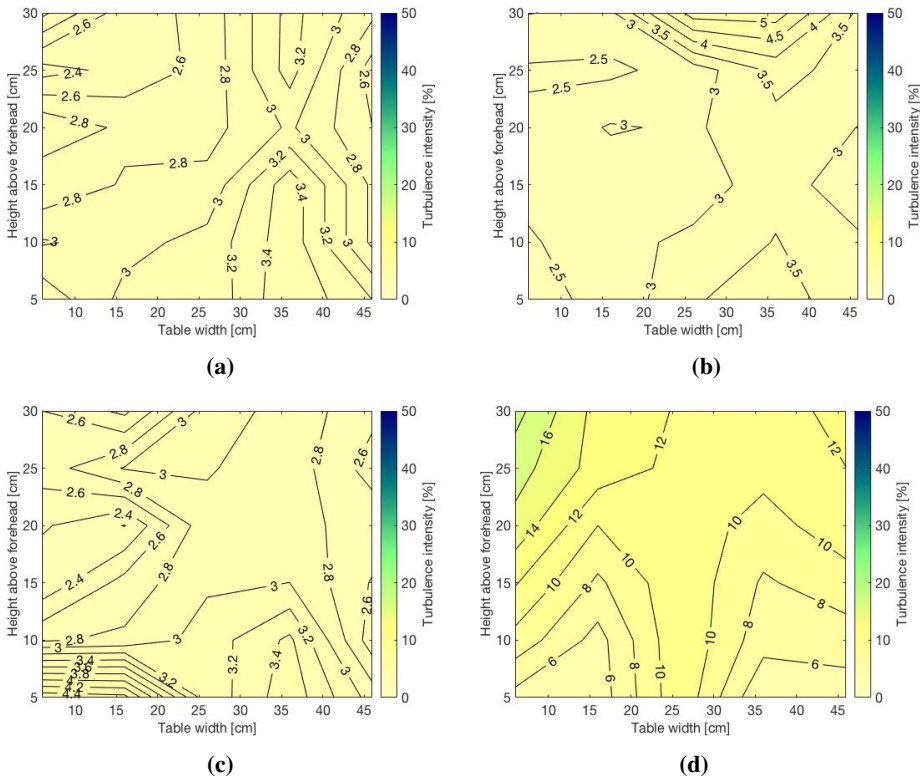
Figure 5.12: Case 2: Turbulence intensity contours above the forehead

Turbulence intensity distribution above chest

The contours above the chest are displayed in Figure 5.14. Figure 5.13a and Figure 5.13b both display values varying around 3 %, with the highest values appearing at the bottom of both figures.

There appears to be a diagonal division of the contour in Figure 5.13c, with lower values in the top right corner and higher values in the bottom left corner. The values range from 3 to 9 %. Figure 5.13d shows a profile where higher values stretch from the middle of the top towards the bottom left. There is a tendency of higher values to the left, and the highest value is located in the bottom left corner. The values range from 4 to 9 %.

(a)

(b)

(c)

(d)
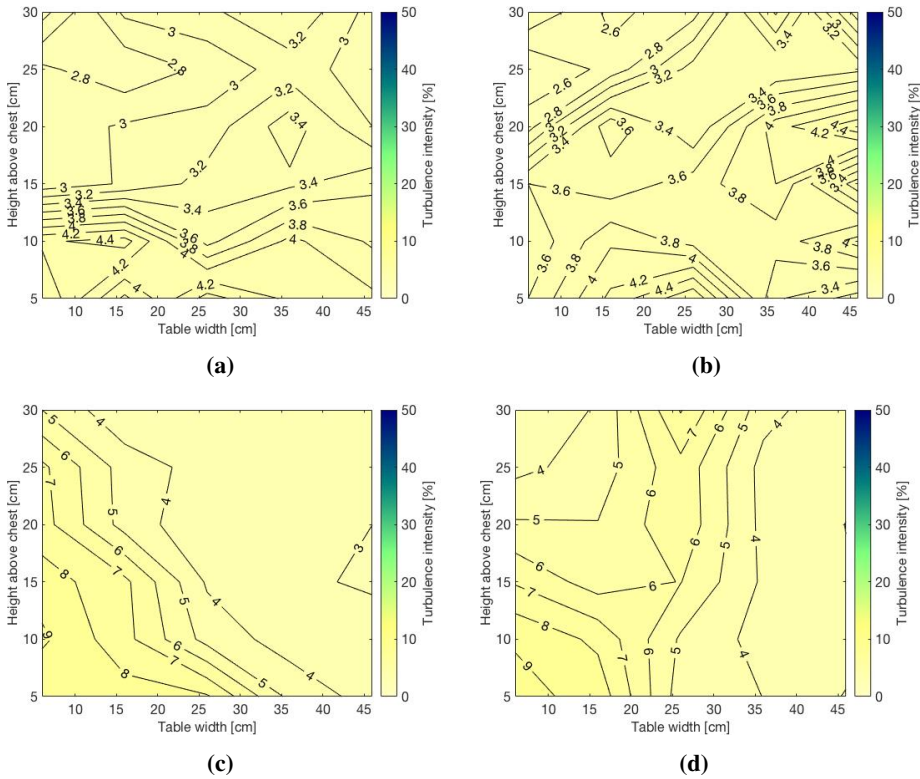
Figure 5.13: Case 2: Turbulence intensity contours above the chest

Turbulence intensity distribution above waist

The contours above the waist are displayed in Figure 5.14. Figure 5.14a shows the contour above an empty operating table. The values range from 3 to 12 %, and the highest values are encountered in the bottom left corner. Figure 5.14b, Figure 5.14c and Figure 5.14d all display higher values in the left part of the contour, with the highest values occurring closest to the patient. All three contours also have their minimum value in the top right corner. The ranges of Figure 5.14b, Figure 5.14c and Figure 5.14d are 5-35, 5-25 and 4-18 %, respectively.
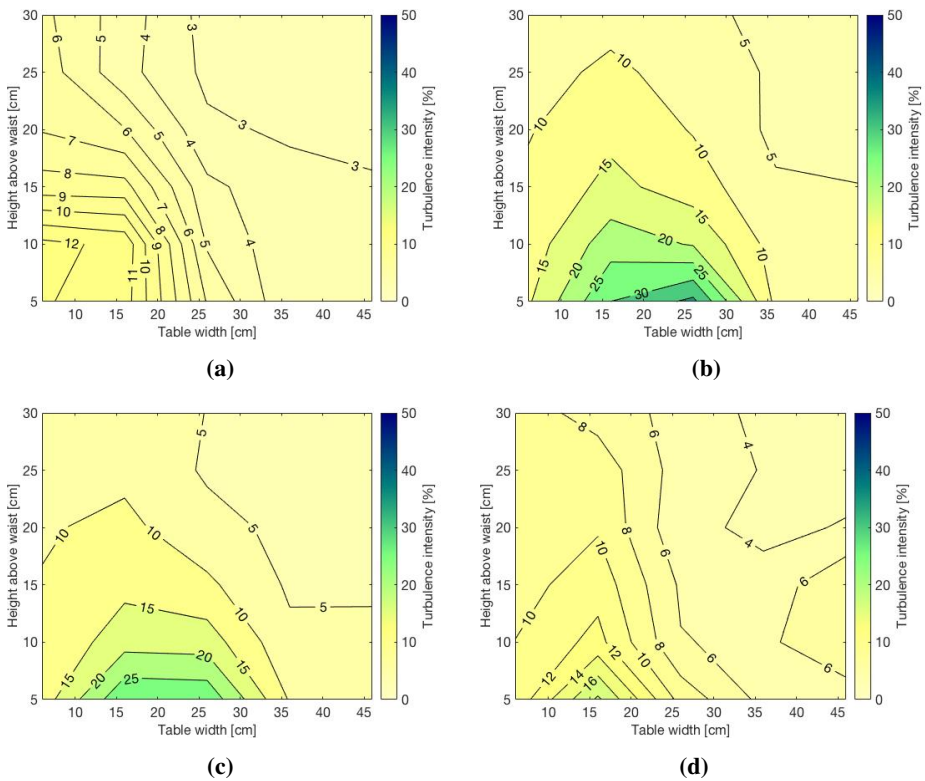
Figure 5.14: Case 2: Turbulence intensity contours above the waist

Turbulence intensity distribution above pelvis

The contours above the pelvis are displayed in Figure 5.15. Figure 5.15a serves as the reference and the contour displays values ranging from 3 to 11 %, with the highest values located to the left and the lowest to the right. Figure 5.15b demonstrates very high values in the bottom center, and values throughout the contour vary between 10 and 80 %. The top right corner features the lowest values. Note that the values of the color bar in Figure 5.15b range from 0 to 80 %.

Figure 5.15c shows higher values in the left part close to the patient. Values throughout the figure are lying in the interval of 5 to 35 %. Also, Figure 5.15c features lower values in the top right corner. The levels of turbulence in Figure 5.15d range from 5 to 25 %. The highest values appear near the top right corner.

(a)

(b)

(c)

(d)
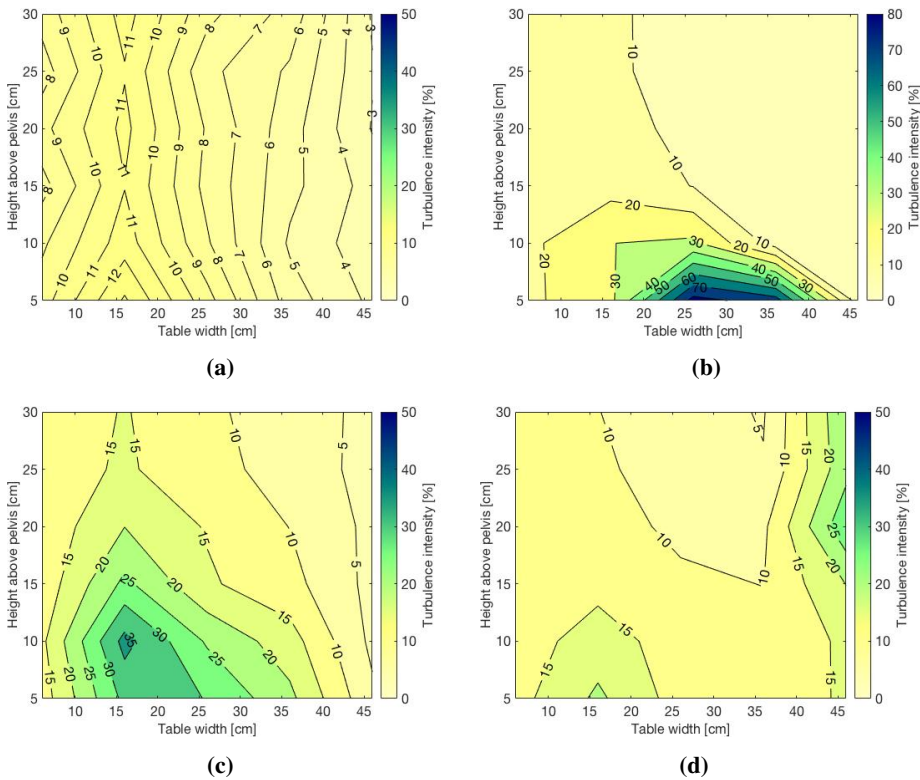
Figure 5.15: Case 2: Turbulence intensity contours above the pelvis

5.3 Case 3: Experiment with a thermal manikin in an operating theatre with a mixing system

This section will present the results of the experiment performed in an operating theatre with a mixing system. The results are based on the experimental setup explained in Chapter 4.3 and will be presented in a similar way as in Chapter 5.2. Each of the contours presented in this chapter is based on recordings from 30 different measurement points, where each point is the average value over a period of three minutes. The order of the cross-sections: chest, waist, pelvis. The markings (a) - (d) below the plots correspond to Scenario 1 - 4.

5.3.1 Velocity contours

The following part presents the velocity contours from the measurements in an operating theatre with a mixing system.

Velocity distribution above chest

Figure 5.16 displays the velocity contours above the chest. All of the contours in Figure 5.16 show a tendency of lower values in the top right quadrant than in the top left quadrant. Also, the maximum values in all the plots occur in the top left corner. The pattern in Figure 5.16a shows higher values in the top left corner and the values in the plot range from 0.16 to 0.23 m/s. Figure 5.16b shows a profile where the bottom half displays the low values, with the lowest occurring closest to the patient. The values vary between 0.16 and 0.22 m/s.

The pattern demonstrated in Figure 5.16c is characterized by lower values appearing from 5-15 cm above the patient, with the values in the contour ranging from 0.16 to 0.25 m/s. The profile in Figure 5.16d has an S-shaped appearance, with lower values in the right part than in the left. The values span from 0.17 to 0.23 m/s.
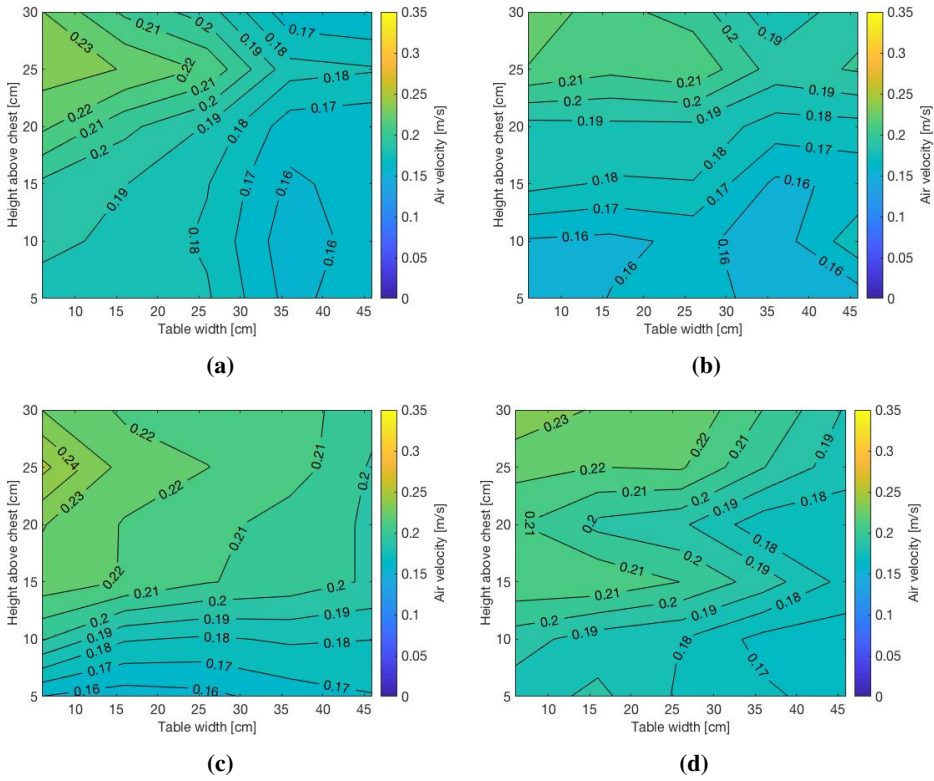
Figure 5.16: Case 3: Velocity contours above the chest

Velocity distribution above waist

The velocity contours above the waist are presented in Figure 5.17. All the contours in Figure 5.17 show high values near the top and low values close to the bottom. In Figure 5.17a, Figure 5.17c and Figure 5.17d do the lowest values appear in the bottom right corner. Also, they show a tendency of higher values in the left part of the contour. The values in Figure 5.17a span from 0.15 to 0.23 m/s. The lower values in Figure 5.17b appear below a height of 15 cm. However, there is an area with a velocity of 0.17 m/s near the top right corner. The values in the plot range from 0.14 to 0.20 m/s.

The pattern in Figure 5.17c is dominated by a large area with a velocity of 0.16 m/s, located in the bottom half. The velocity interval is 0.16-0.26 m/s. There is a peak of 0.20 m/s in the center of Figure 5.17d. The values in this plot span from 0.15 to 0.21 m/s.
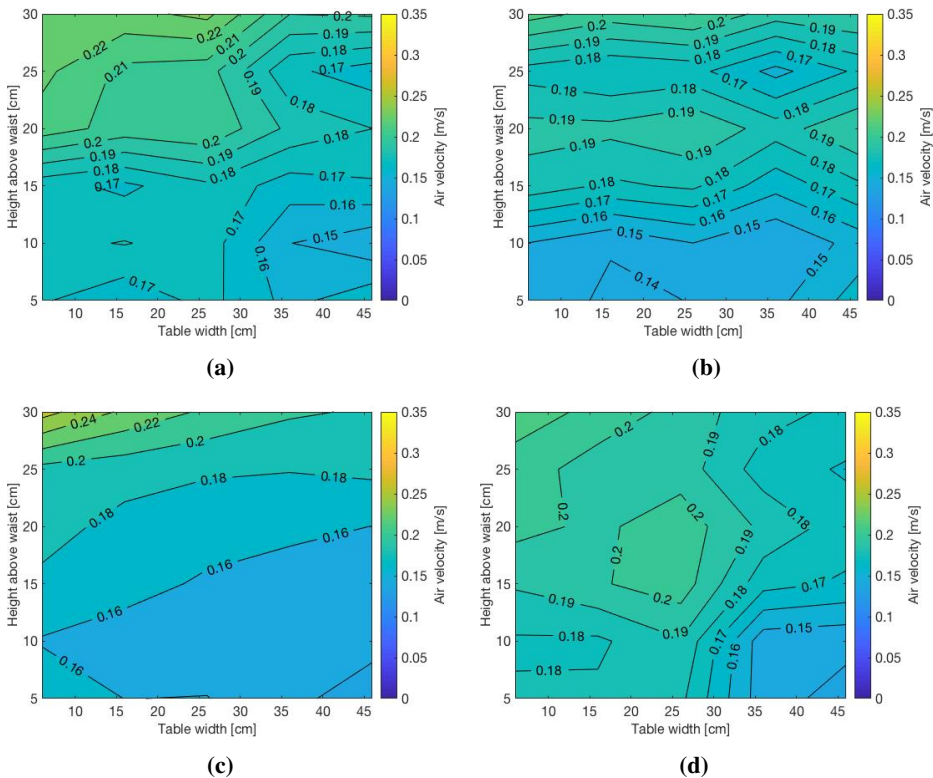
Figure 5.17: Case 3: Velocity contours above the waist

Velocity distribution above pelvis

Figure 5.18 shows the velocity contours above the pelvis. All of the contours in Figure 5.18 demonstrate a tendency of lower values in the bottom half. Figure 5.18a, Figure 5.18c and Figure 5.18d all display lower values in the right part than in the left. The values in Figure 5.18a range from 0.14 to 0.19 m/s.

In Figure 5.18b, Figure 5.18c and Figure 5.18d do the minimum values appear closest to the patient. The ranges of Figure 5.18b, Figure 5.18c and Figure 5.18d are 0.145-0.18, 0.11-0.19 and 0.13-0.21 m/s, respectively. The pattern in Figure 5.18d is dominated by a large area of 0.19 m/s stretching from the top right corner towards the bottom left corner.
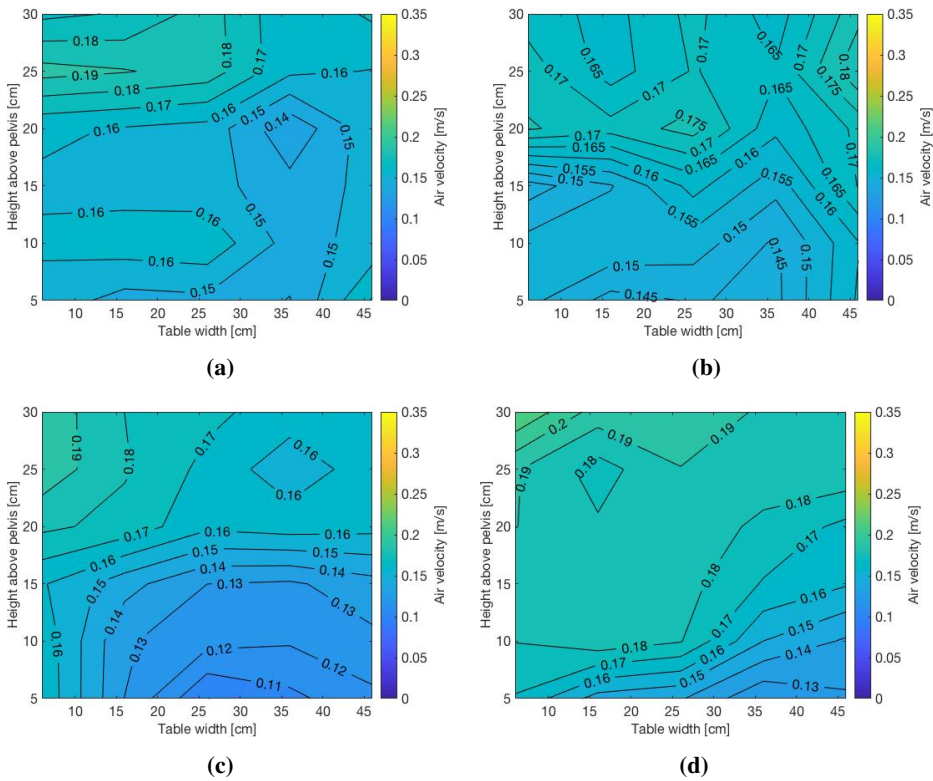
Figure 5.18: Case 3: Velocity contours above the pelvis

5.3.2 Temperature contours

The following part presents the temperature contours from the measurements in an operating theatre with a mixing system.

Temperature distribution above chest

Figure 5.19 displays the contours above the chest. The highest values in both Figure 5.19a and Figure 5.19b occur at the bottom center of the contours. Their values range from 21.86 to 22.04 and from 22.0 to 22.60°C, respectively. The profile in Figure 5.19b is characterized by stratification in the bottom half and homogeneous temperatures in the top half. Figure 5.19c shows a pattern with axis symmetry around the line of a table width equal to 26 cm. The highest values occur both in the top and bottom center of the contour. The values span from 22.05 to 22.20°C. The profile in Figure 5.19d is dominated by higher values occurring in the top half of the contour, with the maximum value being located in the top center. The maximum value is 24.6°C and the minimum 22.6°C. Note that the range of the color bar in Figure 5.19d deviates from the other contours in Figure 5.19, with a minimum and maximum value of 22 and 25°C, respectively.
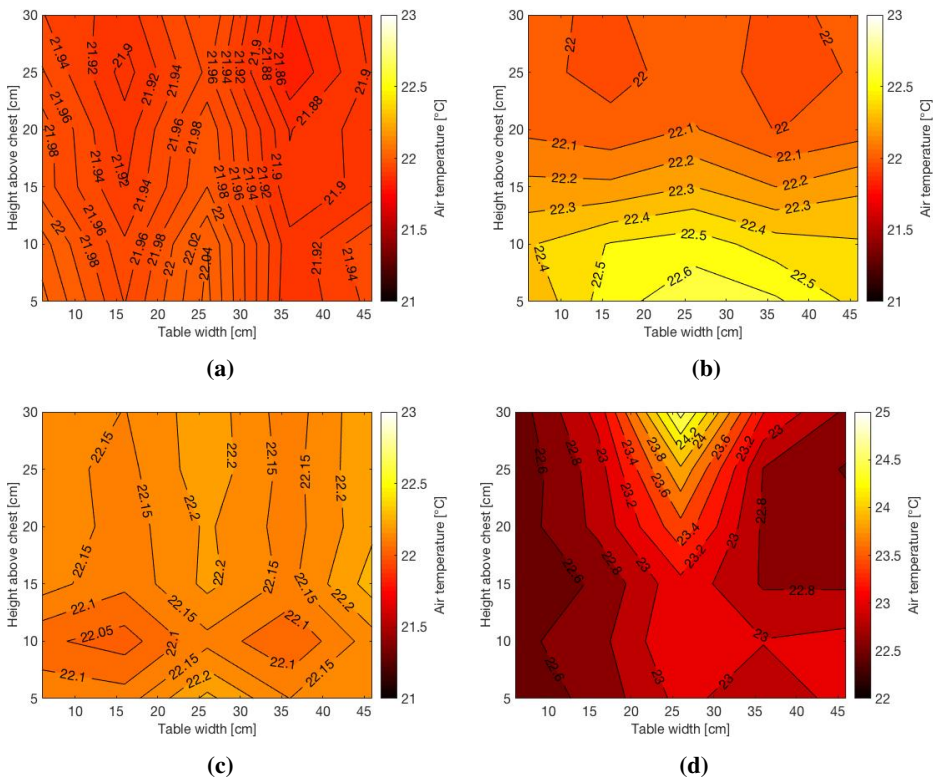
Figure 5.19: Case 3: Temperature contours above chest

Temperature distribution above waist

The temperature contours above the waist are presented in Figure 5.20. All of the contours in Figure 5.20 demonstrate a pattern of higher temperatures occurring below a height of 15 cm, and also a tendency of larger temperature variations in the bottom half. Both Figure 5.20a and Figure 5.20b display higher temperatures to the left than to the right, and also a tendency of symmetry about the line of a table width equal to 26 cm. Their ranges are 21.85-22.15 and 22.00-22.50°C, respectively.

The highest values in Figure 5.20c are found near the bottom right corner, and temperatures are in general higher in the right than in the left bottom quadrant. The values lie between 22.30 and 23.30°C. The profile in Figure 5.20d has a symmetrical appearance. The highest value is 25.50 and the lowest 23.00°C. Note that the range of the color bar in Figure 5.20a and Figure 5.20b are equal, whereas both Figure 5.20c and Figure 5.20d have individual bars.

(a)

(b)

(c)

(d)
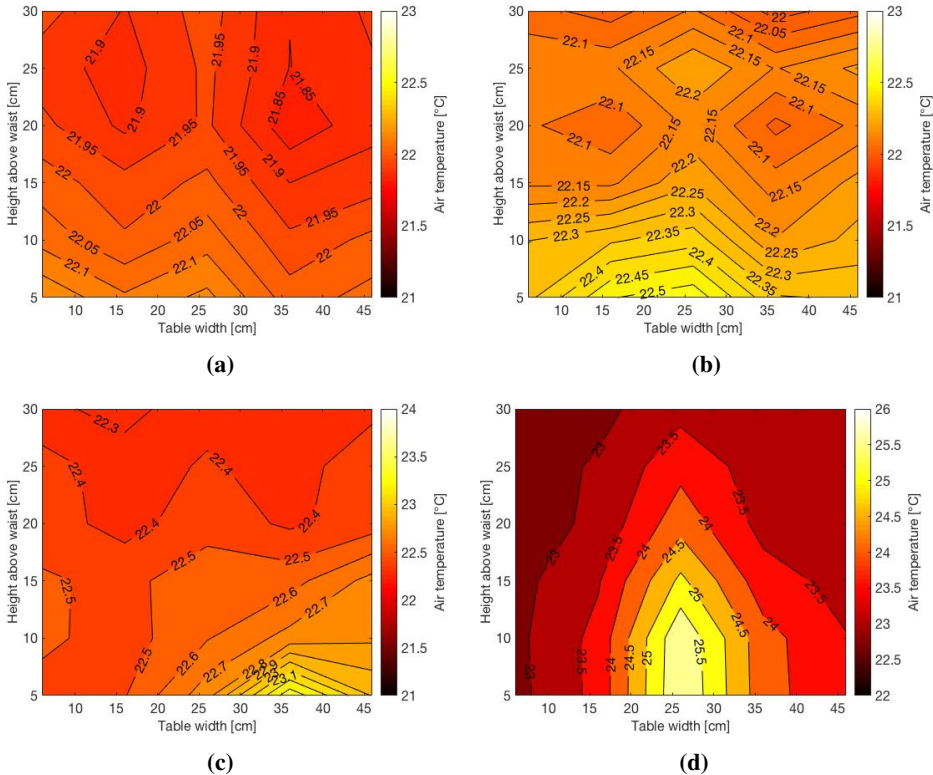
Figure 5.20: Case 3: Temperature contours above the waist

Temperature distribution above pelvis

The temperature contours above the pelvis are displayed in Figure 5.21. Figure 5.21a shows a pattern where the higher values occur in the upper half of the contour and larger temperature differences in the bottom half. The temperatures range from 21.60 to 22.20°C. Figure 5.21b, Figure 5.21c and Figure 5.21d all show a tendency of higher temperatures and larger temperature variations below a height of 15 cm. The contours in Figure 5.21b and 5.21c shows stratification, and the ranges are 22.10-22.55 and 22.70-23.70°C, respectively. The lowest and highest value in Figure 5.21d are 23.00 and 26.50°C, respectively. Note that the range of the colour bar in Figure 5.21a and Figure 5.21b are equal, whereas both Figure 5.21c and Figure 5.21d have individual bars.
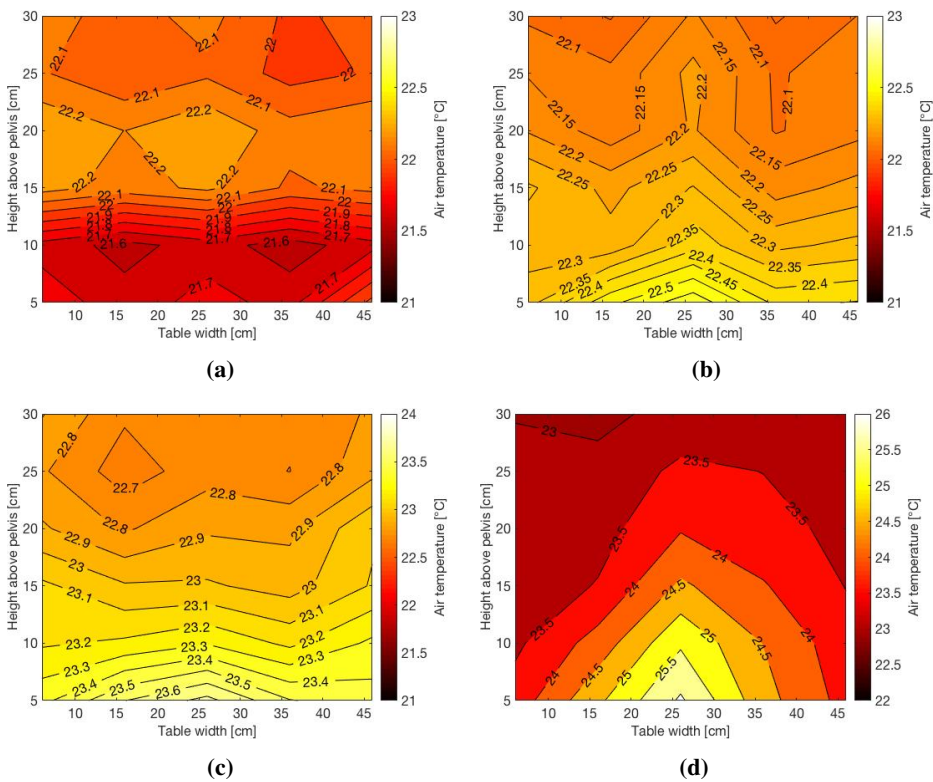
Figure 5.21: Case 3: Temperature contours above the pelvis

5.3.3 Turbulence intensity contours

The following part presents the turbulence intensity contours from the experiment in an operating theatre with a mixing system.

Turbulence intensity distribution above chest

The turbulence intensity contours above the chest are presented in Figure 5.22. The pattern in Figure 5.22a is characterized by higher values in the upper part, with a maximum value of 39 % located in the top centre. The lowest value is 28 %. Figure 5.22b shows a profile with evenly distributed values. The highest value is 33 % and occurs at 20 cm above the chest, and the minimum value is 27 %.

Both Figure 5.22c and Figure 5.22d demonstrate patterns where the higher values can be found below a height of 15 cm. Also, their maximum values appear in the bottom centre of the plots. The values in Figure 5.22c span from 32 to 41 %. The pattern in Figure 5.22d is dominated by a large area of 34 %, and the values in the contour range from 30 to 44 %.
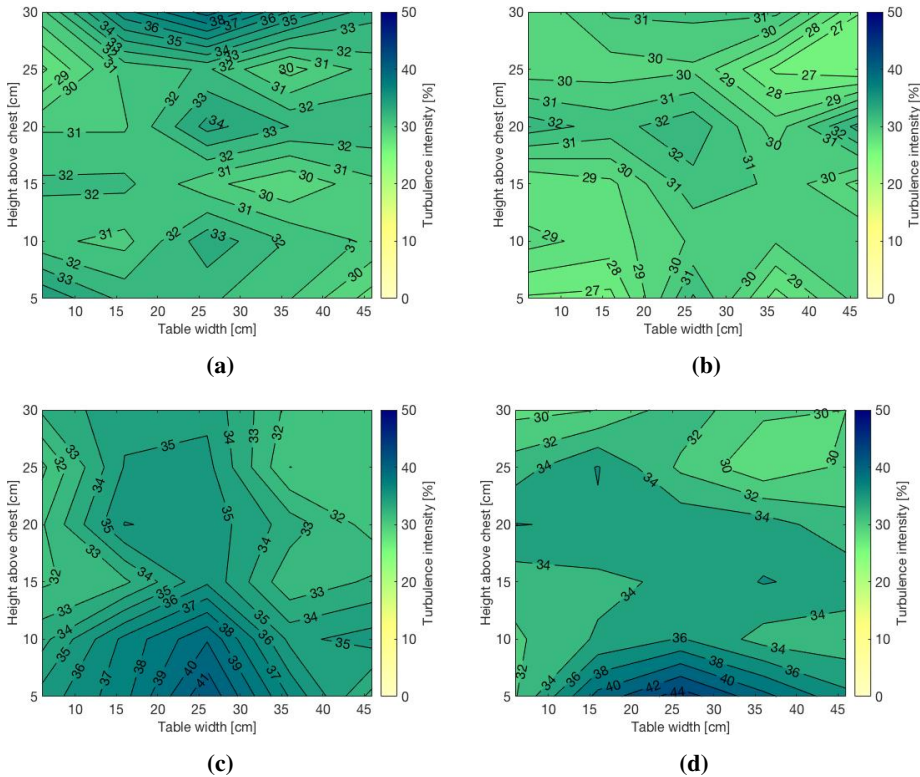
Figure 5.22: Case 3: Turbulence intensity contours above the chest

Turbulence intensity distribution above waist

Figure 5.23 displays the turbulence intensity contours above the waist. All of the contours in Figure 5.23 demonstrate a tendency of higher values being located below a height of 15 cm, as well as single peaks of high values occurring in the upper part. Figure 5.23a and Figure 5.23c feature higher values in the left part of the contour than in the left. The values in these two figures range from 29 to 38 and from 30 to 40 %, respectively.

The highest values of Figure 5.23a and Figure 5.23c are both located 10 cm above the waist, in the center, while the maximum values of Figure 5.23b and Figure 5.23d are located at a height of 5 cm. The values in Figure 5.23b lie between 27 and 37 %. Figure 5.23d displays values ranging from 26 to 36 %, with small areas of higher values.
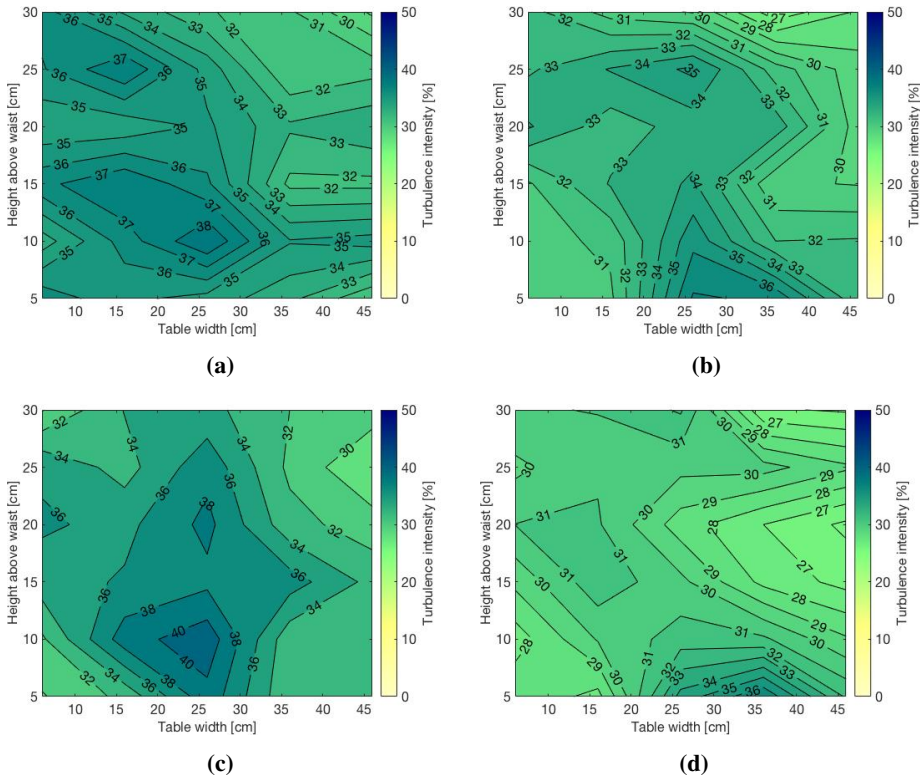
Figure 5.23: Case 3: Turbulence intensity contours above the waist

Turbulence intensity distribution above pelvis

Figure 5.24 displays the contours above the pelvis. Figure 5.24a demonstrates a pattern where a ridge of higher values stretches horizontally across the upper half. Also, the contour features higher values to the left than to the right. Values range from 31 to 39 %. The plot in Figure 5.24b shows that the highest value occurs closest to the patient near the bottom right corner, while a peak of higher values is located at the center. The values span from 26 to 40 %.

The profile of Scenario 3, shown in Figure 5.24c, is characterized by higher values being located below a height of 15 cm, as well as higher values to the right than to the left. Values in the contour span from 22 to 34 %. The higher values in Figure 5.24d appear close to the patient, with a maximum of 32 %. The lowest value, 22 %, appears both near the top right and the bottom left corner.
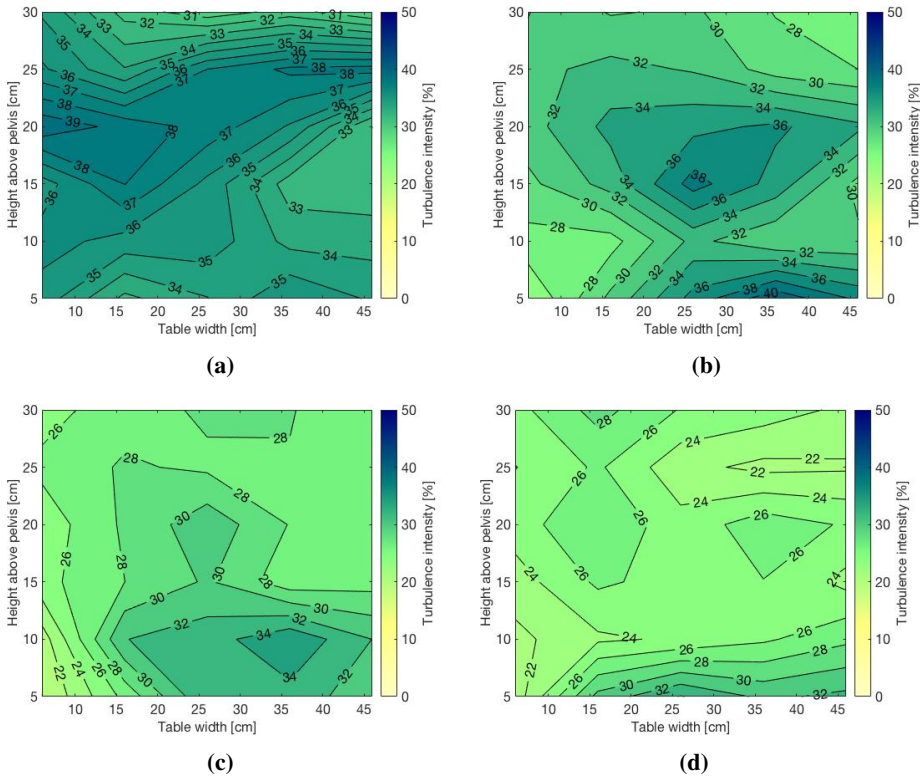
Figure 5.24: Case 3: Turbulence intensity contours above the pelvis

Chapter 6

Discussion

The chapter contains a discussion and comparison of the results presented in Chapter 5. Practical limitations, suggestions for future design specifications, as well as suggestions for future studies, will be presented.

6.1 Comparison of results

This part includes a comparison of the results in Case 2 with those of previous studies, a comparison of the results from Case 2 and 3, as well as a comparison of the mathematical models in Chapter 3 and the experimental results of Chapter 5.1. There is a limited number of scientific articles investigating the airflow distribution above the patient for a mixing and a LAF system through experimental methods, especially for mixing systems, which complicates a comparison. Therefore will the results of Case 2 and 3 be compared to each other in order to discuss differences potentially caused by the ventilation systems. The comparison will only comprise the cross-sections above the chest, waist, and pelvis, as they were investigated in both cases. Regarding the thermal plume from a human in a supine position are there few studies, which makes also that comparison difficult.

6.1.1 Case 1

One of the objectives for Case 1 was to investigate the thermal plume above real human beings. Measurements above five males in a supine position were conducted, and the results will be compared to mathematical models presented in Chapter 3. As only the middle sensor consistently recorded values above 0.05 m/s is it impossible to determine or estimate the plume boundary based on the measurement data, and thus will the comparisons only focus at the centerline velocities. The mean centerline velocities above the forehead, chest, waist, and pelvis presented in Chapter 5.1 will serve as references to which the mathematical models are compared. These velocities are shown in Figure 6.1.
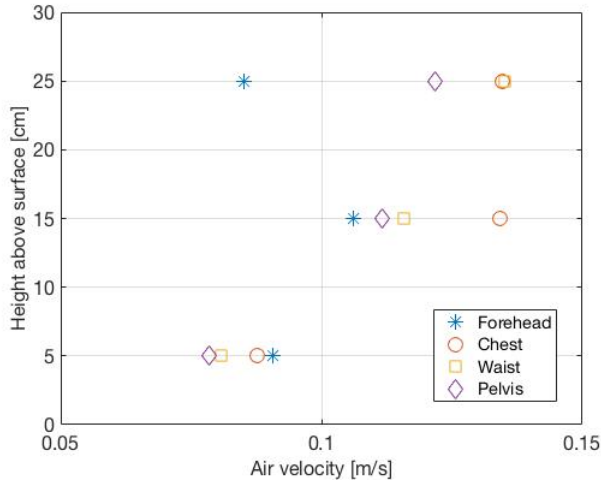
Figure 6.1: Measured centerline velocities

Since the mean centerline velocities are used, it was decided to base calculation of the body surface area on the average height and weight of the human subjects. The surface temperature of the average human was assumed to be uniform over the entire body at a value of $32.0°C$. According to Hanssen (1991, as cited in Novakovic *et al.* 2014) is $32.0°C$ in the lower end of human skin temperature under normal conditions, and since the insulating effect of clothing will reduce the surface temperature of the subjects was this value chosen. The air temperature in the climate chamber was assumed to be $23.0°C$.

Table 6.1 provides an overview of calculated values based on Equation 3.1, 3.2, 3.3 and 3.4 in Chapter 3.1, subject data from Table 4.2 and the temperatures from the foregoing paragraph.

Table 6.1: Calculated values for convective heat output

Variable	Calculated value
A	1.9542 m^2
A_c	1.5849 m^2
ΔT	9
h_c	$1.9776 \text{ W/m}^2\text{K}$
$\dot{Q}_k$	28.2083 W

Figure 6.2 shows the experimentally obtained data of Case 1, compared to the line source models of Storås and Skaret. Storås' (2017) model in Figure 6.2 is the one from Equation 3.14, where the whole body of a thermal manikin was modeled as a line source with an experimentally determined proportionality factor. Skaret's (2000) model, on the other hand, is a general equation for a line source. Figure 6.2 shows that none of the models coincide with the recorded values. The two models each show constant velocities, where the values are significantly higher than the measured velocities. However, the centerline velocities above the waist and pelvis show a tendency of increasing values with height, so the models of Skaret and Storås could prove more accurate at increased heights. The deviations could be caused by the fact that none of the models have been based on measurements above real humans, which have complex body geometries. Storås' model appears to be the best match, which is reasonable given how it was developed.
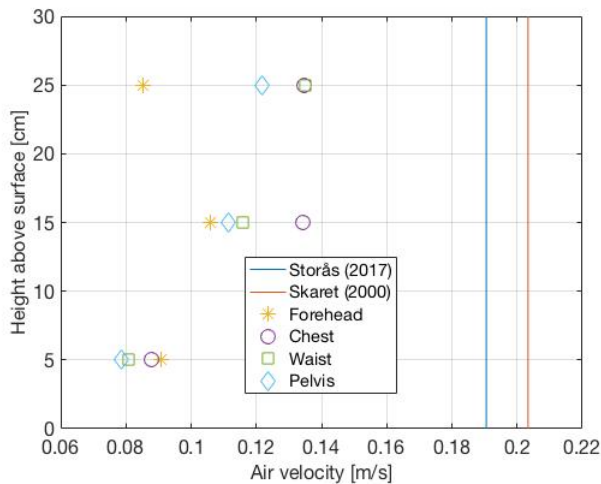
Figure 6.2: Comparison of results from experiments and line source equations

Based on the results in Figure 6.1, it was decided to try to model the torso of the human body as a point source. An important assumption for the mathematical models was the use of the total convective heat output of a body in the models. The reason behind this is the difficulty associated with determining the portion of the total convective heat output originating from the torso. Therefore, the convective heat output was set to 28.2083 W.

Another simplification was to base the diameter of the heat source on the dimensions of the thermal manikin. This can be considered a fair assumption due to the human-like shape and geometry of the manikin. The diameter of the torso was set to 0.30 m, which was the average of the width measured at the chest, waist, and pelvis. By the use of Equation 3.9 was then a distance of 0.795 m to the virtual origin, z_0, calculated.

Figure 6.3 demonstrate large differences between Equation 3.7 and Equation 3.15, by Skaret and Storås respectively, and the measured velocities. One explanation for the large deviations between the models and the experimental results is related to the calculation of the distance to the virtual origin. As shown in Chapter 3.2.1 have different authors suggested various equations for the calculation of z_0, and z_0 has a major impact on the spread angle and thus the proportionality constant, C_b. Another important aspect is that neither of the models in Figure 6.3 were developed from measurements above real humans. Equation 3.7 by Skaret is a general equation for a point source, whereas Equation 3.15 by Storås is based on measurements above a thermal manikin. The simplification of the convective heat output and diameter of the heat source are also elements that affect the models and potentially increase the differences.
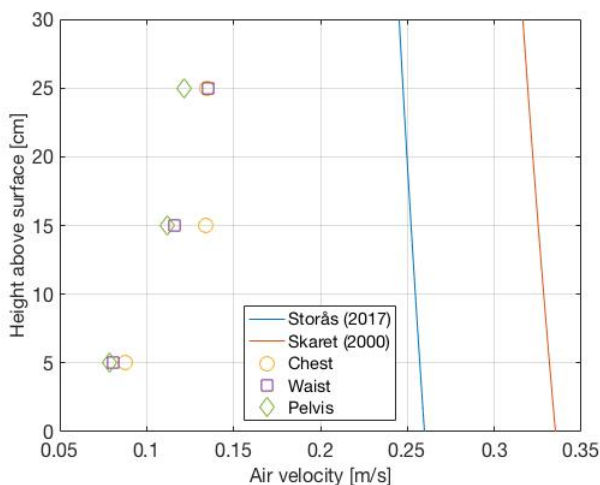
Figure 6.3: Comparison of results from experiments and point source equations

The relatively large differences between the mathematical models and the experimental results in Figure 6.2 and Figure 6.3 indicate that the thermal plume from a person in a supine position is complex and hard to model. There are some insecurities related to the

experimental setup, and the plume itself, that could contribute to these differences. Since the middle sensor was placed along the centerline of the subjects, combined with the fact that it recorded the highest values, was it assumed to measure the centerline velocity of the plume. However, thermal plumes are known to be elusive and sensitive to changes, and therefore it is likely that the sensor did not record the velocity of the actual centerline at all times.

Another consequence of the plume's characteristics and the complex human geometry is that it is uncertain whether the middle sensor was positioned at the location of the centerline in the first place. It is also possible that the mathematical models would have been more accurate at increased heights, as the measurements were performed very close to the subjects. This could mean that parts of the investigated region were in the CBL around the patient and not in the region of self-similarity of mean motion (Zukowska, Popiolek, and Melikov, 2010).

6.1.2 Case 2 and previous studies

Case 2 investigated the airflow distribution above the patient in an operating theatre with a LAF system. None of the velocity contours for Scenario 1 demonstrated a pattern of uniform velocity as each of them showed velocity variations exceeding 0.02 m/s, which is the accuracy of the instruments. Also, the contours showed that there were significant differences between the cross sections and the velocities ranged from 0.16 to 0.28 m/s. The Health Technical Memorandum, HTM, published by the United Kingdom National Health Service Estates provides guidance for ventilation of healthcare facilities and recommends a minimum velocity of 0.2 m/s above the operating table (Department of Health UK, 2007). A substantial part of the measured airflow velocities in Scenario 1 are lower than 0.2 m/s, and also well below the Norwegian guideline of 0.25-0.28 m/s (Aune, 2015), which means that even above an empty operating table is the ventilation system unable to fulfill the requirements.

The introduction of the patient has a pronounced impact on the velocity distribution. Figure 5.4b, Figure 5.5b, Figure 5.6b and Figure 5.7b all show a pattern where the velocities in general have dropped compared to the previous scenario. It is likely that it is caused by the upward movement of the convective airflow from the patient which counteracts the supply airflow (Cao *et al.*, 2017), and thus reduces the total airflow velocity. Also, the minimum velocities of all the contours are located closest to the patient in the bottom center. The location could be explained by the fact that the centerline velocity in a thermal plume represents the highest velocity in the plume (Skåret, 2000).

The velocity contour above the forehead for Scenario 4, deviates from the airflow patterns shown in the corresponding contours at different cross sections, as well as the one for Scenario 3. The contour displays the lowest values near the top, a vertical line of lower values in the right part, and a peak of higher velocities in the left part. The turbulence intensity contour for Scenario 4, Figure 5.12d, shows elevated levels of turbulence compared to the previous scenarios with the highest values appearing in the top half of the contour. Surgical lamps interfere with and block the supply airflow, and thus wakes form downstream of the lamps. Since one of the surgical lamps was positioned directly above the forehead of the patient, could this explain the pattern in Figure 5.4d and Figure 5.12d. In the wakes eddies form (Brohus, Balling, and Jeppesen, 2006) and areas of calmer air may also be encountered (Sadrizadeh, Holmberg, and Tammelin, 2014). The influence of the lamp would be in accordance with the findings of Chow and Yang (2005), Brohus, Balling and Jeppesen (2006), Sadrizadeh, Holmberg and Tammelin (2014) and Aganovic *et al.* (2017), which all point to the presence and positioning of surgical lamps as one of the most influencing factors on the airflow distribution close to the patient.

6.1.3   Case 2 and 3

Case 2 and 3 investigated the airflow distribution in close proximity to the patient in an operating theatre with a LAF and a mixing system, respectively. It is evident when comparing the velocity contours for the two cases that the airflow distributions above the patient display different characteristics. The contours for the LAF system show a wide range of values in each velocity contour, with each contour demonstrating velocity differences of 0.10 m/s or more. In contrast to this do the velocity contours for Case 3 display smaller differences and the only contour with a difference of 0.10 m/s or more is found in Figure 5.17c, where the difference is 0.12 m/s. In addition, more extreme values occur in the contours of Case 2, where the minimum and maximum velocities are 0.06 and 0.32 m/s, respectively. The corresponding numbers for Case 3 are 0.11 and 0.26 m/s. There is also a difference in terms of airflow patterns shown in the velocity contours. The patterns clearly change from Scenario 2 through to Scenario 4 for each cross section in Case 3, whereas most contours in Case 2 maintain their shape over the same interval. The difference could be attributed to the design and objective of the two ventilation systems as a mixing system constantly stirs the air in the entire room, while the LAF system provides a constant and unidirectional airflow.

A common feature for both cases is that the velocity contours are drastically changed from Scenario 1 to Scenario 2 for each cross-section, indicating the influence of the thermal plume of the patient. However, the thermal plume of the patient appears to have a greater impact on the velocity in a LAF system than in a mixing system, as can be seen by comparing the difference between Scenario 1 and Scenario 2 for both cases. In principle, this could be explained by the fact that the supply airflow in a LAF system and the thermal plume arising from the patient cause air movement in opposite directions, thus lowering the total velocity. The airflow direction in Case 3 however, is impossible to determine due to the use of omnidirectional anemometers.

All of the velocity contours for Case 3 indicate that the changes from scenario to scenario, in terms of both values and pattern, principally occur below the height of 15 cm above the surface. This area also demonstrates large velocity differences, and the lowest velocities are always located here. The tendency of larger variations and of changes occurring below 15 cm, can also be spotted in the majority of the corresponding temperature and turbulence intensity contours for Case 3. However, exceptions from this tendency can be found in Figure 5.19c, Figure 5.19d and Figure 5.23b. The velocity contours for Case 2 show the same tendency as the corresponding contours in Case 3.

The surgical lamps impact the velocity contours for each cross-section in both Case 2 and 3. Compared to the corresponding contours for Scenario 3, all contours for Scenario 4 demonstrate increased velocities in general. For the velocity contours of Case 3, the airflow patterns also change significantly from Scenario 3 to 4. This impact could be caused by the light from the lamps since the lamps were positioned above the head and foot end of the operating table with the light focused on the pelvis area. As none of the lamps were upstream of the chest, waist or pelvis in Case 2, in which the direction of

the supply airflow is known, it seems more likely that the impact of the lamps could be related to the light rather than the lamps. In terms of turbulence intensity, the surgical lamps appear to have a calming effect on some of the cross-sections. The contours above the pelvis and waist for both cases, Figure 5.14d and Figure 5.23d, and Figure 5.15d and Figure 5.24d, demonstrate lower levels of turbulence compared to the preceding scenario. However, this effect can not be spotted in the contours above the chest in Figure 5.13d and 5.22d. The reason could be that the angle and height of the lamp above the head end caused light to pass only through the cross-sections above the waist and pelvis.

In terms of turbulence intensity, it can be seen from the results of Case 2 and 3 that the general level of turbulence is higher in Case 3 than in Case 2. The values in Case 3 span from 22 to 44 %, while the values in Case 2 range from 2.8 to 80 %. It should be noted that values above 35 % in Case 2 only appear in a small area above the pelvis in Figure 5.15b. As for turbulence intensity contours for Case 2, all demonstrate values way higher than the limit of 12.5 % which Karthikeyan and Samuel (2008) referred to as a high level of turbulence in an operating theatre. The difference between the two cases is most likely connected to the ventilation principles. A mixing system supplies air at high velocities and levels of turbulence, while a LAF system aims to provide an airflow with low levels of turbulence. The contours of Case 2 indicate that the airflow distribution is more likely to experience large changes of turbulence intensity with a LAF than with a mixing system.

The temperature contours in Case 3 do in general show higher temperatures than their counterparts in Case 2, even though the setpoint temperature was 22.0°C in both operating theatres. In Case 2, the temperatures in every contour are, except Figure 5.11d, around 22.0°C with no values equal to or above 23.0°C. On the other hand, a part of the temperature contours for Case 3 display values above 23.0°C. Especially in Scenario 3 and 4, the contours above the waist and pelvis for Case 3 show substantially higher values than the corresponding contours for Case 2, as can be seen comparing the mentioned contours in Figure 5.10 to Figure 5.20 and Figure 5.11 to Figure 5.21. This could indicate that a mixing system is less efficient than a LAF system when it comes to keeping the temperature of the air in close proximity to the patient, near the setpoint temperature in the room. The increased temperatures close to the patient could actually enhance the healing process, as they promote vasodilatation (Harper, Young and McNaught, 2014). On the other hand, some of the measured temperatures are outside the temperature range of 18-24 °C recommended by C.b.z (2004, cited in Nastase *et al.*, 2016) and D.D.G.f (2002, cited in Nastase *et al.*, 2016). The elevated temperatures for Scenario 3 and 4 in Case 3 could be related to the fact that the cylinders representing the surgical staff did not only supply additional heat, but also acted as hinders for the airflow and reduced the cooling capacity of the airflow.

Some of the temperature contours for Scenario 4, Figure 5.9d, Figure 5.10d and Figure 5.20d, display higher values near the top, which is most likely caused by light from the lamps hitting the sensors and thus elevating the temperature. The highest recorded temperatures for Case 2 and 3 were 23.6 and 26.0 °C, respectively. Both occurred closest to the patient in Scenario 4, as can be seen in Figure 5.11d and Figure 5.21d. The area around

the pelvis was illuminated by the lights, which most likely caused the cloth to absorb a part of the thermal radiation from the lamps and increase the local temperature.

6.2 Suggestions and guidance to design the airflow distribution in operating theatres

One of the task in the assignment text of this thesis was to provide suggestions and guidance to design the airflow distribution in operating theatres, and based on the experimental results from Case 2 and 3 will some suggestions be presented.

In a study by Lewis *et al.* (1969), the content of microorganisms in the human microenvironment was found to clearly exceed the levels found in ambient air. According to Memarzadeh and Manning (2002), the dominant way of bacteria transport during surgery is by the release of skin cells from uncovered parts of the team performing the surgery. The authors also claim that these cells are so small that they are transported not only by convection in an operating room, but also by diffusion caused by the turbulence (ibid.). Both these studies therefore indicate that the ventilation system should provide an airflow of clean, fresh air capable of swiftly removing airborne particles and bacteria.

The results from Case 2 indicated that the ventilation system of "Operasjonsstue 8" was unable to deliver an airflow that kept the air velocity close to the patient, above or equal to 0.20 m/s, as recommended in the HTM (Department of Health UK, 2007). They also demonstrated elevated levels of turbulence intensity in Scenario 2 to 4. Both the air velocity and turbulence intensity affect the convective heat loss of the wound (Murakami, Kato and Zeng, 1997). The results from Case 3 could indicate that the velocity and turbulence intensity distributions with a mixing system is less affected by thermal plumes than with a LAF system. The temperature contours for Case 3 on the other hand, demonstrated increased values, especially in Scenario 4.

Based on observations and analysis of the results from Case 2 and 3, it could be wise to take the influence of the patient, the surgical staff and surgical lamps into consideration during the design phase of the ventilation system. The same would be smart for the design of mixing systems. It is important to underline that their impacts both as heat sources and physical obstacles should be evaluated.

6.3 Practical limitations

The main objective of this thesis was to characterize the airflow distribution in close proximity to a patient in supine position in operating theatres with different ventilation systems, and it is important to underline that this thesis solely focused on the airflow distribution. Bacteria dispersion and measurements of bacteria were not a part of the objective, and consequently the results from cannot be used to establish a relation between SSIs and the measured airflow distributions. However, the experimental results from Case 2 and 3 can

contribute to a better understanding of the interaction between the ventilation system and the patient, surgical staff and surgical lamps, and how the airflow distribution close to the patient is affected.

Due to the use of omnidirectional anemometers do the results not show the direction of the airflows. For Case 2, the direction can be assumed as the direction of the supply airflow and the airflow inside the thermal plumes are opposite. The directions of the measured airflows in Case 3 on the other hand, are not obtainable from the measurement results. The fact that the anemometers have a lower range limit of 0.05 m/s, caused limitations for Case 1.

The thermal manikin and its heating system caused some limitations, as significant surface temperature differences were observed within small areas. This means that the reliability of the results was affected. The clothing of the thermal manikin also causes some limitations for the results in Case 2 and 3, as a patient during surgery is likely to expose areas of skin and tissue to the ambient air. A second limitation of the thermal manikin is the lack of breathing mechanisms, as airflows originating from breathing could affect the results. Besides the different ventilation systems, the two operating theatres in Case 2 and 3 were not identical, hence posing some limitations on the comparison of the airflow distributions caused by the two systems.

A major limitation in this thesis is the lack of information from previous studies. Many of the studies regarding ventilation of operating rooms were simulations based on computational fluid dynamics (CFD), and not experimental measurements. Most of them focused on LAF and studies on mixing systems in ORs were hard to find, making a complete comparison challenging. Studies on the thermal plume from a person in supine position were also hard to come by, as articles regarding the human thermal plume mainly focused on the plume from a sedentary or standing person. The surgical staff were simulated as metal cylinders and this imposes limitations on the assessment of the influence of the surgical staff. The reason for this is that the surgical staff could affect the airflow not only by their thermal plume, but also by their posture and activity.

6.4   Future work

The topic for this master thesis is a relatively new one and further work is needed before reliable conclusions can be drawn. Therefore, based on observations from the experiments and the results in this thesis, will the section provide a list of suggestions and recommendations for future work.

- Conduct measurements of the thermal plumes of humans in supine position with a larger sample of people and with numerous sensors, in order to develop a mathematical model of the thermal plume of a human in supine position.

- Use instruments with greater accuracy and with the capability of measuring velocities below 0.05 m/s. Also, instruments or techniques that can determine the direction

of the airflow, like Particle Image Velocimetry (PIV), should be used. This is especially relevant for operating theatres with mixing systems.

- The heating system of the thermal manikin should be improved. The system should be carefully designed in order to be able to keep the surface temperatures uniform over each regulated section, and the system should also include more sections for temperature control.

- Implement a breathing system for the manikin.

- Investigate and establish which levels of turbulence intensity that should be considered low, medium or high for mixing and LAF systems in operating theatres.

- Investigate and measure the airflow in an entire operating theatre equipped with a mixing system, in order to find out whether the airflow conditions actually are similar at all locations.

- Perform experiments in operating theatres with real humans and surgical staff in order to obtain more realistic and reliable results.

- Run measurement data through a Kalman filter in order to get more accurate data.

Chapter 7

Conclusion

This master thesis experimentally investigated the airflow distributions in close proximity to a human in supine position in two operating theatres with different ventilation systems; mixing and LAF systems. The thesis was structured into three main cases. The objective of Case 1 was to investigate the thermal plume above real humans in supine position and calibrate the settings of a thermal manikin according to the findings. Case 2 and 3 had similar objectives, but for different ventilation systems, as they both aimed at characterizing the airflow distribution in close proximity to a lying human body in an operating theatre.

Case 1 investigated the thermal plumes from humans in supine position in quiescent surroundings. From the results it appears that the centerline velocity varies depending on the cross sections above the body. Also, the results demonstrate individual differences among humans and that the standard deviations may increase with increasing height above the body. The highest mean velocity of 0.135 m/s indicates that the thermal plume of a human in supine position could affect the airflow distribution in a room. The comparison between the mathematical models and the measurement data indicates that a model of the human thermal plume should be based on measurements above real humans.

The results of Case 2 and 3 suggest that the airflow distributions alter following the addition of heat sources and physical obstacles. The measured velocities in Case 2 could imply that the LAF system was unable to suppress the impact of the heat sources as the measured values dropped. The velocity contours of Case 2 suggests that the laminar supply airflow may be decelerated by the thermal plumes, thus reducing the total velocity of the airflow and causing non-uniform conditions. Surgical lamps in Case 2 also proved to impact the airflow distribution downstream, as the airflow pattern changed and the levels of turbulence increased.

Results from both Case 2 and 3 suggest that the surgical lamps may increase airflow velocities and reduce levels of turbulence intensity in cross-sections where they are not positioned directly above the region. This impact should be investigated in future studies.

The results from Case 3 suggests that the levels of turbulence intensity are higher and that the airflow velocities are less affected by heat sources and obstacles for a mixing than a LAF system. Turbulence intensity values in Case 3 ranged from 22 to 44 %, while the velocities were between 0.11 and 0.26 m/s. The results from Case 3 demonstrate that the most significant changes from scenario to scenario took place within 15 cm above the surface of the manikin.

There are many uncertainties and limitations associated with the experiments. The most significant one is that the anemometers were unable to measure the direction of the airflow, which complicated the analysis of the results. Yet, some of the findings in this master thesis may prove valuable when designing ventilation systems for operating theatres.

Bibliography

Aganovic, A., Cao, G., Stenstad, L. and Skogås, J. (2017). Impact of surgical lights on the velocity distribution and airborne contamination level in an operating room with laminar airflow system. *Building and Environment*, 126, pp.42-53.

Agodi, A., Auxilia, F., Barchitta, M., Cristina, M., D'Alessandro, D., Mura, I., Nobile, M., Pasquarella, C., Avondo, S., Bellocchi, P., Canino, R., Capozzi, C., Casarin, R., Cavasin, M., Contegiacomo, P., Deriu, M., Evola, F., Farsetti, P., Grandi, A., Guareschi, D., Longhitano, A., Longo, G., Malatesta, R., Marenghi, P., Marras, F., Maso, A., Mattaliano, A., Montella, M., Moscato, U., Navone, P., Romeo, M., Rossi, F., Ruffino, M., Santangelo, C., Sartini, M., Sessa, G., Tardivo, S., Tranquilli Leali, P., Torregrossa, M. and Vitali, P. (2015). Operating theatre ventilation systems and microbial air contamination in total joint replacement surgery: results of the GISIO-ISChIA study. *Journal of Hospital Infection*, 90(3), pp.213-219.

Alsved, M., Civilis, A., Ekolind, P., Tammelin, A., Andersson, A., Jakobsson, J., Svensson, T., Ramstorp, M., Sadrizadeh, S., Larsson, P., Bohgard, M., Šantl-Temkiv, T. and Löndahl, J. (2018). Temperature-controlled airflow ventilation in operating rooms compared with laminar airflow and turbulent mixed airflow. *Journal of Hospital Infection*, 98(2), pp.181-190.

Andrew, M., Myhr, K. and Skulberg, A. (1997). *Retningslinjer for mikrobiologisk kontroll av luft i rom hvor det foretas operative inngrep og større invasive prosedyrer (operasjonsrom).* Statens helsetilsyn.

Arnesen, H. (2018). *vasodilatasjon - Store medisinske leksikon.* [online] Store norske leksikon. Available at: https://sml.snl.no/vasodilatasjon [Accessed 4 May 2018].

Aune, K. (2015). *Design, Commissioning and Testing of Operating Theatre Isolating Rooms in Norway.*

Bailly, C. and Comte-Bellot, G. (2015). *Turbulence.* Springer International Publishing.

Bischoff, P., Kubilay, N., Allegranzi, B., Egger, M. and Gastmeier, P. (2017). Effect of laminar airflow ventilation on surgical site infections: a systematic review and meta-analysis. *The Lancet Infectious Diseases*, 17(5), pp.553-561.

Blowers, R. and Crew, B. (1960). Ventilation of operating-theatres. *Journal of Hygiene*, 58(4), pp.427-448

Brohus, H., Balling, K. and Jeppesen, D. (2006). Influence of movements on contaminant transport in an operating room. *Indoor Air*, 16(5), pp.356-372.

Buchanan, C. and Dunn-Rankin, D. (1998). Transport of Surgically Produced Aerosols in an Operating Room. *AIHAJ*, 59(6), pp.393-402.

Cao, G., Storås, M., Aganovic, A., Stenstad, L. and Skogås, J. (2018). Do surgeons and surgical facilities disturb the clean air distribution close to a surgical patient in an orthopedic operating room with laminar airflow?. *American Journal of Infection Control*.

Chow, T., Lin, Z. and Bai, W. (2006). The Integrated Effect of Medical Lamp Position and Diffuser Discharge Velocity on Ultra-clean Ventilation Performance in an Operating Theatre. *Indoor and Built Environment*, 15(4), pp.315-331.

Chow, T. and Wang, J. (2012). Dynamic simulation on impact of surgeon bending movement on bacteria-carrying particles distribution in operating theatre. *Building and Environment*, 57, pp.68-80.

Chow, T. and Yang, X. (2005). Ventilation performance in the operating theatre against airborne infection: numerical study on an ultra-clean system. *Journal of Hospital Infection*, 59(2), pp.138-147.

Department of Health UK (2007). *Health Technical Memorandum 03-01: Specialised ventilation for healthcare premises. Part A - Design and installation*. Edinburgh: TSO.

Erichsen Andersson, A., Petzold, M., Bergh, I., Karlsson, J., Eriksson, B. and Nilsson, K. (2014). Comparison between mixed and laminar airflow systems in operating rooms and the influence of human factors: Experiences from a Swedish orthopedic center. *American Journal of Infection Control*, 42(6), pp.665-669.

Essex-Lopresti, M. (1999). Operating theatre design. *The Lancet*, 353(9157), pp.1007-1010.

Folkehelseinstituttet. (2016). *Infeksjoner etter kirurgi, NOIS-POSI 2015*.

French, G. and Cheng, A. (1991). Measurement of the costs of hospital infection by prevalence surveys. *Journal of Hospital Infection*, 18, pp.65-72.

Friberg, B. (1998). Ultraclean Laminar Airflow ORs. *AORN Journal*, 67(4), pp.841-851.

Friberg, B., Friberg, S. and Burman, L. (1996). Zoned vertical ultraclean operating room ventilation: A novel concept making long side walls unnecessary. *Acta Orthopaedica Scandinavica*, 67(6), pp.578-582.

Goodfellow, H. and Tähti, E. (2001). *Industrial ventilation design guidebook*. San Diego: United States: Academic Press.

Haley, R., Schaberg, D., Crossley, K., Von Allmen, S. and McGowan, J. (1981). Extra charges and prolongation of stay attributable to nosocomial infections: A prospective interhospital comparison. *The American Journal of Medicine*, 70(1), pp.51-58.

Harper, D., Young, A. and McNaught, C. (2014). The physiology of wound healing. *Surgery (Oxford)*, 32(9), pp.445-450.

Incropera, F., Dewitt, D., Bergman, T. and Lavine, A. (2013). *Principles of heat and mass transfer*. 7th ed. Singapore: John Wiley Sons.

Kaoutar, B., Joly, C., L'Hériteau, F., Barbut, F., Robert, J., Denis, M., Espinasse, F., Merrer, J., Doit, C., Costa, Y., Daumal, F., Blanchard, H., Eveillard, M., Botherel, A., Brücker, G. and Astagneau, P. (2004). Nosocomial infections and hospital mortality: a multicentre epidemiological study. *Journal of Hospital Infection*, 58(4), pp.268-275.

Karthikeyan, C. and Samuel, A. (2008). CO2-dispersion studies in an operation theatre under transient conditions. *Energy and Buildings*, 40(3), pp.231-239.

KLS Martin Group (2008). *Operating lights: marLED® with VariLUX and Outstanding and LED light of the 2nd and generation*. [ebook] Available at: http://www.kebomed.no/files/155/kls_martin_marled_v10_og_v16.pdf [Accessed 25 May 2018].

Kondrashov, A., Sboev, I. and Dunaev, P. (2016). Evolution of convective plumes adjacent to localized heat sources of various shapes. *International Journal of Heat and Mass Transfer*, 103, pp.298-304.

Kruse, C., Nuutila, K., Lee, C., Kiwanuka, E., Singh, M., Caterson, E., Eriksson, E. and Sørensen, J. (2015). The external microenvironment of healing skin wounds. *Wound Repair and Regeneration*, 23(4), pp.456-464.

Kurazumi, Y., Tsuchikawa, T., Ishii, J., Fukagawa, K., Yamato, Y. and Matsubara, N. (2008a). Radiative and convective heat transfer coefficients of the human body in natural convection. *Building and Environment*, 43(12), pp.2142-2153.

Kurazumi, Y., Tsuchikawa, T., Matsubara, N. and Horikoshi, T. (2004). Convective heat transfer area of the human body. *European Journal of Applied Physiology*, 93(3), pp.273-285.

Kurazumi, Y., Tsuchikawa, T., Matsubara, N. and Horikoshi, T. (2008b). Effect of posture on the heat transfer areas of the human body. *Building and Environment*, 43(10), pp.1555-1565.

Lewis, H., Foster, A., Mullan, B., Cox, R. and Clark, R. (1969). AERODYNAMICS OF THE HUMAN MICROENVIRONMENT. *The Lancet*, 293(7609), pp.1273-1277.

Lidwell, O. (1981). Airborne bacteria and surgical infection. *The American Journal of Medicine*, 70(3), pp.693-697.

Lidwell, O., Lowbury, E., Whyte, W., Blowers, R., Stanley, S. and Lowe, D. (1982). Effect of ultraclean air in operating rooms on deep sepsis in the joint after total hip or knee replacement: a randomised study. *BMJ*, 285(6334), pp.10-14.

Lister, J. (1867). On the Antiseptic Principle of the Practice of Surgery. *The Lancet*, 90(2299), pp.353-356.

McHugh, S., Hill, A. and Humphreys, H. (2015). Laminar airflow and the prevention of surgical site infection. More harm than good?. *The Surgeon*, 13(1), pp.52-58.

Memarzadeh, F. and Manning, A. (2002). Comparison of operating room ventilation systems in the protection of the surgical site. *ASHRAE Transactions*, 108(2), pp.3-15.

Murakami, S., Kato, S. and Zeng, J. (1997). Flow and temperature fields around human body with various room air distribution, Part 1 - CFD study on computational thermal manikin. *ASHRAE Transactions*, 103(1), pp.3-15.

Nastase, I., Croitoru, C., Vartires, A. and Tataranu, L. (2016). Indoor Environmental Quality in Operating Rooms: An European Standards Review with Regard to Romanian Guidelines. *Energy Procedia*, 85, pp.375-382.

Nilsson, P. (2003). *Achieving the desired indoor climate*. Lund: Studentlitteratur.

Novakovic, V., Hanssen, S., Thue, J., Wangensteen, I. and Gjerstad, F. (2014). *ENØK i bygninger: effektiv energibruk*. 3rd ed. Gyldendal undervisning.

Poggio, J. (2013). Perioperative Strategies to Prevent Surgical-Site Infection. *Clinics in Colon and Rectal Surgery*, 26(03), pp.168-173.

Rezapoor, M., Alvand, A., Jacek, E., Paziuk, T., Maltenfort, M. and Parvizi, J. (2018). Operating Room Traffic Increases Aerosolized Particles and Compromises the Air Quality: A Simulated Study. *The Journal of Arthroplasty*, 33(3), pp.851-855.

Chris Rousseau, P. (2011). *Health Care Standard Update - Innovation - Newcomb Boyd*. [online] Newcomb-boyd.com. Available at: http://www.newcomb-boyd.com/publications-presentations-seminar-notes/health-care-standard-update/ [Accessed 2 Mar. 2018].

Sadrizadeh, S. and Holmberg, S. (2014). Surgical clothing systems in laminar airflow operating room: a numerical assessment. *Journal of Infection and Public Health*, 7(6), pp.508-516.

Sadrizadeh, S., Holmberg, S. and Tammelin, A. (2014). A numerical investigation of vertical and horizontal laminar airflow ventilation in an operating room. *Building and Environment*, 82, pp.517-525.

Sadrizadeh, S., Tammelin, A., Ekolind, P. and Holmberg, S. (2014). Influence of staff number and internal constellation on surgical site infection in an operating room. *Particuology*, 13, pp.42-51.

Scalise, A., Bianchi, A., Tartaglione, C., Bolletta, E., Pierangeli, M., Torresetti, M., Marazzi, M. and Di Benedetto, G. (2015). Microenvironment and microbiology of skin wounds: the role of bacterial biofilms and related factors. *Seminars in Vascular Surgery*, 28(3-4), pp.151-159.

Scaltriti, S., Cencetti, S., Rovesti, S., Marchesi, I., Bargellini, A. and Borella, P. (2007). Risk factors for particulate and microbial contamination of air in operating theatres. *Journal of Hospital Infection*, 66(4), pp.320-326.

Skåret, E. (2000) *Ventilasjonsteknisk håndbok.* Oslo: Norges byggforskningsinstitutt.

Smith, E., Raphael, I., Maltenfort, M., Honsawek, S., Dolan, K. and Younkins, E. (2013). The Effect of Laminar Air Flow and Door Openings on Operating Room Contamination. *The Journal of Arthroplasty*, 28(9), pp.1482-1485.

Stacey, A. and Humphreys, H. (2002). A UK historical perspective on operating theatre ventilation. *Journal of Hospital Infection*, 52(2), pp.77-80.

Storås, M.C.A. (2017) *Characterization of the airflow distribution in close proximity to a patient in operating rooms with laminar airflow at St. Olavs Hospital.* Master thesis. Norwegian University of Science and Technology.

Tammelin, A., Ljungqvist, B. and Reinmüller, B. (2012). Comparison of three distinct surgical clothing systems for protection from air-borne bacteria: A prospective observational study. *Patient Safety in Surgery*, 6(1), p.23.

Vranckx, J., Slama, J., Preuss, S., Perez, N., Svensjø, T., Visovatti, S., Breuing, K., Bartlett, R., Pribaz, J., Weiss, D. and Eriksson, E. (2002). Wet Wound Healing. *Plastic and Reconstructive Surgery*, 110(7), pp.1680-1687.

Weinstein, R. and Bonten, M. (2017). Laminar airflow and surgical site infections: the evidence is blowing in the wind. *The Lancet Infectious Diseases*, 17(5), pp.472-473.

Whyte, W., Hodgson, R. and Tinkler, J. (1982). The importance of airborne bacterial contamination of wounds. *Journal of Hospital Infection*, 3(2), pp.123-135.

Yu, C., Lin, C. and Yang, Y. (2010). Human body surface area database and estimation formula. *Burns*, 36(5), pp.616-629.

Zoon, W., Loomans, M. and Hensen, J. (2011). Testing the effectiveness of operating room ventilation with regard to removal of airborne bacteria. *Building and Environment*, 46(12), pp.2570-2577.

Zukowska, D., Popiolek, Z. and Melikov, A. (2010). Determination of the integral characteristics of an asymmetrical thermal plume from air speed/velocity and temperature measurements. *Experimental Thermal and Fluid Science*, 34(8), pp.1205-1216.

Appendix

A.1 Risk assessment for the master thesis

Enhet: Fremtidens operasjonsrom, St. Olavs hospital

Linjeleder: Jan Gunnar Skogås

Deltakere ved kartleggingen (m/ funksjon)**: Ansvarlig veileder Guangyu Cao, medveileder Liv-Inger Stenstad, medveileder Jan Gunnar Skogås, student Anders Mostrøm Nilssen**
(Ansv. veileder, student, evt. medveiledere, evt. andre m. kompetanse)

Kort beskrivelse av hovedaktivitet/hovedprosess: Masteroppgave student Anders Mostrøm Nilssen. Tittel på oppgave: Characterization of the airflow distribution in close proximity to the patient in an operating room

Er oppgaven rent teoretisk? (JA/NEI): **Nei** *«JA» betyr at veileder innestår for at oppgaven ikke inneholder noen aktiviteter som krever risikovurdering. Dersom «JA»: Beskriv kort aktiviteten i kartleggingsskjemaet under. Risikovurdering trenger ikke å fylles ut.*

Signaturer: Ansvarlig veileder: Student:

Dato: 26.01.18

ID nr.	Aktivitet/prosess	Ansvarlig	Eksisterende dokumentasjon	Eksisterende sikringstiltak	Lov, forskrift o.l.	Kommentar
	Feltmålinger med pasient	Guangyu Cao	Risk Assessment Report: Thermal plume experiment (pdf)	Mikrobiologisk kontrol av luft i operasjonsstuer (pdf)	Forskrift om smittevern i helsetjenesten	
	Feltmålinger uten pasient	Guangyu Cao	Risk Assessment Report: Thermal plume experiment (pdf)	Mikrobiologisk kontroll av luft i operasjonsstuer (pdf)	Forskrift om smittevern i helsetjenesten	

NTNU
HMS

Risikovurdering

	Utarbeidet av	Nummer	Dato
	HMS-avd.	HMSRV2603	22.03.2011
	Godkjent av		Erstatter
	Rektor		01.12.2006

Enhet: Fremtidens operasjonsrom, St. Olavs hospital   **Dato: 26.01.18**

Linjeleder: Jan Gunnar Skogås

Deltakere ved kartleggingen (m/ funksjon): Ansvarlig veileder Guangyu Cao, medveileder Liv-Inger Stenstad, medveileder Jan Gunnar Skogås, student Anders Mostrøm Nilssen

(Ansv. Veileder, student, evt. medveiledere, evt. andre m. kompetanse)

Risikovurderingen gjelder hovedaktivitet: Masteroppgave student Anders Mostrøm Nilssen. Tittel på oppgave: Characterization of the airflow distribution in close proximity to the patient in an operating room

Signaturer: *Ansvarlig veileder:*   *Student:*

ID nr	Aktivitet fra kartleggings-skjemaet	Mulig uønsket hendelse/ belastning	Vurdering av sannsyn-lighet (1-5)	Vurdering av konsekvens:				Risiko-Verdi (menn-eske)	Kommentarer/status Forslag til tiltak
				Menneske (A-E)	Ytre miljø (A-E)	Øk/ materiell (A-E)	Om-dømme (A-E)		
	Feltmålinger med pasient	Ingen	1	A	A	A	A	A1	Denne studien medfører ingen risiko for pasient, ansatte, utstyr eller materiale
	Feltmålinger uten pasient	Ingen	1	A	A	A	A	A1	Denne studien medfører ingen risiko for pasient, ansatte, utstyr eller materiale

NTNU		Utarbeidet av	Nummer	Dato
HMS	Risikovurdering	HMS-avd.	HMSRV2603	22.03.2011
		Godkjent av		Erstatter
		Rektor		01.12.2006

Sannsynlighet vurderes etter følgende kriterier:

Svært liten 1	Liten 2	Middels 3	Stor 4	Svært stor 5
1 gang pr 50 år eller sjeldnere	1 gang pr 10 år eller sjeldnere	1 gang pr år eller sjeldnere	1 gang pr måned eller sjeldnere	Skjer ukentlig

Konsekvens vurderes etter følgende kriterier:

Gradering	Menneske	Ytre miljø Vann, jord og luft	Øk/materiell	Omdømme
E Svært Alvorlig	Død	Svært langvarig og ikke reversibel skade	Drifts- eller aktivitetsstans >1 år.	Troverdighet og respekt betydelig og varig svekket
D Alvorlig	Alvorlig personskade. Mulig uførhet.	Langvarig skade. Lang restitusjonstid	Driftsstans > ½ år Aktivitetsstans i opp til 1 år	Troverdighet og respekt betydelig svekket
C Moderat	Alvorlig personskade.	Mindre skade og lang restitusjonstid	Drifts- eller aktivitetsstans < 1 mnd	Troverdighet og respekt svekket
B Liten	Skade som krever medisinsk behandling	Mindre skade og kort restitusjonstid	Drifts- eller aktivitetsstans < 1uke	Negativ påvirkning på troverdighet og respekt
A Svært liten	Skade som krever førstehjelp	Ubetydelig skade og kort restitusjonstid	Drifts- eller aktivitetsstans < 1dag	Liten påvirkning på troverdighet og respekt

Risikoverdi = Sannsynlighet x Konsekvens
Beregn risikoverdi for Menneske. Enheten vurderer selv om de i tillegg vil beregne risikoverdi for Ytre miljø, Økonomi/materiell og Omdømme. I så fall beregnes disse hver for seg.

Til kolonnen "Kommentarer/status, forslag til forebyggende og korrigerende tiltak":
Tiltak kan påvirke både sannsynlighet og konsekvens. Prioriter tiltak som kan forhindre at hendelsen inntreffer, dvs. sannsynlighetsreduserende tiltak foran skjerpet beredskap, dvs. konsekvensreduserende tiltak.

NTNU [logo] HMS/KS	Risikomatrise	utarbeidet av HMS-avd.	Nummer HMSRV2604	Dato 08.03.2010
		godkjent av Rektor	Erstatter	09.02.2010

MATRISE FOR RISIKOVURDERINGER ved NTNU

KONSEKVENS	Svært alvorlig	E1	E2	E3	E4	E5
	Alvorlig	D1	D2	D3	D4	D5
	Moderat	C1	C2	C3	C4	C5
	Liten	B1	B2	B3	B4	B5
	Svært liten	A1	A2	A3	A4	A5
		Svært liten	Liten	Middels	Stor	Svært stor
				SANNSYNLIGHET		

Prinsipp over akseptkriterium. Forklaring av fargene som er brukt i risikomatrisen.

Farge	Beskrivelse
Rød	Uakseptabel risiko. Tiltak skal gjennomføres for å redusere risikoen.
Gul	Vurderingsområde. Tiltak skal vurderes.
Grønn	Akseptabel risiko. Tiltak kan vurderes ut fra andre hensyn.

A.2 Assessment from NSD

NSD

Guangyu Cao
Realfagbygget E1-145, Høgskoleringen 5
7491 TRONDHEIM

Vår dato: 26.04.2018   Vår ref: 60169 / 3 / LT   Deres dato: Deres ref:

Forenklet vurdering fra NSD Personvernombudet for forskning

Vi viser til melding om behandling av personopplysninger, mottatt 04.04.2018.
Meldingen gjelder prosjektet:

60169	Characterization of the airflow distribution in close proximity to the patient in an operating room
Behandlingsansvarlig	NTNU, ved institusjonens øverste leder
Daglig ansvarlig	Guangyu Cao
Student	Anders Moström Nilssen

Vurdering
Etter gjennomgang av opplysningene i meldeskjemaet med vedlegg, vurderer vi at prosjektet er omfattet
av personopplysningsloven § 31. Personopplysningene som blir samlet inn er ikke sensitive, prosjektet er
samtykkebasert og har lav personvernulempe. Prosjektet har derfor fått en forenklet vurdering. Du kan
gå i gang med prosjektet. Du har selvstendig ansvar for å følge vilkårene under og sette deg inn i
veiledningen i dette brevet.

Vilkår for vår vurdering
Vår anbefaling forutsetter at du gjennomfører prosjektet i tråd med:
- opplysningene gitt i meldeskjemaet
- krav til informert samtykke
- at du ikke innhenter sensitive opplysninger
- veiledning i dette brevet
- NTNU sine retningslinjer for datasikkerhet

Veiledning

Krav til informert samtykke
Utvalget skal få skriftlig og/eller muntlig informasjon om prosjektet og samtykke til deltakelse.
Informasjon må minst omfatte:
- at NTNU er behandlingsansvarlig institusjon for prosjektet
- daglig ansvarlig (eventuelt student og veileders) sine kontaktopplysninger
- prosjektets formål og hva opplysningene skal brukes til

Dokumentet er elektronisk produsert og godkjent ved NSDs rutiner for elektronisk godkjenning.

- hvilke opplysninger som skal innhentes og hvordan opplysningene innhentes
- når prosjektet skal avsluttes og når personopplysningene skal anonymiseres/slettes

På nettsidene våre finner du mer informasjon og en veiledende mal for informasjonsskriv.

Forskningsetiske retningslinjer
Sett deg inn i forskningsetiske retningslinjer.

Meld fra hvis du gjør vesentlige endringer i prosjektet
Dersom prosjektet endrer seg, kan det være nødvendig å sende inn endringsmelding. På våre nettsider finner du svar på hvilke endringer du må melde, samt endringsskjema.

Opplysninger om prosjektet blir lagt ut på våre nettsider og i Meldingsarkivet
Vi har lagt ut opplysninger om prosjektet på nettsidene våre. Alle våre institusjoner har også tilgang til egne prosjekter i Meldingsarkivet.

Vi tar kontakt om status for behandling av personopplysninger ved prosjektslutt
Ved prosjektslutt 16.06.2018 vil vi ta kontakt for å avklare status for behandlingen av personopplysninger.

Gjelder dette ditt prosjekt?

Dersom du skal bruke databehandler
Dersom du skal bruke databehandler (ekstern transkriberingsassistent/spørreskjemaleverandør) må du inngå en databehandleravtale med vedkommende. For råd om hva databehandleravtalen bør inneholde, se Datatilsynets veileder.

Hvis utvalget har taushetsplikt
Vi minner om at noen grupper (f.eks. opplærings- og helsepersonell/forvaltningsansatte) har taushetsplikt. De kan derfor ikke gi deg identifiserende opplysninger om andre, med mindre de får samtykke fra den det gjelder.

Dersom du forsker på egen arbeidsplass
Vi minner om at når du forsker på egen arbeidsplass må du være bevisst din dobbeltrolle som både forsker og ansatt. Ved rekruttering er det spesielt viktig at forespørsel rettes på en slik måte at frivilligheten ved deltakelse ivaretas.

Se våre nettsider eller ta kontakt med oss dersom du har spørsmål. Vi ønsker lykke til med prosjektet!

Vennlig hilsen

Marianne Høgetveit Myhren

Lis Tenold

Kontaktperson: Lis Tenold tlf: 55 58 33 77 / lis.tenold@nsd.no
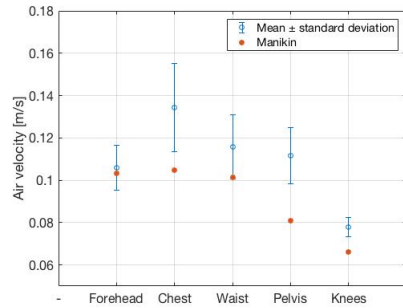
A.3 Results

A.3.1 Case 1

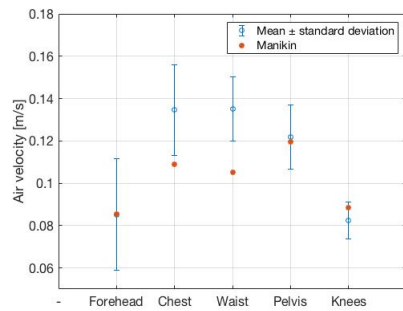**Figure A.1:** Centerline velocities 15 cm including knees

Figure A.2: Centerline velocities 25 cm including knees

A.3.2 Case 2

Velocity distribution above knees

Figure A.3 presents the velocity contours above the knees for case 2. Figure A.3a displays a velocity range of 0.10-0.15 m/s, where the lowest values can be found near the bottom left corner and the highest in the top right corner. The contour in figure A.3b is divided diagonally with a large area of low, almost identical values in the left bottom half, while the upper right half shows a larger variation. The minimum velocity of 0.06 m/s and can be found at a table width of 36 cm, and the velocities range from from 0.06 to 0.16 m/s.

The contour in figure A.3c is dominated by a large area of equal velocity stretching diagonally towards the top left corner. The area has a velocity of 0.07 m/s, which is the minimum value in the figure, and layers around it shows increasing values with distance. In terms of range, does the values lie between 0.07 and 0.15 m/s. Figure A.3d demonstrates a pattern where the lowest velocity is found near the bottom right corner, and a large area with a velocity of 0.16 m/s stretching diagonally across the plot. The range is 0.10-0.22 m/s.
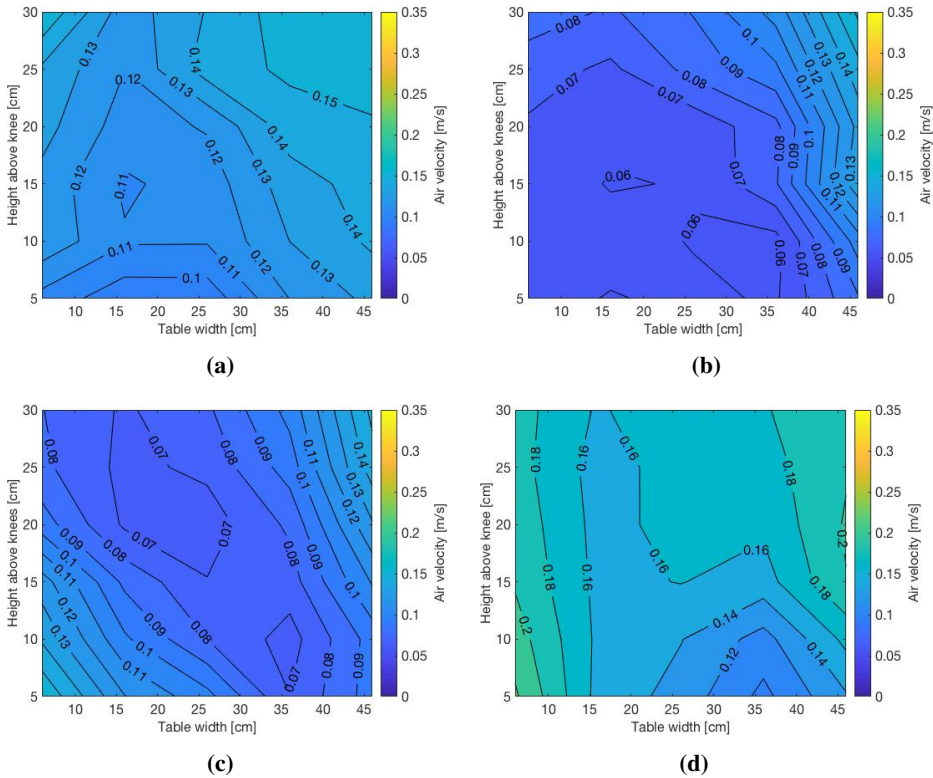
Figure A.3: Case 2: Velocity contours above the knees

Temperature distribution above knees

The contours above the knees are displayed in figure A.4. Figure A.4a shows the temperature field above an empty operating table and the temperature variations in this plot are very small, with temperatures ranging from 21.52 to 21.70 °C. All figures in A.4 shows a tendency of higher values to the left and lower to the right.

The highest temperatures in both figure A.4b and A.4c occurs closest to the patient, and the temperatures range from 21.90 to 22.50 and from 21.95 to 22.30 °C, respectively. The pattern in figure A.4d is characterized by higher values in the top half of the contour, with the maximum temperature being located at the top centre. The temperatures vary between 21.90 to 22.50 °C.

(a)

(b)

(c)
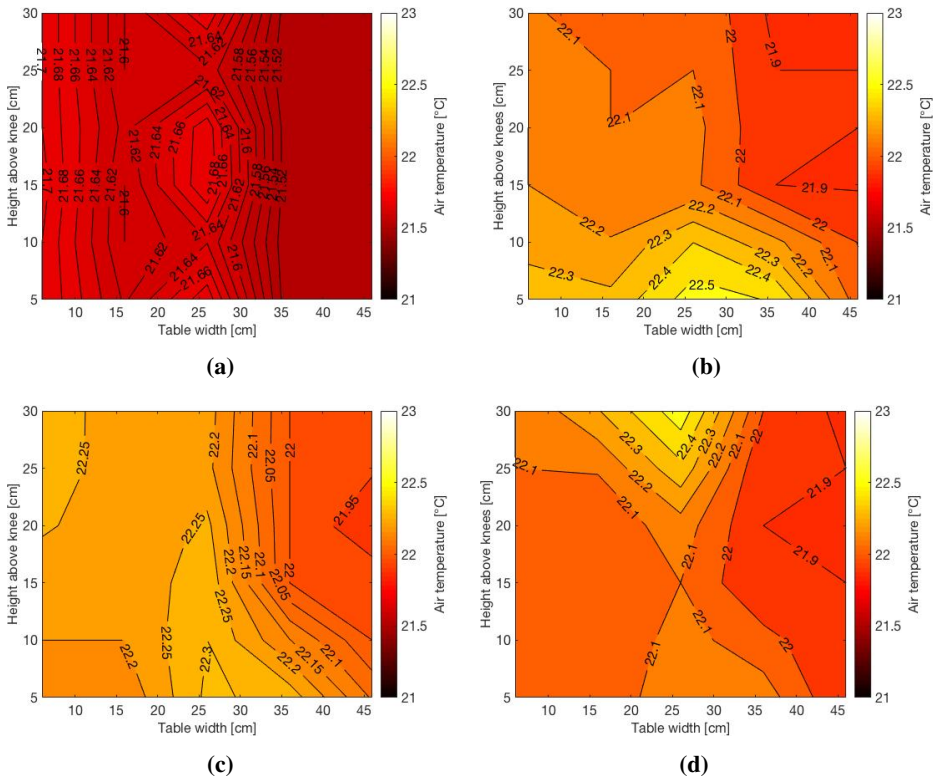
(d)

Figure A.4: Case 2: Temperature contours above the knees

Turbulence intensity distribution above knees

The turbulence intensity contours above the knees are presented in figure A.5. The results from the measurements above an empty operating table are shown in figure A.5a. The values range from 4 to 22 %, with the highest values occurring in the left part and the lowest values in the right part of the contour. Figure A.5b displays highest values at the bottom, while the left part features the highest mean value. Also, the range of the colour bar spans from 10 to 70 %.

The pattern in figure A.5c demonstrates an area of elevated levels stretching diagonally across the contour, from the bottom right to the top left corner. The area features three peaks, all with a value of 35 %. The values in the plot range from 10 to 35 %. The values in figure A.5d range from 6 to 20 %, and the contour displays a profile where the majority of the values are closer to the lower end of the range. The highest values are found close to the patient near the bottom right corner.
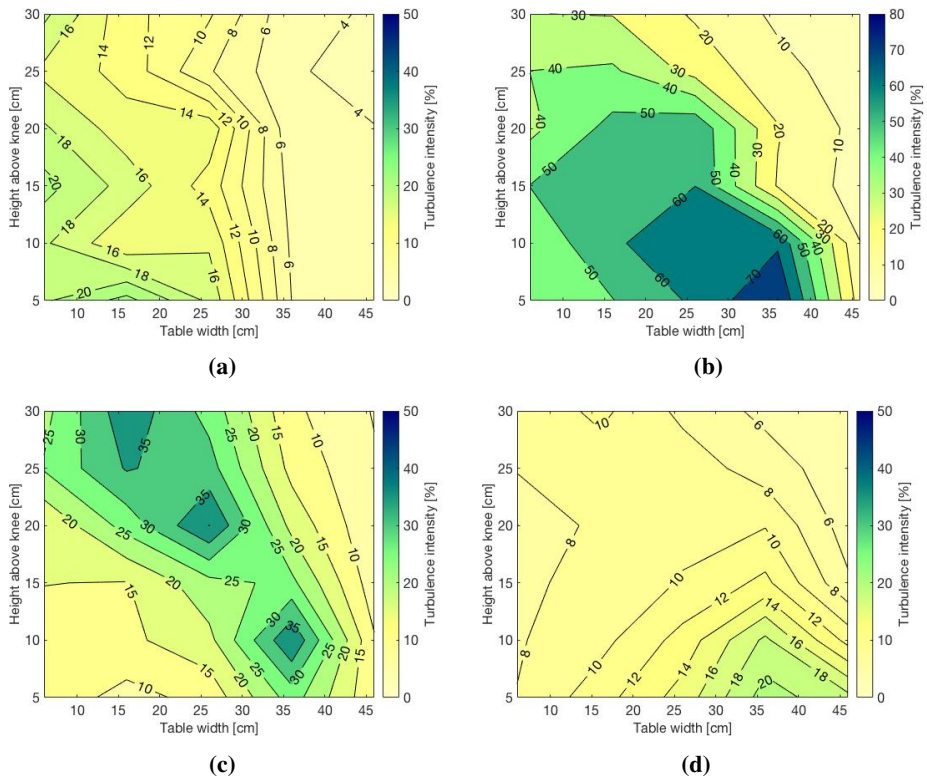

(a)

(b)

(c)

(d)

Figure A.5: Case 2: Turbulence intensity contours above the knees

A.4 Risk assessment for thermal plume experiment

A.4.1 Risk Assessment report

NTNU   **SINTEF**

Risk Assessment Report

Thermal plume experiment

Prosjektnavn	Characterization of the airflow distribution in close proximity to the patient in an operating room
Apparatur	Klimarom, VVS-lab
Enhet	NTNU
Apparaturansvarlig	Guangyu Cao
Prosjektleder	Guangyu Cao
HMS-koordinator	Morten Grønli
HMS-ansvarlig (linjeleder)	Terese Løvås
Plassering	Klimarom, Varmetekniske laboratorier
Romnummer	C247C, 2. etg i klimalab, Varmetekniske laboratorier
Risikovurdering utført av	

Approval:

Apparatur kort (UNIT CARD) valid for:	6 månader
Forsøk pågår kort (EXPERIMENT IN PROGRESS) valid for:	6 månader

Rolle	Navn	Dato	Signatur
Prosjektleder	Guangyu Cao	18.1.2018	Gm Cao
HMS koordinator	Morten Grønli		
HMS ansvarlig (linjeleder)	Terese Løvås		

NTNU

SINTEF

TABLE OF CONTENTS

◼ NTNU   **◉ SINTEF**

1   INTRODUCTION

The purpose of the experiment is to investigate the thermal plume rising from a supine occupant.

The experiment will be performed in several steps:
   i.   Calibrating the anemometers.
   ii.   Measurements of the air velocity above the thermal manikin.
   iii.   Measurements of the air velocity above a living human.

2   ORGANISATION

Rolle	
Prosjektleder	Guangyu Cao
Apparaturansvarlig	Guangyu Cao
Romansvarlig	Lars Konrad Sørensen
HMS koordinator	Morten Grønli
HMS ansvarlig (linjeleder):	Terese Løvås

3   RISK MANAGEMENT IN THE PROJECT

Hovedaktiviteter risikostyring	Nødvendige tiltak, dokumentasjon	DATE
Prosjekt initiering	Prosjekt initiering mal	21.08.17
Veiledningsmøte Guidance Meeting	Skjema for Veiledningsmøte med pre-risikovurdering	22.09.17
Innledende risikovurdering Initial Assessment	Fareidentifikasjon – HAZID Skjema grovanalyse	22.09.17
Vurdering av teknisk sikkerhet Evaluation of technical security	Prosess-HAZOP Tekniske dokumentasjoner	03.11.17
Vurdering av operasjonell sikkerhet Evaluation of operational safety	Prosedyre-HAZOP Opplæringsplan for operatører	
Sluttvurdering, kvalitetssikring Final assessment, quality assurance	Uavhengig kontroll Utstedelse av apparaturkort Utstedelse av forsøk pågår kort	

4 DESCRIPTIONS OF EXPERIMENTAL SETUP

The setup of the experiment will be as shown in figure 1. The air velocity will be measured above the thermal manikin/living human.
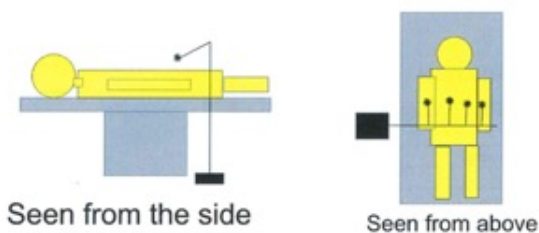
Figure 1: Setup for the experiment at C247C.

The air velocity will be measured close to the thermal manikin/living human, without ventilation. The manikin is fitted with a heating cable, and the heat load of the cable can be adjusted by dimmers.

List of instruments:
- Anemometer
- Thermal manikin

5 EVACUATION FROM THE EXPERIMENTAL AREA

Evacuate at signal from the alarm system or local gas alarms with its own local alert with sound and light outside the room in question, see 6.2

Evacuation from the rigging area takes place through the marked emergency exits to the assembly point, (corner of Old Chemistry Kjelhuset or parking 1a-b.)

Action on rig before evacuation:
The power to the thermal manikin and the exhaust fan should be turned off in case of evacuation.

2

◻ NTNU   **◯ SINTEF**

6   WARNING

6.1   Before experiments

Send an e-mail with information about the planned experiment to:
iept-experiments@ivt.ntnu.no

The e-mail must include the following information:
* Name of responsible person:
* Experimental setup/rig:
* Start Experiments: (date and time)
* Stop Experiments: (date and time)

You must get the approval back from the laboratory management before start up. All
running experiments are notified in the activity calendar for the lab to be sure they are
coordinated with other activity.

6.2   Abnormal situation

FIRE
If you are NOT able to extinguish the fire, activate the nearest fire alarm and evacuate area.
Be then available for fire brigade and building caretaker to detect fire place.
If possible, notify:

NTNU	SINTEF
Morten Grønli, Mob: 918 97 515	Harald Mæhlum, Mob: 930 14 986
Terese Løvås: Mob: 918 97 007	Petter Røkke, Mob: 901 20 221
NTNU – SINTEF Beredskapstelefon	800 80 388

GAS ALARM
If a gas alarm occurs, close gas bottles immediately and ventilate the area. If the level of the
gas concentration does not decrease within a reasonable time, activate the fire alarm and
evacuate the lab. Designated personnel or fire department checks the leak to determine
whether it is possible to seal the leak and ventilate the area in a responsible manner.

Alert Order is in the above paragraph.

PERSONAL INJURY
* First aid kit in the fire / first aid stations
* Shout for help
* Start life-saving first aid
* CALL 113 if there is any doubt whether there is a serious injury

OTHER ABNORMAL SITUATIONS

NTNU:
You will find the reporting form for non-conformance on:
https://innsida.ntnu.no/wiki/-/wiki/Norsk/Melde+avvik

SINTEF:

3

7 ASSESSMENT OF TECHNICAL SAFETY

7.1 HAZOP

See Chapter 13 "Guide to the report template".

The experiment set up is divided into the following nodes:

Node 1	Test rig in Klimalab
Node 2	

Attachments, Form: Hazop_mal
Conclusion: (Safety taken care of)

7.2 Flammable, reactive and pressurized substances and gas

Are any flammable, reactive and pressurized substances and gases in use?

YES	Explosion document has to be made and/or documented pressure test, (See 8.3)
NO	NO

Attachments: EX zones?
Conclusion:

7.3 Pressurized equipment

Is any pressurized equipment in use?

YES	The equipment has to undergo pressure testes in accordance with the norms and be documented
NO	NO

Attachments: Certificate for pressurized equipment (see Attachment to Risk Assessment)
Conclusion:

7.4 Effects on the environment (emissions, noise, temperature, vibration, smell)

Will the experiments generate emission of smoke, gas, odour or unusual waste?
Is there a need for a discharge permit, extraordinary measures?

YES	
NO	NO

Attachments:
Conclusion:

7.5 Radiation

See Chapter 13 "Guide to the report template".

YES	Radiation Sources need to have an own risk assessment
NO	NO

4

Attachments:
Conclusion:

7.6 Chemicals

Will any chemicals or other harmful substances be used in the experiments? Describe how the chemicals should be handled (stored, disposed, etc.) Evaluate the risk according to safety datasheets, MSDS. Is there a need for protective actions given in the operational procedure?

YES	Do a risk assessment of the use
NO	NO

Attachments: MSDS
Conclusion:

7.7 Electricity safety (deviations from the norms/standards)

YES	Electricity safety has to be assessed
NO	NO

Attachments:
Conclusion:

8   ASSESSMENT OF OPERATIONAL SAFETY

Ensure that the procedures cover all identified risk factors that must be taken care of. Ensure that the operators and technical performance have sufficient expertise.

8.1   Procedure HAZOP

See Chapter 13 "Guide to the report template".
The method is a procedure to identify causes and sources of danger to operational problems.

Attachments:: HAZOP_MAL_Prosedyre

8.2   Operation procedure and emergency shutdown procedure

See Chapter 13 "Guide to the report template".
The operating procedure is a checklist that must be filled out for each experiment.
Emergency procedure should attempt to set the experiment set up in a harmless state by unforeseen events.

Attachments: Procedure for running experiments
Emergency shutdown procedure:

5

8.3 Training of operators

A Document showing training plan for operators
- *What are the requirements for the training of operators?*
- *What it takes to be an independent operator*
- *Job Description for operators*

Attachments: Training program for operators

8.4 Technical modifications

- *Technical modifications made by the operator (e.g.Replacement of components, equal to equal)*
- *Technical modifications that must be made by Technical staff (for example, modification of pressure equipment).*
- *What technical modifications give a need for a new risk assessment(by changing the risk picture)?*

Conclusion:

8.5 Personal protective equipment

- *It is mandatory use of eye protection in the rig zone*
- *It is mandatory use of protective shoes in the rig zone.*
- *Use gloves when there is opportunity for contact with hot/cold surfaces.*
- *Use of respiratory protection apparatus*

Conclusion:

8.6 General Safety

- *The area around the staging attempts shielded.*
- *Gantry crane and truck driving should not take place close to the experiment.*
- *Gas cylinders shall be placed in an approved carrier with shut-off valve within easy reach.*
- *Monitoring, can experiment run unattended, how should monitoring be?*

8.7 Safety equipment

- *Have portable gas detectors to be used during test execution?*
- *Warning signs, see the Regulations on Safety signs and signaling in the workplace*

8.8 Special predations

For example:
- *Monitoring.*
- *Safety preparedness.*
- *Safe Job Analysis of modifications, (SJA)*
- *Working at heights*
- *Flammable / toxic gases or chemicals*

◉ NTNU   **◉ SINTEF**

9   QUANTIFYING OF RISK - RISK MATRIX

The risk matrix will provide visualization and an overview of activity risks so that
management and users get the most complete picture of risk factors.

IDnr	Aktivitet-hendelse	Frekv-Sans	Kons	RV
xx	Rotating shaft, sanger of contact	1	C1	
	Much noise, people without protective gear enter the rig site	1	B1	

Conclusion: The *Participants has to make a comprehensive assessment to determine whether the
remaining risks of the activity/process is acceptable.*

NTNU　　　　　　　　　　　**SINTEF**

10　REGULATIONS AND GUIDELINES

Se http://www.arbeidstilsynet.no/regelverk/index.html
- Lov om tilsyn med elektriske anlegg og elektrisk utstyr (1929)
- Arbeidsmiljøloven
- Forskrift om systematisk helse-, miljø- og sikkerhetsarbeid (HMS Internkontrollforskrift)
- Forskrift om sikkerhet ved arbeid og drift av elektriske anlegg (FSE 2006)
- Forskrift om elektriske forsyningsanlegg (FEF 2006)
- Forskrift om utstyr og sikkerhetssystem til bruk i eksplosjonsfarlig område NEK 420
- Forskrift om håndtering av brannfarlig, reaksjonsfarlig og trykksatt stoff samt utstyr og anlegg som benyttes ved håndteringen
- Forskrift om Håndtering av eksplosjonsfarlig stoff
- Forskrift om bruk av arbeidsutstyr.
- Forskrift om Arbeidsplasser og arbeidslokaler
- Forskrift om Bruk av personlig verneutstyr på arbeidsplassen
- Forskrift om Helse og sikkerhet i eksplosjonsfarlige atmosfærer
- Forskrift om Høytrykksspyling
- Forskrift om Maskiner
- Forskrift om Sikkerhetsskilting og signalgivning på arbeidsplassen
- Forskrift om Stillaser, stiger og arbeid på tak m.m.
- Forskrift om Sveising, termisk skjæring, termisk sprøyting, kullbuemeisling, lodding og sliping (varmt arbeid)
- Forskrift om Tekniske innretninger
- Forskrift om Tungt og ensformig arbeid
- Forskrift om Vern mot eksponering for kjemikalier på arbeidsplassen (Kjemikalieforskriften)
- Forskrift om Vern mot kunstig optisk stråling på arbeidsplassen
- Forskrift om Vern mot mekaniske vibrasjoner
- Forskrift om Vern mot støy på arbeidsplassen

Veiledninger fra arbeidstilsynet
se: http://www.arbeidstilsynet.no/regelverk/veiledninger.html

11　DOCUMENTATION

- Tegninger, foto, beskrivelser av forsøksoppsetningen
- Hazop_mal
- Sertifikat for trykkpåkjent utstyr
- Håndtering avfall i NTNU
- Sikker bruk av LASERE, retningslinje
- HAZOP_MAL_Prosedyre
- Forsøksprosedyre
- Opplæringsplan for operatører
- Skjema for sikker jobb analyse, (SJA)
- Apparaturkortet
- Forsøk pågår kort

12   GUIDANCE TO RISK ASSESSMENT TEMPLATE

Chapter 7 Assessment of technical safety.

Ensure that the design of the experiment set up is optimized in terms of technical safety.
Identifying risk factors related to the selected design, and possibly to initiate re-design to ensure that risk is eliminated as much as possible through technical security.
This should describe what the experimental setup actually are able to manage and acceptance for emission.

7.1 HAZOP

The experimental set up is divided into nodes (eg motor unit, pump unit, cooling unit.). By using guidewords to identify causes, consequences and safeguards, recommendations and conclusions are made according to if necessary safety is obtained. When actions are performed the HAZOP is completed.
(e.g. "No flow", cause: the pipe is deformed, consequence: pump runs hot, precaution: measurement of flow with a link to the emergency or if the consequence is not critical used manual monitoring and are written into the operational procedure.)

7.2 Flammable, reactive and pressurized substances and gas.

According to the Regulations for handling of flammable, reactive and pressurized substances and equipment and facilities used for this:

Flammable material: Solid, liquid or gaseous substance, preparation, and substance with occurrence or combination of these conditions, by its flash point, contact with other substances, pressure, temperature or other chemical properties represent a danger of fire.

Reactive substances: Solid, liquid, or gaseous substances, preparations and substances that occur in combinations of these conditions, which on contact with water, by its pressure, temperature or chemical conditions, represents a potentially dangerous reaction, explosion or release of hazardous gas, steam, dust or fog.

Pressurized : Other solid, liquid or gaseous substance or mixes having fire or hazardous material response, when under pressure, and thus may represent a risk of uncontrolled emissions

Further criteria for the classification of flammable, reactive and pressurized substances are set out in Annex 1 of the Guide to the Regulations "Flammable, reactive and pressurized substances"
http://www.dsb.no/Global/Publikasjoner/2009/Veiledning/Generell%20veiledning.pdf
http://www.dsb.no/Global/Publikasjoner/2010/Tema/Temaveiledning_bruk_av_farlig_stoff_Del_1.pdf

Experiment setup area should be reviewed with respect to the assessment of Ex zone
• Zone 0: Always explosive atmosphere, such as inside the tank with gas, flammable liquid.
• Zone 1: Primary zone, sometimes explosive atmosphere such as a complete drain point
• Zone 2: secondary discharge could cause an explosive atmosphere by accident, such as flanges, valves and connection points

7.4 Effects on the environment

With pollution means: bringing solids, liquid or gas to air, water or ground, noise and vibrations, influence of temperature that may cause damage or inconvenience effect to the environment.

Regulations: http://www.lovdata.no/all/hl-19810313-006.html#6

NTNU guidance to handling of waste:http://www.ntnu.no/hms/retningslinjer/HMSR18B.pdf

7.5 Radiation

Definition of radiation

Ionizing radiation: Electromagnetic radiation (in radiation issues with wawelength <100 nm) or rapid atomic particles (e.g. alpha and beta particles) with the ability to stream ionized atoms or molecules.
Non ionizing radiation: Electromagnetic radiation (wavelength >100 nm), og ultrasound$_1$ with small or no capability to ionize.
Radiation sources: All ionizing and powerful non-ionizing radiation sources.
Ionizing radiation sources: Sources giving ionizing radiation e.g. all types of radiation sources, x-ray, and electron microscopes.
Powerful non ionizing radiation sources: Sources giving powerful non ionizing radiation which can harm health and/or environment, e.g. class 3B and 4. MR$_2$ systems, UVC$_3$ sources, powerful IR sources$_4$.
$_1$Ultrasound is an acoustic radiation ("sound") over the audible frequency range (> 20 kHz). In radiation protection regulations are referred to ultrasound with electromagnetic non-ionizing radiation.
$_2$MR (e.g. NMR) - nuclear magnetic resonance method that is used to "depict" inner structures of different materials.
$_3$UVC is electromagnetic radiation in the wavelength range 100-280 nm.
$_4$IR is electromagnetic radiation in the wavelength range 700 nm - 1 mm.

For each laser there should be an information binder (HMSRV3404B) which shall include:
- General information
- Name of the instrument manager, deputy, and local radiation protection coordinator
- Key data on the apparatus
- Instrument-specific documentation
- References to (or copies of) data sheets, radiation protection regulations, etc.
- Assessments of risk factors
- Instructions for users
- Instructions for practical use, startup, operation, shutdown, safety precautions, logging, locking, or use of radiation sensor, etc.
- Emergency procedures
- See NTNU for laser: http://www.ntnu.no/hms/retningslinjer/HMSR34B.pdf

7.6 The use and handling of chemicals.

In the meaning chemicals, a element that can pose a danger to employee safety and health

See: http://www.lovdata.no/cgi-wift/ldles?doc=/sf/sf/sf-20010430-0443.html

Safety datasheet is to be kept in the HSE binder for the experiment set up and registered in the database for chemicals.

Chapter 8 Assessment of operational procedures.

Ensures that established procedures meet all identified risk factors that must be taken care of through operational barriers and that the operators and technical performance have sufficient expertise.

8.1 Procedure Hazop
Procedural HAZOP is a systematic review of the current procedure, using the fixed HAZOP methodology and defined guidewords. The procedure is broken into individual operations (nodes) and analyzed using guidewords to identify possible nonconformity, confusion or sources of inadequate performance and failure.

8.2 Procedure for running experiments and emergency shutdown.
Have to be prepared for all experiment setups.

The operating procedure has to describe stepwise preparation, startup, during and ending conditions of an experiment. The procedure should describe the assumptions and conditions for starting, operating parameters with the deviation allowed before aborting the experiment and the condition of the rig to be abandoned.

Emergency procedure describes how an emergency shutdown have to be done, (conducted by the uninitiated),

what happens when emergency shutdown, is activated. (electricity / gas supply) and
which events will activate the emergency shutdown (fire, leakage).

Chapter 9 Quantifying of RISK
Quantifying of the residue hazards, Risk matrix

To illustrate the overall risk, compared to the risk assessment, each activity is plotted with values for the probability and consequence into the matrix. Use task IDnr.

Example: If activity IDnr. 1 has been given a probability 3 and D for consequence the risk value become D3, red. This is done for all activities giving them risk values.

In the matrix are different degrees of risk highlighted in red, yellow or green. When an activity ends up on a red risk (= unacceptable risk), risk reducing action has to be taken

CONSEQUENSES						
	Catastrophic	E1	E2	E3	E4	E5
	Major	D1	D2	D3	D4	D5
	Moderate	C1	C2	C3	C4	C5
	Minor	B1	B2	B3	B4	B5
	Insignificant	A1	A2	A3	A4	A5
		Rare	Unlikely	Possible	Likely	Almost
		PROBABILITY				

Table 8. Risk's Matrix

NTNU   SINTEF

Table 9. The principle of the acceptance criterion. Explanation of the colors used in the matrix

COLOUR		DESCRIPTION
Red		Unacceptable risk Action has to be taken to reduce risk
Yellow		Assessment area. Actions has to be considered
Green		Acceptable risk. Action can be taken based on other criteria

A.4.2 Attachement to Risk Assessment report

NTNU   **SINTEF**

Attachment to Risk Assessment report

Thermal plume experiment

Prosjektnavn	Characterization of the airflow distribution in close proximity to the patient in an operating room
Apparatur	Klimarom VVS-lab
Enhet	NTNU
Apparaturansvarlig	Guangyu Cao
Prosjektleder	Guangyu Cao
HMS-koordinator	Morten Grønli
HMS-ansvarlig (linjeleder)	Terese Løvås
Plassering	Klimarom, Varmetekniske laboratorier
Romnummer	C247C, 2. etg i klimalab, Varmetekniske laboratorier
Risikovurdering utført av	

TABLE OF CONTENTS

NTNU

SINTEF

1

NTNU · **SINTEF**

ATTACHMENT B: HAZOP TEMPLATE

Project: Characterization of the airflow distribution in close proximity to the patient in an operating room

Node: 1

Page:

Ref	Guideword	Causes	Consequences	Safeguards	Recommendations	Action	Date/Sign
Low risk	Lower or higher temperature in thermal manikin	Wrong level of current for the heating system	The thermal manikin could become hotter than expected, and in extreme cases may cause burns or fire	Make sure that the electrical equipment is correctly set up, following the guidelines of the equipment	To follow the guidelines of the equipment.	Adjust input current/watt in order to control the temperature of the heating system	

NTNU   **SINTEF**

ATTACHMENT C: TEST CERTIFICATE FOR LOCAL PRESSURE TESTING

Trykkpåkjent utstyr:	
Benyttes i rigg:	
Design trykk for utstyr (bara):	
Maksimum tillatt trykk (bara): (i.e. burst pressure om kjent)	
Maksimum driftstrykk i denne rigg:	

Prøvetrykket skal fastlegges i følge standarden og med hensyn til maksimum tillatt trykk.

Prøvetrykk (bara):			
X maksimum driftstrykk: I følge standard			
Test medium:			
Temperatur (°C)			
Start tid:		Trykk (bara):	
Slutt tid:		Trykk (bara):	
Maksimum driftstrykk i denne rigg:			

Eventuelle repetisjoner fra atm. trykk til maksimum prøvetrykk:................

Test trykket, dato for testing og maksimum tillatt driftstrykk skal markers på (skilt eller innslått)

_____   _____
Sted og dato   Signatur

3

NTNU ☐   ⊙ SINTEF

ATTACHMENT D: HAZOP PROCEDURE (TEMPLATE)

Project:
Node: 1

Page

Ref#	Guideword	Causes	Consequences	Safeguards	Recommendations	Action	Date/Sign
	Not clear procedure	Procedure is to ambitious, or confusingly					
	Step in the wrong place	The procedure can lead to actions done in the wrong pattern or sequence					
	Wrong actions	Procedure improperly specified					
	Incorrect information	Information provided in advance of the specified action is wrong					
	Step missing	Missing step, or step requires too much of operator					
	Step unsuccessful	Step has a high probability of failure					
	Influence and effects from other	Procedure's performance can be affected by other sources					

4

113

▣ NTNU

◎ SINTEF

ATTACHMENT E: PROCEDURE FOR RUNNING EXPERIMENTS

Prosjekt: Characterization of the airflow distribution in close proximity to the patient in an operating room	Dato	Signatur
Apparatur Thermal manikin experiment		
Prosjektleder Guangyu Cao	18.1.2018	

Conditions for the experiment:	Completed
Experiments should be run in normal working hours, 08:00-16:00 during winter time and 08.00-15.00 during summer time. Experiments outside normal working hours shall be approved.	✓
One person must always be present while running experiments, and should be approved as an experimental leader.	✓
An early warning is given according to the lab rules, and accepted by authorized personnel.	✓
Be sure that everyone taking part of the experiment is wearing the necessary protecting equipment and is aware of the shut down procedure and escape routes.	✓
Preparations	**Carried out**
Post the "Experiment in progress" sign.	✓
Measure initial air temperature in the room. Check at 3-4 different heights to make sure that there is little stratification.	✓
Measure wall surface temperature in case of radiation influence on the thermal manikin.	✓
Position thermal manikin/human and the sensors at starting locations.	✓
Heat up manikin to the correct surface temperature.	✓
During the experiment	
Measurements of velocity at the chosen points.	✓
Open door between measurements, in order to ventilate and avoid heating of the room.	✓
End of experiment	
Turn off heat source.	✓
Remove all obstructions/barriers/signs around the experiment.	✓
Tidy up and return all tools and equipment.	✓
Tidy and cleanup work areas.	✓
Return equipment and systems back to their normal operation settings (fire alarm)	✓
To reflect on before the next experiment and experience useful for others	
Was the experiment completed as planned and on scheduled in professional terms?	
Was the competence which was needed for security and completion of the experiment available to you?	✓

5

114

	Do you have any information/ knowledge from the experiment that you should document and share with fellow colleagues?	✓

Operator(s):

Navn	Dato	Signatur
ANDERS MOSTROM NLSSEN	18.01.18	Anders Mosfröm Nilssen

O NTNU   **O SINTEF**

ATTACHMENT F: TRAINING OF OPERATORS

Prosjekt: Characterization of the airflow distribution in close proximity to the patient in an operating room	Dato	Signatur
Apparatur: Klimalab		
Prosjektleder: Guangyu Cao	18. 1. 2018	*Gyu Cao*

	Knowledge about EPT LAB in general	
	Lab • Access • routines and rules • working hour	
	Knowledge about the evacuation procedures.	
	Activity calendar for the Lab	
	Early warning, iept-experiments@ivt.ntnu.no	
	Knowledge about the experiments	
	Procedures for the experiments	
	Emergency shutdown.	
	Nearest fire and first aid station.	

I hereby declare that I have read and understood the regulatory requirements has received appropriate training to run this experiment and are aware of my personal responsibility by working in EPT laboratories.

Operator(s):

Navn	Dato	Signatur
ANDERS MOSTRØM NILSEN	18.09.18	Anders Moström Nilsen

NTNU

SINTEF

ATTACHMENT G: FORM FOR SAFE JOB ANALYSIS

SJA name:	
Date:	Location:
Mark for completed checklist:	

Participators:		
SJA-responsible:		

Specification of work (What and how?):

Risks associated with the work:

Safeguards: (plan for actions, see next page):

Conclusions/comments:

Recommended/approved	Date/Signature:	Recommended/approved	Date/Signature:
SJA-responsible:		HSE responsible:	
Responsible for work:		Other, (position):	

8

117

HSE aspect	Yes	No	NA	Comments / actions	Resp.
Documentation, experience, qualifications					
Known operation or work?					
Knowledge of experiences / incidents from similar operations?					
Necessary personnel?					
Communication and coordinating					
Potential conflicts with other operations?					
Handling of an eventually incident (alarm, evacuation)?					
Need for extra assistance / watch?					
Working area					
Unusual working position					
Work in tanks, manhole?					
Work in ditch, shaft or pit?					
Clean and tidy?					
Protective equipment beyond the personal?					
Weather, wind, visibility, lighting, ventilation?					
Usage of scaffolding/lifts/belts/ straps, anti-falling device?					
Work at hights?					
Ionizing radiation?					
Influence of escape routes?					
Chemical hazards					
Usage of hazardous/toxic/corrosive chemicals?					
Usage of flammable or explosive chemicals?					
Risk assessment of usage?					
Biological materials/substances?					
Dust/asbestos/dust from insulation?					
Mechanical hazards					
Stability/strength/tension?					
Crush/clamp/cut/hit?					
Dust/pressure/temperature?					
Handling of waste disposal?					
Need of special tools?					
Electrical hazards					
Current/Voltage/over 1000V?					
Current surge, short circuit?					
Loss of current supply?					
Area					
Need for inspection?					
Marking/system of signs/rope off?					
Environmental consequences?					
Key physical security systems					
Work on or demounting of safety systems?					
Other					

9

NTNU ⬤ SINTEF

APPARATURKORT / UNITCARD

Dette kortet SKAL henges godt synlig på apparaturen!
This card MUST be posted on a visible place on the unit!

Apparatur (Unit)	
Thermal manikin experiment	
Prosjektleder (Project Leader)	**Telefon mobil/privat** (Phone no. mobile/private)
Guangyu Cao	918 97 689
Apparaturansvarlig (Unit Responsible)	**Telefon mobil/privat** (Phone no. mobile/private)
Guangyu Cao	918 97 689
Sikkerhetsrisikoer (Safety hazards)	
Do not touch the thermal manikin while it is plugged	
Sikkerhetsregler (Safety rules)	
Turn off the thermal when not in use	
Nødstopp prosedyre (Emergency shutdown) Switch off and unplug thermal manikin	

Her finner du (Here you will find):

Prosedyrer (Procedures)	In the room
Bruksanvisning (Users manual)	In the room

Nærmeste (Nearest)

Brannslukningsapparat (fire extinguisher)	First floor VVS-lab(syd)
Førstehjelpsskap (first aid cabinet)	First floor VVS-lab(syd)

NTNU
Institutt for energi og prosessteknikk

SINTEF Energi
Avdeling energiprosesser

Dato

Dato

_____

_____

Signert

Signert

_____

_____

_____

10

☐ NTNU   ◉ SINTEF

FORSØK PÅGÅR /EXPERIMENT IN PROGRESS

Dette kortet SKAL henges opp før forsøk kan starte!
This card MUST be posted on the unit before the experiment startup!

Apparatur (Unit)	
Thermal manikin experiment	
Prosjektleder (Project Leader)	**Telefon mobil/privat** (Phone no. mobile/private)
Guangyu Cao	9189 7689
Apparaturansvarlig (Unit Responsible)	**Telefon mobil/privat** (Phone no. mobile/private)
Guangyu Cao	9189 76 89
Godkjente operatører (Approved Operators)	**Telefon mobil/privat** (Phone no. mobile/private)
Anders Mostrøm Nilssen	9181 7565

Prosjekt (Project)
Characterization of the airflow distribution in close proximity to the patient in an operating room

Forsøkstid / Experimental time (start - stop)

08.11.17-19.01.18

Kort beskrivelse av forsøket og relaterte farer (Short description of the experiment and related hazards)

Measure the air velocity in close proximity to a thermal manikin/living human in supine position. The door should be closed during the experiment. Do not touch the thermal manikin while it is plugged, as the manikin could be hot and there also may be a risk of electrical shock due to the heating method of the manikin.

NTNU
Institutt for energi og prosessteknikk

SINTEF Energi
Avdeling energiprosesser

Dato

Dato

_____

_____

Signert

Signert

_____

_____

11

A.5   Article for IndoorAir2018

The effect of the thermal obstructions on the velocity and temperature field in an operating room with laminar airflow

Anders Mostrøm Nilssen[1], Amar Aganovic[1], Guangyu Cao[1], Liv-Inger Stenstad[2], Jan G. Skogås[2]

[1]Kolbjørn Hejes vei 1b, 7491 Trondheim, Norway, Department of Energy and Process Engineering, Norwegian University of Science and Technology, Trondheim, Norway

[2]Postboks 3250 Sluppen, 7006, Trondheim, Norway, St. Olavs Hospital, Trondheim, Norway

Corresponding email: andersmn@stud.ntnu.no

SUMMARY

In modern hospitals, among surgical patients surgical-site infections (SSIs) are the most common hospital-acquired infections. The objective of this study is to characterize the airflow distribution in close proximity to the patient in an operating room (OR) with laminar airflow (LAF) system. Field measurements of the air temperature and velocity were conducted at St. Olavs hospital, Norway. The patient was simulated by persons of different height and age in supine position, while the indoor environmental conditions of the operating room were set equal to those of a real surgery. The results show that the airflow above the patient is affected by the supply air from the ceiling being counteracted by the thermal plume of the patient, resulting in lower velocity above the patient than the surroundings.

KEYWORDS

Laminar airflow ventilation; Airflow velocity; Surgical site infections; Operating room

1 INTRODUCTION

Nosocomial infections pose a major problem for both patients and hospitals, and calculations have indicated that the hospital stay for an affected patient may be prolonged by 4-7 days (Kjønniksen et al., 2002). Among patients who have undergone surgery, Surgical Site Infection (SSIs) are the most prevalent sort of nosocomial infections, accounting for 36 % (Poggio, 2013). Patients in surgery involving knee or hip replacement are especially prone to SSIs as the tissue is exposed to ambient air for a relatively long time and because a large amount of tissue is exposed. A recent study at St. Olavs hospital showed that of 587 patients included in the study, 1.7 % had developed a deep and 1.7 % a superficial SSI following an orthopaedic procedure (Hagen, 2016). The total number of infected in the mentioned study of Hagen is higher than the national average for Norway of 1.8 % (Helsenorge, 2016) following surgery.

There are several factors that may contribute to the risk of SSIs. These factors include among others age and weight of the patient, underlying patient illness, the surgical staff's abilities, attention to hygiene, and contamination levels of bacteria and particles in the operating room (OR) (Weinstein and Bonten, 2017). The role of the ventilation system in an OR has also been investigated in several studies. A large study executed in the 1970s by Lidwell and colleagues, stated that ultra-clean air provided through a LAF system and fine-meshed filters could reduce the risk of developing a deep sepsis following a knee or hip replacement from 1.5 % to 0.6 % (Lidwell et al., 1982). However, a study performed by Bischoff and colleagues reviewed 12

previous studies comparing conventional ventilation with LAF ventilation, and concluded that LAF ventilation had no advantage regarding SSIs (Bischoff et al., 2017). A second study, performed by McHugh and colleagues, concluded that the supposed correlation between LAF and lower rates of SSIs is uncertain, and that recent studies actually suggests LAF to be linked to higher rates (McHugh et al., 2015).

During surgery, a patient in supine position will experience heat transfer in different ways: convection to the surrounding air, radiation to the surrounding surfaces, conduction to the solid materials in direct contact, evaporation from the skin, and respiration. The heat loss caused by convection is due to the fact that the skin has higher temperature than the surrounding air, resulting in heating of the air close to the skin. The heated air will then rise due to reduced density, causing a thermal plume (Goodfellow and Tähti, 2001, p. 518). As the air rises, more surrounding air will be entrained in the plume. The flow inside the plume will be turbulent (Zukowska, Popiolek and Melikov, 2010). The amount of air that the plume entrains depends on the power and geometry of the heat source, as well as the temperature of the surrounding air (Goodfellow and Tähti, 2001, p. 517). A thermal plume caused by a human in supine position is extremely individual. This is due to the complex geometry of a human body, as well as biological differences like skin temperature, metabolism, age and height among others. The plume itself is also elusive and sensitive to changes in the surroundings (Zukowska, Popiolek and Melikov, 2010).

When considering a wound and its healing process, a distinction between the internal and external wound microenvironment can be made. According to Kruse and colleagues the external microenvironment is the outer part of the wound which borders to the wound surface (Kruse et al., 2015). Parameters in the external microenvironment that affect the wound healing are temperature, pressure, presence of certain gases, microbes, hydration and pH (ibid.). The wound temperature is dependent on both the blood flow and the ambient air temperature, and an increased wound temperature is associated with vasodilatation (ibid.). Vasodilatation is the phenomenon of increased interior diameter in the blood vessels (MedicineNet, 2016) and increases the transport of nutrients and oxygen to the wound (Kruse et al., 2015), thus enhancing the healing. Heat loss due to evaporation may lower the wound temperature and promote vasoconstriction, which is the opposite of vasodilatation (MedicineNet, 2016). The velocity of the ambient air and the turbulence intensity both affect the convective heat loss of the wound (Murakami, Kato and Zeng, 1997).

Based on this, the focus of this study was to investigate air temperature and velocity in the external microenvironment of the hip area during a mock up surgery. The external microenvironment was defined as a square with a base area of 0.245 m^2 and a height of 15 cm.

2 METHODS

Field measurements were conducted in this study. The investigated area of the body was the area around the top of the femur.

The operating room
The OR in which the experiments took place was Operating Room of the Future's OR, at the department of orthopaedic procedures. The OR features a LAF ventilation system including high efficiency particulate air (HEPA) filters, and air supply happens through filters in the ceiling. The ceiling height is 3 meters and the floor area 56.58 m^2. In the middle of the room there is a clean zone of 11.56 m^2, which is equal to and positioned directly beneath the supply

area of the ventilation system. The OR is connected to a hallway with an automatic sliding door with an area of 3 m². The door remained closed during the measurements. Relative humidity is regulated at the operation central of the hospital after common HVAC principles, while the air temperature can be controlled from a display inside the OR. The set point range of these parameters were set to 30 ± 7 % and 22 ± 1 °C, respectively. The supply air velocity is controlled centrally and set to 0.3 m/s.

Instrumentation
Both the air temperature and speed were performed using 8 of the omnidirectional thermoanemometer SENSOANEMO 5100FS.

Table 1. Measurement range and accuracy of instruments

	Measurement range	Accuracy
Air speed [m/s]	0.05 - 5.00	±0.02, ±1 % of readings
Temperature [°C]	-10 - +50	±0.2

The recording time was 3 minutes for each measurement, and for every two second a velocity was logged.

Experimental set up
The top of the femur was found for the patient, and then 25 cm up and down from that location were measured and indicated. Based on this a grid of 48 measurement points at each height above the patient was created, with 6 rows and 8 columns. The distance between each row and column, was set to 10 and 7 cm respectively, meaning that the grid covered an area of 0.245 m². Two heights, 10 and 15 cm above the patient, were chosen for the measurement grid, resulting in a total of 96 points. The vertical distances were measured from the top of the supine patient, at the same location as the top of the femur.

Two scenarios were considered for this study. Scenario 1 included a patient in supine position and two persons mimicking the activity level and presence of surgeons. Scenario 2 was similar to scenario 1, but additionally featured specific surgical lighting. The patient was a 26-year-old male of 194 cm and 86 kg. The surgeons were mimicked by the same persons for both scenarios. The patient and the surgeons were equally dressed, and the clothing included a protective hood, a short-sleeved shirt, light pants, socks, underwear and shoes, corresponding to 0.5-0.6 clo. The surgical lamps in scenario 2 were positioned according to the German standard DIN1946 as the abdomen was illuminated. The two lamps had a hemispherical shape and a diameter of 0.6 and 0.85 m respectively, and both featured halogen bulbs with filters preventing heat dissipation on the operating field.

Figure 1 shows a sketch of the setup along, and also a photo taken during the experiments at St. Olavs hospital.
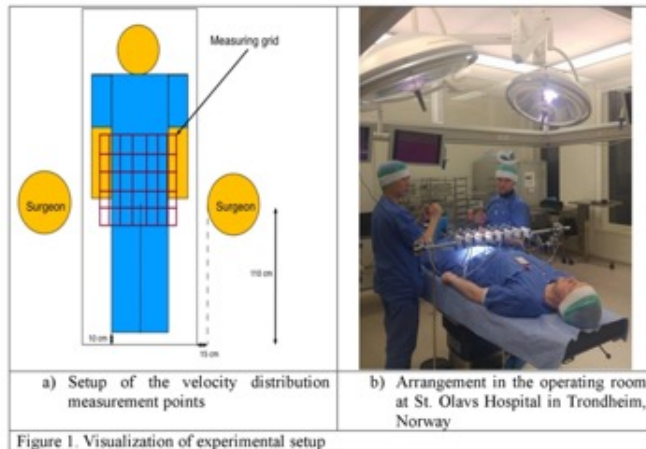
| a) Setup of the velocity distribution measurement points | b) Arrangement in the operating room at St. Olavs Hospital in Trondheim, Norway |

Figure 1. Visualization of experimental setup

3 RESULTS

The arithmetic mean for each measuring point and measurement was calculated and then plotted in contour plots for both the air velocity and temperature. Figure 2 shows that the temperature is somewhat higher in the central, lower part of the plot. This corresponds to the groin of the patient, and an elevated temperature in this area could be caused by the fact that this is a junctional area between the thighs. Therefore, the surfaces of the inner thighs could come in contact, reducing the total surface area exposed to air and thus increasing the surface temperature compared to other areas. Temperature plots for both scenarios show that the air temperature is in general higher closer to the patient.

Figure 2. Temperature distribution measurements for Scenario 1 10 cm (left) and 15 cm (right) above simulated patient in an operating room with laminar airflow.

fig/IA5.jpg

Figure 5. Temperature distribution measurements 10 cm (left) and 15 cm (right) for Scenario 2 above simulated patient in an operating room with laminar airflow.
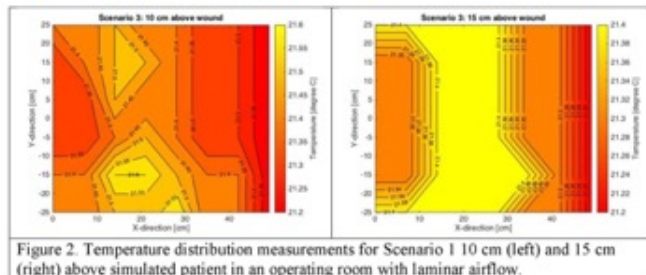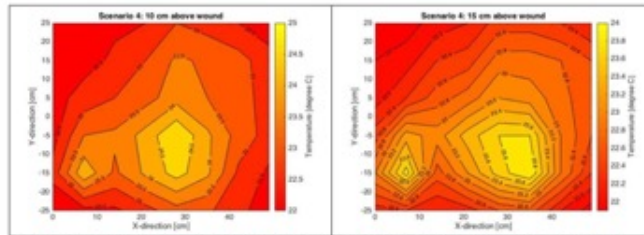
In Figure 6 one can observe the same case as in Figure 5 regarding the velocity of the air, that the velocity seems to decrease with increasing height above the patient. The point of highest velocity in Figure 6 seems to coincide with a small point of higher temperature in Figure 5, whereas the major hot spot in Figure 5 does not have a corresponding spot in any of the plots in Figure 6.
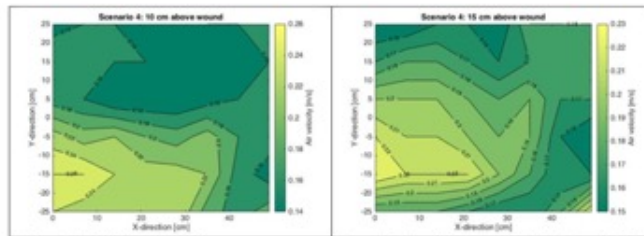
Figure 6. Velocity distribution measurements 10 cm (left) and 15 cm (right) for Scenario 2 above simulated patient in an operating room with laminar airflow.

4 DISCUSSION

The plots for the scenario without surgical lights shows small temperature differences in the measurement grid. This could be explained by high ventilation rates in the sterile zone. A powerful heat source is required in order to heat the vast amount of air that is constantly flowing towards the patient, and produce a significant thermal footprint in the measurements. From the plots in figure 2 it seems that the thermal plume caused by the patient in this scenario is only strong enough to leave this footprint at the height closest to the patient.

Figure 2 also shows that the highest recorded temperatures occur around the centreline of the x-axis in both plots. Figure 3 and 4 show that the lowest recorded velocities occur around the same centreline as in figure 2. The elevated temperatures indicate the presence of a thermal plume, and air inside the plume will move upwards. As a consequence will air movement caused by the ventilation system and the thermal plume have opposite directions, meaning

that the thermal plume decelerates the airflow from the ventilation system. This could explain the velocity plots in figure 3 and 4, as the lower velocities appear along the centreline of the x-axis.

The temperatures in the scenario with surgical lights are substantially higher than in the case without lights, and could be caused by absorption of light at the illuminated area. They imply that the thermal plume of the scenario with lamps could be stronger than the one without.

The airflow pattern in the scenario with surgical lighting appears more chaotic than the pattern in the scenario without. The lack of symmetry in the velocity plots in figure 6 deviates from the quasisymmetric plots in figure 3 and 4. Another feature of the plots in figure 6 is that the highest velocities appear closest to the patient, in contradiction to what is observed in the scenario without surgical lighting. This could indicate that the airflow pattern is fundamentally different for the two scenarios. As the surgical lamps interfere with and block the laminar airflow from the ceiling, they cause formation of wakes downstream. The wakes change the airflow and could explain the velocity plots in figure 4. In previous studies have both Chow and Yang (2005) and Brohus et al. (2006) identified the presence and positioning of surgical lamps as one of the most influencing factors on the airflow distribution close to the patient.

The tendency of higher temperatures and lower velocities in the left part of the grid in the scenario with surgical lamps, may have several causes. One of them could be that the bar with the sensors were not located directly above the patient, but that it was placed somewhat more to the right. Another possibility is that the distance between the sensors on the right side was larger than it was supposed to be, causing the outermost right sensor to be farther away from the middle of the patient than the outermost left sensor. A third option includes uneven positioning of the measurement rig after moving it between the rows in the grid. A fourth explanation is that the patient moved during the measurements.

During both scenarios clothing covered the intended wound area of the patient, and the additional thermal resistance of the clothing could affect the results. In the scenario with surgical lighting the clothing will most likely absorb a larger absorb a larger part of the thermal radiation from the lamps, as skin has greater emissivity than cloth (Incropera et al., 2013).

5 CONCLUSIONS

The supply air flow from the LAF system appears to be decelerated, and disturbed by the thermal plume from the patient, which results in unstable distribution close to the patient. Surgical lamps also had a major impact on the air flow, due to their heating of the wound area and interference with the supply air flow. Therefore, the intended laminar air flow near the patient was altered and the characteristics are more complex than what the design was meant to provide. Therefore, future guidelines and design specifications should more carefully consider the effect of thermal plumes and obstructions on the laminar airflow in operating rooms.

6 REFERENCES

Bischoff P, Zeynep Kubilay N, Allegranzi B, Egger M, Gastmeier P. (2017) Effect of laminar airflow ventilation on surgical site infections: a systematic review and meta-analysis. *The Lance Infectious Diseases*, 17(5), pp. 553-561

Brohus H, Balling K, Jeppesen D. (2006) Influence of movements on contaminant transport in an operating room. *Indoor Air*, 16(5), pp. 356-372

Chow T, Yang X. (2005) Ventilation performance in the operating theatre against airborne infection: numerical study on ultra-clean system. *Journal of Hospital Infection*, 59(2), pp. 138-147

Goodfellow H, Tähti E. (2001) *Industrial Ventilation Design Guidebook*. London: Academic Press

Hagen L. (2016) *Postoperative sårinfeksjoner, en observasjonsstuide ved St. Olavs hospital, Roros Sykehus*. Master thesis. Norges teknisk-naturvitenskapelige universitet

Helsenorge. (2016) *Forekomst av helsetjenesteassosierte infeksjoner i sykehus*. Available from: https://helsenorge.no/Kvalitetsindikatorer/infeksjoner/sykehusinfeksjoner#Se-resultater (Accessed: 11.12.2017)

Incropera F, Dewitt D, Bergman T, Lavine A. (2013) Principles of heat and mass transfer. 7th ed. Singapore: Wiley, pp. 1080-1010

Kjønniksen I, Segadal L, Haugsbø A, Hotvedt R, Jacobsen T, Kristiansen IS, Nordsletten L, Søndenaa VG. (2002) Ventilasjon av operasjonsstuer, *Tidsskr Nor Legeforen*, 122(5), pp. 545-547. Available from: http://tidsskriftet.no/2002/02/kronikk/ventilasjon-av-operasjonsstuer (Accessed: 11.12.2017)

Kruse CR, Nuutila K, Lee CC, Kiwanuka E, Singh M, Caterson EJ, Eriksson E, Sørensen JA. (2015) The external microenvironment of healing skin wounds, *Wound repair regen*, 23(4), pp. 456-464

Lidwell OM, Lowbury EJ, Whyte W, Blowers R, Stanley SJ, Lowe D. (1982) Effect of ultra-clean air in operating rooms on deep sepsis in the joint after total hip or knee replacement: a randomized study, *British Medical Journal*, 285(10), pp. 10-14

McHugh SM, Hill ADK, Humphreys H. (2015) Laminar airflow and the prevention of surgical site infection. More harm than good?, *The Surgeon*, 13(1), pp. 52-58

MedicineNet. (2016) *Vasodilation*. Available from: https://www.medicinenet.com/script/main/art.asp?articlekey=5965 (Accessed: 12.12.2017)

Murakami S, Kato S, Zeng J. (1997) Flow and Temperature Fields Around Human Body with Various Room Air Distribution, Part 1 – CFD Study on Computational Thermal Manikin, *ASHRAE Transactions*, 103(1), pp. 3-15

Poggio JL. (2013) Perioperative Strategies to Prevent Surgical-Site Infection, *Clinics in Colon and Rectal Surgery*, 26(3), pp. 168-173. Available from: https://www.ncbi.nlm.nih.gov/pmc/articles/PMC3747289/pdf/10-1055-s-0033-1351133.pdf (Accessed: 11.12.2017)

Weinstein RA, Bonten MJM. (2017) Laminar airflow and surgical site infections: the evidence is blowing in the wind, *The Lancet Infectious Diseases*, 17(5), pp. 472-473. Available from: https://www.sciencedirect.com/science/article/pii/S1473309917300609 (Accessed: 11.12.2017)

Zukowska D, Popiolek Z, Melikov A. (2010) Determination of the integral characteristics of an asymmetrical thermal plume from air speed/velocity and temperature measurements, *Experimental Thermal and Fluid Science*, 34(8), pp. 1205-1216

A.6 Article for Roomventilation2018

FIELD MEASUREMENTS OF THE AIRFLOW DISTRIBUTION IN CLOSE PROXIMITY TO A PATIENT IN AN OPERATING ROOM

Anders Mostrøm Nilssen[1,*], Amar Aganovic[1], Guangyu Cao [1], Liv-Inger Stenstad[2], Jan G. Skogås[2]

[1]Kolbjørn Hejes vei 1b, 7491 Trondheim, Norway, Department of Energy and Process Engineering, Norwegian University of Science and Technology, Trondheim, Norway
[2]Postboks 3250 Sluppen, 7006 Trondheim, Norway, St. Olavs Hospital, Trondheim, Norway
Corresponding email: andersmosnil@gmail.com

SUMMARY

In modern hospitals among surgical patients are surgical-site infections the most common hospital-acquired infections. The objective of this study is to characterize the airflow distribution in close proximity to the patient in an operating room with a laminar airflow system. Field measurements of air velocity were conducted at St. Olavs hospital, Norway. The patient was simulated by a person in supine position, while the indoor environmental conditions were set equal to those of a real surgery. The results show that the airflow above the patient is affected by the supply air from the ceiling being counteracted by the thermal plume of the patient, resulting in lower velocities above the patient than the surroundings. They also show that the presence of surgical lamps have a major impact on the airflow distribution.

Keywords: ventilation, hospital, airflow, velocity, measurements.

1 INTRODUCTION

Nosocomial infections pose a major problem for both patients and hospitals, and calculations have indicated that the hospital stay for an affected patient may be prolonged by 4-7 days (Kjønniksen et al., 2002). Among patients who have undergone surgery are surgical-site infections (SSIs) the most prevalent sort of nosocomial infections, accounting for 36 % (Poggio, 2013). Surgery involving knee or hip replacement is especially prone to SSIs due to the fact that a large amount of tissue is exposed to ambient air for a relatively long period of time. A recent study at St. Olavs hospital showed that of 587 patients included in the study, 1.7 % had developed a deep and 1.7 % a superficial SSI following an orthopaedic procedure (Hagen, 2016). The total number of infected in the mentioned study of Hagen (ibid.) is higher than the national average in Norway of 1.8 % (Helsenorge, 2016) following surgery.

Factors that may contribute to the risk of SSIs include among others; age and weight of the patient, underlying patient illness, the surgical staff's abilities, attention to hygiene, and contamination levels of bacteria and particles in the operating room (OR) (Weinstein and Bonten, 2017). Also, the role of the ventilation system in the OR has been investigated in several studies. A large study executed in the 1970s and 1980s by Lidwell et al., stated that ultra-clean air provided through a laminar airflow (LAF) system and fine-meshed filters could reduce the risk of developing a deep sepsis following a knee or hip replacement from 1.5 % to 0.6 % (Lidwell et al., 1982). However, in a study by McHugh et al. the authors concluded that the supposed correlation between LAF and lower rates of SSIs is uncertain, and that recent studies actually suggests LAF to be linked to higher rates (McHugh et al., 2015). A study performed by Bischoff et al. reviewed 12 previous studies comparing conventional ventilation with LAF ventilation, and concluded that LAF ventilation held no advantage regarding SSIs (Bischoff et al., 2017).

During surgery, a patient in supine position will experience convective heat loss to the surrounding air. The heat loss caused by convection is due to the temperature of the skin being higher than the surrounding air, resulting in heating of the air close to the skin. The heated air will then rise due to

reduced density, causing a thermal plume (Goodfellow and Tähti, 2001). As the air rises, more surrounding air will be entrained in the plume. The flow inside the plume will be turbulent (Zukowska et al., 2010). The amount of air that the plume entrains depends on the power and geometry of the heat source, and the temperature of the surrounding air (Goodfellow and Tähti, 2001). A thermal plume caused by a human in supine position is extremely individual due to the complex geometry of a human body, as well as biological differences like skin temperature, metabolism, age and height. The plume itself is elusive and sensitive to changes in the surroundings (Zukowska et al., 2010).

When considering a wound and its healing process, a distinction between the internal and external wound microenvironment can be made. According to Kruse et al. the external microenvironment is the outer part of the wound which borders to wound surface (Kruse et al., 2015). Parameters in the external microenvironment that affect the wound healing are temperature, pressure, presence of certain gasses, microbes, hydration and pH (ibid.). The velocity and the turbulence intensity of the ambient air both affect the convective heat loss of the wound (Murakami et al., 1997).

Based on this, the objective of this study was to investigate the air velocity distribution in the external microenvironment of the hip area during a mock-up surgery. The external microenvironment was defined as a square with a base area of 0.245 m^2 and a height of 0.15 m.

2 METHODS

2.1 The operating room

The OR in which the experiments took place was Operating Room of the Future's OR, at the department of orthopaedic procedures. The OR features a LAF ventilation system including high efficiency particulate air (HEPA) filters, and air supply happens through filters in the ceiling. The ceiling height is 3 meters and the floor area 56.58 m^2. In the middle of the room there is a clean zone of 11.56 m^2, which is equal to and positioned directly beneath the supply area of the ventilation system. The OR is connected to a hallway with an automatic sliding door with an area of 3 m^2. The door remained closed during the measurements. Relative humidity is regulated at the operation central of the hospital after common HVAC principles, while the air temperature can be controlled from a display inside the OR. The set point range of these parameters were set to 30 ± 7 % and 22 ± 1 °C, respectively. The supply air velocity is controlled centrally and set to 0.3 m/s.

2.2 Instrumentation

The air velocity measurements were performed using 8 copies of the omnidirectional thermoanemometer SENSOANEMO 5100FS.

Table 1. Measurement range and accuracy of instruments

	Measurement range	Accuracy
Air velocity [m/s]	0.05 – 5.00	±0.02, ±1 % of readings

The recording time was 3 minutes for each measurement, and for every two seconds a velocity was logged.

2.3 Experimental set up

The top of the femur was found for the patient, and then 25 cm up and down from that location were measured and indicated. Based on this a grid of 48 measurement points at each height above the patient was created, with 6 rows and 8 columns. The distance between each row and column, was set to 10 and 7 cm respectively, meaning that the grid covered an area of 0.245 m^2. Two heights, 10 and 15 cm above

the patient, were chosen for the measuring grid, resulting in a total of 96 measuring points. The vertical distances were measured from the top of the supine patient, at the same location as the top of the femur.

Two scenarios were considered for this study. Scenario 1 included a patient in supine position and two persons mimicking the activity level and presence of surgeons. Scenario 2 was similar to scenario 1, but additionally featured specific surgical lighting. The patient was a 26-year-old male of 194 cm and 86 kg. The surgeons were mimicked by the same persons for both scenarios. The patient and the surgeons were equally dressed, and the clothing included a protective hood, a short-sleeved shirt, light pants, socks, underwear and shoes, corresponding to 0.5-0.6 clo. The surgical lamps in scenario 2 were positioned according to the German standard DIN1946 as the abdomen was illuminated. The two lamps had a hemispherical shape and a diameter of 0.6 and 0.85 m respectively, and both featured halogen bulbs with filters preventing heat dissipation on the operating field.
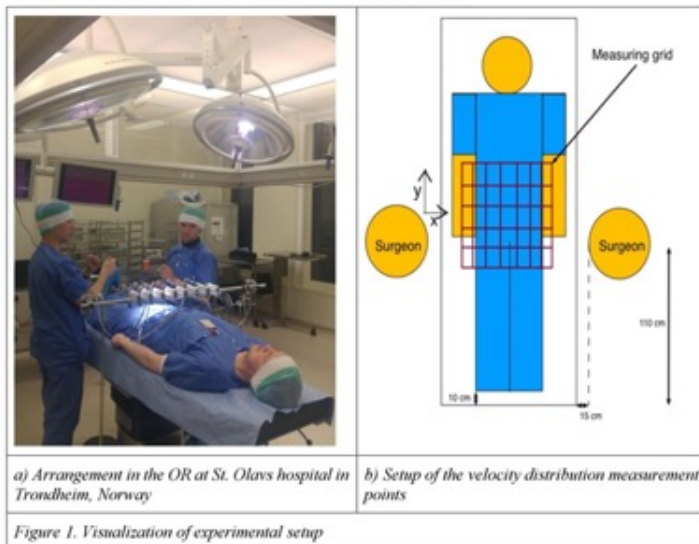

a) Arrangement in the OR at St. Olavs hospital in Trondheim, Norway	b) Setup of the velocity distribution measurement points

Figure 1. Visualization of experimental setup

3 RESULTS

The arithmetic mean for each measuring point and measurement was calculated and then plotted in contour plots. It can be seen from figure 2 and 3, that the velocities closer to the patient are in general lower and more varied. This could be caused by the fact that the supply laminar airflow is being counteracted by the upward air movement caused by the patient's thermal plume. As a thermal plume

rises from its source more ambient air is entrained, and the velocity of the plume is gradually reduced, resulting in a flatter velocity distribution in the plume.
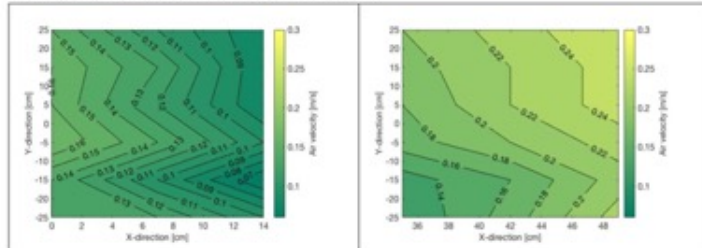

Figure 2. Velocity distributions measurements 10 cm for Scenario 1 above simulated patient in an operating room with laminar airflow. The plot had to be split in two due to two malfunctioning sensors.
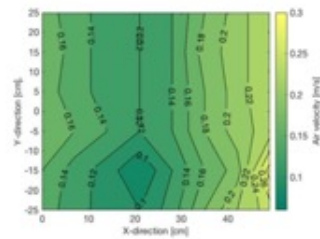

Figure 3. Velocity distribution measurements for Scenario 1 15cm above the simulated patient in an operating room with laminar airflow.

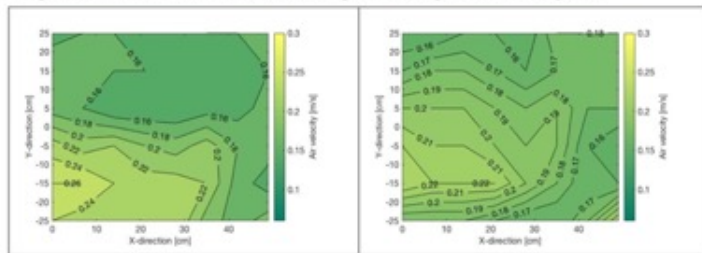In figure 4 one can observe that the velocities in general are higher closer to the patient.

Figure 4. Velocity distribution measurements 10 cm (left) and 15 cm (right) for Scenario 2 above simulated patient in an operating room with laminar airflow.

4 DISCUSSION

The plots for the scenario without surgical lighting show that the thermal plume of the patient decelerates the supply airflow, causing the air velocities in the external microenvironment to be lower than the supply air velocity of 0.3 m/s. The airflow patterns in figure 2 and 3 indicate that the thermal plume of the patient is strongest along the centreline of the x-axis, as that is where the lowest velocities are recorded.

The airflow pattern in scenario 2 deviates from the one in scenario 1, as there is no sort of symmetry around the centreline of the x-axis. Also, unlike the figures for scenario 1, figure 4 shows higher velocities closer to the patient. This, in addition to the lack of symmetry, could indicate that the airflow distribution is fundamentally different for the two scenarios and that the direction of the airflow could be harder to predict in scenario 2. Since the surgical lamps interfere with and partly block the airflow, wakes form downstream of the lamps. The wakes change the airflow, and could explain the distributions shown in figure 4. This would be in the accordance with the findings of both Chow and Yang (Chow and Yang, 2005) and Brohus et al. (Brohus et al., 2006), as they point to the positioning and presence of surgical lamps as one of the most influencing factors on the airflow distribution close to the patient. Another factor that could affect the airflow pattern in figure 4, is the fact that some of the light from the lamps could be absorbed as heat at the illuminated area and increase the local temperature. The increased temperature could then amplify the thermal plume.

During both scenarios, clothing covered the intended wound area of the patient and the additional thermal resistance of the clothing could affect the results. In the scenario with surgical lighting the clothing will most likely absorb a larger part of the thermal radiation from the lamps, as the emissivity of skin is higher than cloth (Incropera et al., 2013). A factor influencing the interpretation of the results, is the accuracy of the instruments of ±0.02 m/s, ±1 % of readings.

Real people were acting both surgeons and patient, and they could cause variations in the velocity recordings due to movement. The standard deviation for each measurement point in both scenarios was calculated, and it ranged from 0.00 to 0.05 m/s.

5 CONCLUSIONS

The laminar airflow from the ventilation system appears to be decelerated and disturbed by the thermal plume of the patient. Surgical lamps had a major impact due to their interference with and blocking of the airflow, and possibly by providing additional heat. As a result, the intended laminar airflow near the patient was altered and the characteristics became more complex than what the design was meant to provide. Hence, the effects of both thermal plumes and obstructions should be taken into account when making new guidelines and design specifications.

ACKNOWLEDGEMENTS

REFERENCES (STYLE: HEADING 1)

Bischoff, P., Zeynep Kubilay, N., Allegranzi, B., Egger, M., Gastmeier, P. (2017) Effect of laminar airflow ventilation on surgical site infections: a systematic review and meta-analysis. *The Lance Infectious Diseases*, 17(5), pp. 553-561, doi: 10.1016/ S1473-3099(17)30059-2

Brohus, H., Balling, K. and Jeppesen, D. (2006). Influence of movements on contaminant transport in an operating room. *Indoor Air*, 16(5), pp.356-372.

Chow, T. and Yang, X. (2005). Ventilation performance in the operating theatre against airborne infection: numerical study on an ultra-clean system. *Journal of Hospital Infection*, 59(2), pp.138-147.

Goodfellow, H., Tähti, E. (2001) *Industrial Ventilation Design Guidebook*. London: Academic Press

Hagen, L. (2016) *Postoperative sårinfeksjoner, en observasjonsstudie ved St. Olavs hospital, Røros Sykehus*. Master thesis. Norges teknisk-naturvitenskapelige universitet

Helsenorge. (2016) *Forekomst av helsetjenesteassosierte infeksjoner i sykehus*. Available from: https://helsenorge.no/Kvalitetsindikatorer/infeksjoner/sykehusinfeksjoner#Se-resultater (Accessed: 11.12.2017)

Incropera, F., Dewitt, D., Bergman, T. and Lavine, A. (2013). Principles of heat and mass transfer . 7th ed. Singapore: Wiley, pp.1008-1010.

Kjønniksen, I., Segadal, L., Haugsbø, A., Hotvedt, R., Jacobsen, T., Kristiansen, I S., Nordsletten, L., Søndenaa, V G. (2002) Ventilasjon av operasjonsstuer, *Tidsskr Nor Legeforen*, 122(5), pp. 545-547. Available from: http://tidsskriftet.no/2002/02/kronikk/ventilasjon-av-operasjonsstuer (Accessed: 11.12.2017)

Kruse, C R., Nuutila, K., Lee, C C., Kiwanuka, E., Singh, M., Caterson, E J., Eriksson, E., Sørensen, J A. (2015) The external microenvironment of healing skin wounds, *Wound repair regen*, 23(4), pp. 456-464, doi: 10.1111/wrr.12303

Lidwell, O M., Lowbury, E J., Whyte, W., Blowers, R., Stanley, S J., Lowe, D. (1982) Effect of ultraclean air in operating rooms on deep sepsis in the joint after total hip or knee replacement: a randomized study, *British Medical Journal*, 285(10), pp. 10-14. doi: https://doi.org/10.1136/bmj.285.6334.10

McHugh, S M., Hill, A D K., Humphreys, H. (2015) Laminar airflow and the prevention of surgical site infection. More harm than good?, *The Surgeon*, 13(1), pp. 52-58. doi: https://doi.org/10.1016/j.surge.2014.10.003

Murakami, S., Kato, S., Zeng, J. (1997) Flow and Temperature Fields Around Human Body with Various Room Air Distribution, Part 1 – CFD Study on Computational Thermal Manikin, *ASHRAE Transactions*, 103(1), pp. 3-15

Poggio, J L. (2013) Perioperative Strategies to Prevent Surgical-Site Infection, *Clinics in Colon and Rectal Surgery*, 26(3), pp. 168-173. Available from: https://www.ncbi.nlm.nih.gov/pmc/articles/PMC3747289/pdf/10-1055-s-0033-1351133.pdf (Accessed: 11.12.2017)

Weinstein, R A., Bonten, M J M. (2017) Laminar airflow and surgical site infections: the evidence is blowing in the wind, *The Lancet Infectious Diseases*, 17(5), pp. 472-473. Available from: https://www.sciencedirect.com/science/article/pii/S1473309917300609 (Accessed: 11.12.2017)

Zukowska D, Popiolek Z, Melikov A. (2010) Determination of the integral characteristics of an asymmetrical thermal plume from air speed/velocity and temperature measurements, *Experimental Thermal and Fluid Science*, 34(8), pp. 1205-1216. doi: https://doi.org/10.1016/j.expthermflusci.2010.04.009